NAVAL POSTGRADUATE SCHOOL
Monterey, California

THESIS

HIGH-RESOLUTION RESIDUE ANTENNA ARCHITECTURES FOR WIDEBAND DIRECTION FINDING

by

Luis E. Moita Rodrigues

June 1996

Thesis Advisor: Phillip E. Pace
Thesis Co-Advisor: Robert M. Keolian

Approved for public release; distribution is unlimited.

DISCLAIMER NOTICE

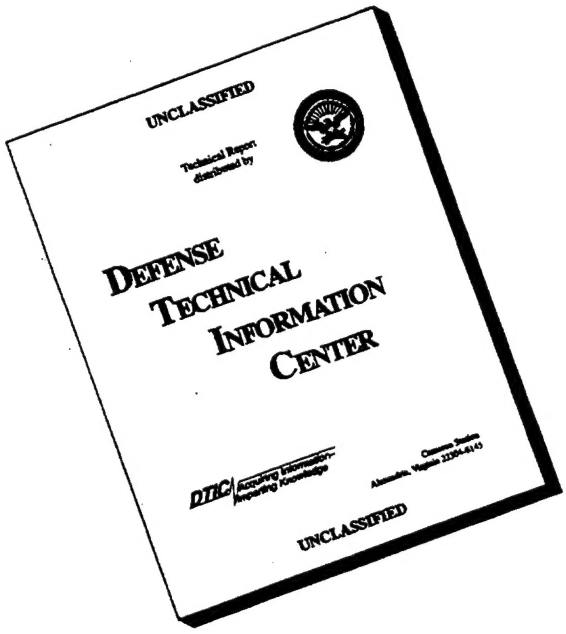

THIS DOCUMENT IS BEST QUALITY AVAILABLE. THE COPY FURNISHED TO DTIC CONTAINED A SIGNIFICANT NUMBER OF PAGES WHICH DO NOT REPRODUCE LEGIBLY.

REPORT DOCUMENTATION PAGE

Form Approved
OMB No. 0704-0188

1. AGENCY USE (Leave Blank)	2. REPORT DATE	3. REPORT TYPE AND DATES COVERED
	June 1996	Master's Thesis

4. TITLE AND SUBTITLE

HIGH-RESOLUTION RESIDUE ANTENNA ARCHITECTURES FOR WIDEBAND DIRECTION FINDING

6. AUTHOR(S)

Rodrigues, Luis E. Moita

7. PERFORMING ORGANIZATION NAME(S) AND ADDRESS(ES)

Naval Postgraduate School
Monterey, CA 93943-5000

8. PERFORMING ORGANIZATION REPORT NUMBER

9. SPONSORING / MONITORING AGENCY NAME(S) AND ADDRESS(ES)

10. SPONSORING / MONITORING AGENCY REPORT NUMBER

11. SUPPLEMENTARY NOTES

The views expressed in this thesis are those of the author and do not reflect the official policy or position of the Department of Defense or the United States Government.

12a. DISTRIBUTION / AVAILABILITY STATEMENT

Approved for public release; distribution is unlimited.

12b. DISTRIBUTION CODE

13. ABSTRACT *(Maximum 200 words)*

The performance of two novel interferometer antenna architectures for high-resolution, wideband direction finding are investigated. The first configuration incorporates a Symmetrical Number System (SNS) encoding of the interferometer amplitude response (symmetrical folding waveform). The second configuration incorporates a Residue Number System (RNS) encoding of the interferometer phase response (saw-tooth waveform). The residue architectures serve as a source for resolution enhancement in an interferometer array by decomposing the analog spatial filtering operation into a number of parallel sub-operations (moduli) that are of smaller computational complexity. Each sub-operation only requires a precision in accordance with the size of the modulus. A much higher resolution is achieved after the N moduli are used and the results of these low precision sub-operations are recombined. A four-element, 3 channel array using the moduli set $m_1 = 3$, $m_2 = 4$ and $m_3 = 5$ was constructed in a ground plane using rectangular waveguide elements with a center frequency of 8.5 GHz. Experimental results are compared with the simulation results to demonstrate the advantages of this approach. The frequency response of the RNS array is investigated numerically. To correct the quantization errors due to any frequency offset, a fast correction algorithm is derived and is shown to have excellent results over a wide bandwidth.

14. SUBJECT TERMS	15. NUMBER OF PAGES
Symmetrical Number System (SNS), Residue Number System (RNS), Direction Finding, Interferometer, Antennas.	110
	16. PRICE CODE

17. SECURITY CLASSIFICATION OF REPORT	18. SECURITY CLASSIFICATION OF THIS PAGE	19. SECURITY CLASSIFICATION OF ABSTRACT	20. LIMITATION OF ABSTRACT
Unclassified	Unclassified	Unclassified	UL

NSN 7540-01-280-5500

Standard Form 298 (Rev. 2-89)
Prescribed by ANSI Std. 239-18

Approved for public release; distribution is unlimited,

HIGH-RESOLUTION RESIDUE ANTENNA ARCHITECTURES FOR WIDEBAND DIRECTION FINDING

LUIS EDUARDO MOITA RODRIGUES
Lieutenant, Portuguese Navy
B.S., Portuguese Naval Academy, 1989

Submitted in partial fulfillment of the
requirements for the degree of

MASTER OF SCIENCE IN APPLIED PHYSICS

from the

NAVAL POSTGRADUATE SCHOOL
June 1996

Author: Luis Eduardo Moita Rodrigues

Luis E. Moita Rodrigues

Approved by:

Phillip E. Pace, Thesis Advisor

Robert Keolian

Robert Mitchell Keolian, Co-Advisor

W. B. Colson

William B. Colson, Chairman
Physics Department

ABSTRACT

The performance of two novel interferometer antenna architectures for high-resolution, wideband direction finding are investigated. The first configuration incorporates a Symmetrical Number System (SNS) encoding of the interferometer amplitude response (symmetrical folding waveform). The second configuration incorporates a Residue Number System (RNS) encoding of the interferometer phase response (saw-tooth waveform). The residue architectures serve as a source for resolution enhancement in an interferometer array by decomposing the analog spatial filtering operation into a number of parallel sub-operations (moduli) that are of smaller computational complexity. Each sub-operation only requires a precision in accordance with the size of the modulus. A much higher resolution is achieved after the N moduli are used and the results of these low precision sub-operations are recombined. A four-element, 3 channel array using the moduli set $m_1 = 3$, $m_2 = 4$ and $m_3 = 5$ was constructed in a ground plane using rectangular waveguide elements with a center frequency of 8.5 GHz. Experimental results are compared with the simulation results to demonstrate the advantages of this approach. The frequency response of the RNS array is investigated numerically. To correct the quantization errors due to any frequency offset, a fast correction algorithm is derived and is shown to have excellent results over a wide bandwidth.

TABLE OF CONTENTS

ACKNOWLEDGMENT

I would like to acknowledge the guidance, precious goodwill and extreme patience of Professor Phillip E. Pace, my thesis advisor. To Professor David C. Jenn, thank you for your direction and advice. To my co-advisor, Professor Robert M. Keolian, thank you for your consideration. I would also like to thank Professor Jeffrey B. Knorr for his suggestions on building the array antenna. To Bob Vitale, from the Microwave Laboratory, thank you for your help and patience in performing some of the experiments on the "anechoic chamber." To Ross Seely and Paul Buczynski, from the Radar Laboratory, thank you for your help in building the array antenna. A special mention goes to the Portuguese Navy for giving me the opportunity to be intellectually challenged at the Naval Postgraduate School. Finally, but most of all, I would like to thank my friend and partner in life, my wife Susana, for her unselfish devotion, patience and love.

This research was supported by the Space and Naval Warfare Systems Command PMW-178.

I. INTRODUCTION

A. OVERVIEW OF DIRECTION FINDING (DF) SYSTEMS

Direction Finding (DF) systems provide an emitter's bearing, or angle of arrival that can be used as an invariant sorting parameter in the deinterleaving of agile pulsed radar signals and in separating closely spaced communications emitters. In addition, the conservation of jamming power in power-managed Electronic Attack (EA) systems depends on the ability of the associated Electronic Warfare Support (ES) system to measure the direction to the victim emitter. Direction-of-arrival measurement systems fall into three main categories: scanning beam, simultaneous-multiple-beam, and interferometer techniques. The mechanically scanning beam requires only a single antenna. However, this technique has the disadvantage of a low probability of intercept. The simultaneous-multiple-beam system uses an antenna or several antennas, forming a number of simultaneous beams, thereby retaining the high sensitivity of the scanning beam approach while providing fast response. However, it requires many parallel receiving channels, each with full frequency coverage. Interferometer systems, based on phase-comparison techniques, have the advantage of a fast response but generally use wide coverage antennas which result in low sensitivity. In addition, they require relatively complex microwave circuitry that must maintain a precise phase match over a wide frequency band under extreme environmental conditions. When high accuracy is required (on the order of 0.1 to 1 degree), wide baseline interferometers are used with ambiguity resolving circuitry. [Ref. 1]

The two primary interferometer techniques used for DF are the amplitude-comparison method and the phase-comparison method. Generally the phase-comparison method has the advantage of greater accuracy, but the amplitude-comparison method is widely used due to its lower complexity and cost. The basic interferometer geometry is

illustrated in Figure1.1 whereby a plane wave arriving at an angle θ is received by one antenna element earlier than the other due to the difference in path length. The time difference can be expressed as a phase difference

$$\Delta\phi = \frac{2\pi d}{\lambda}\sin\theta \qquad (1\text{-}1)$$

where d is the spacing between antennas, and λ is the wavelength. For a two-element interferometer, the spacing *d* must be λ/2 or less to provide unambiguous, or single lobe ±90° coverage.

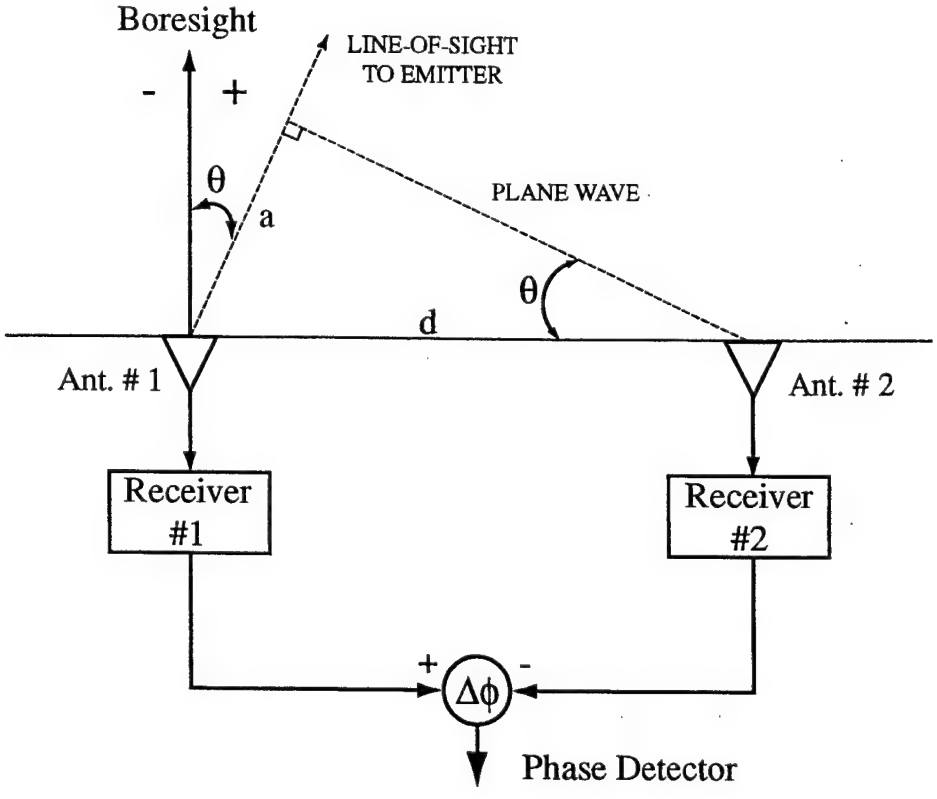

Figure 1.1: Phase Interferometer Principle.

The spacing between antennas must be established for the highest frequency to be received. Interferometers employing multiple antenna elements are called multiple baseline interferometers. Usually the receiver consists of a reference antenna and a series of companion antennas. The spacing between the reference element and the first companion antenna is $\lambda/2$; other secondary elements are placed to form pairs separated by 1, 2, 4, and 8 wavelengths. This multiple baseline interferometer provides a binary angle-of-arrival measurement where each bit of the measurement supplies a more accurate estimate of the emitter's angle of arrival. [Ref. 1]

Another kind of multiple baseline interferometer is the nonharmonic. In nonharmonic interferometers, no pair of elements provides completely unambiguous angle-of-arrival information over the complete field of view. For example, the initial spacing in the nonharmonic interferometer might be λ, while the next companion element spacing is 3 $\lambda/2$. Ambiguities are resolved by truth tables, and hence the accuracy is set by the spacing of the widest baseline antenna pair. Nonharmonic interferometers have been implemented over nine-to-one bandwidths (2 to 18 GHz) with rms accuracy from 0.1 to 1 degree and without ambiguities over $\pm 90°$. The principal advantage of the nonharmonic interferometer over the harmonic interferometer is the increased bandwidth for unambiguous coverage [Ref. 2].

B. PRINCIPAL CONTRIBUTIONS

This thesis investigates the performance of two new interferometer antenna architectures for high-resolution wideband direction finding. The first configuration incorporates a symmetrical number system (SNS) encoding of the interferometer amplitude response (symmetrical folding waveform). The SNS can serve as a source for resolution enhancement in an interferometer by decomposing the analog spatial filtering operation into

a number of parallel sub-operations (moduli) that are of smaller computational complexity. Each sub-operation symmetrically folds the antenna's amplitude response with folding period *equal to twice the modulus*. Thus, each sub-operation only requires a precision in accordance with that modulus. A much higher resolution is achieved after the N different SNS moduli are used and the results of these low precision sub-operations are recombined. Simulation results are used to numerically evaluate the performance of a 4-element (3 channel) array using moduli m_1=3, m_2=4 and m_3=5. The antenna was constructed in a ground plane using rectangular waveguide elements with a center frequency of 8.5 GHz. Experimental (anechoic chamber) results were obtained and compared with the simulation results to demonstrate the feasibility of the approach. The second antenna configuration incorporates a residue number system (RNS) encoding of the interferometer phase response (sawtooth folding waveform). The phase response folds with folding period *equal to the modulus*. Simulation results indicate that the RNS architecture antenna provides a more robust solution to high-resolution DF. The frequency response of the RNS array is investigated numerically. Quantization errors in the resolved direction of arrival when the intercepted frequency is other than the center frequency are demonstrated. A fast correction algorithm that uses the known intercepted frequency (e.g., from an intercept receiver) is derived. The performance of the algorithm is quantified and shown to have excellent results over a large bandwidth.

C. THESIS OUTLINE

Chapter II details the mathematical development of the linear antenna array. A two element interferometer is shown as a special case. The array factor associated with the linear array is derived. Chapter III, is devoted to the encoding of amplitude response with the SNS. First the SNS encoding procedure is briefly introduced. The SNS antenna

architecture is then derived with simulation results shown to demonstrate the array performance. Construction of the antenna hardware is described and experimental results are shown. Chapter IV examines encoding the phase response with the RNS. The RNS encoding procedure is briefly described and simulation results are shown. In Chapter V the antenna frequency response, antenna size and respective accuracy are investigated for the RNS antenna design. The correction algorithm is derived using the intercepted frequency. Chapter VI presents a summary, some concluding remarks and recommendations. The Appendix provides the Matlab™ code that simulates the output of both the SNS and RNS antenna for direction finding, as well as the calculations of the quantization errors.

II. LINEAR ARRAY ANTENNA THEORY

A. OVERVIEW

Several radiation elements can be arranged in space and interconnected to produce a directional radiation pattern. Such a configuration of multiple radiating elements is referred to as an array antenna, or simply an array. In an array of identical elements, the radiation pattern is determined by the type of individual elements used, their orientations, their positions in space, and the amplitude and phase of the current feeding them. To provide specialized radiation patterns, it is necessary that the fields from the elements of the array interfere constructively (add) in the desired signal directions and interfere destructively (cancel each other) in the remaining space. Ideally this can be accomplished, but practically it is only approached. Arrays can be found in many geometrical configurations. The most elementary is that of a *linear array* in which the array element centers lie along a straight line. The elements may be equally or unequally spaced. When the array element centers are located in a plane, it is said to be a *planar array*. Examples of planar arrays are circular and rectangular arrays in which the element centers are disposed on a circle, or are contained within a rectangular area, respectively. Another class of arrays is that of *conformal arrays*. In this application the array element locations must conform to some nonplanar surface such as that found on an aircraft or missile.[Ref. 3]

The simplest and one of the most practical arrays is formed by uniformly distributing the elements along a line. This arrangement is the conventional linear array configuration. Considering that all of the array elements are identical, the principle of pattern multiplication applies. This is stated as: "The electrical field pattern of an array consisting of similar elements is given by the product of the pattern of one of the elements (the element factor (EF)) and the pattern of an array of isotropic point sources with the

same locations, relative amplitudes and phases as the original array (the array factor (AF))" [Ref. 4]. That is,

$$E(\theta, \phi) = EF(\theta, \phi) \cdot AF(\theta) \tag{2-1}$$

where $E(\theta, \phi)$ is the total radiated (or received) electric field intensity in the direction (θ, ϕ).

The array factor may be thought of as a sum of isotropic point sources located at the center of each array element. The array factor is that factor of the radiation pattern which is found from the element currents (amplitudes and phases) and their locations. On the other hand, the element pattern is that factor of the radiation pattern determined by the individual properties of an element (its current distribution and orientation in space).

B. LINEAR ARRAY ANTENNA BEAMFORMING

A typical linear array composed of N_e similar element antennas is shown in Figure 2.1. The output of each array element may be controlled in amplitude and phase as indicated by the phase shifters and attenuators. In addition to the amplitude and phase control imposed on each element represented by I_n ($n = 0, 1, 2, \ldots, N_e-1$), there is relative phase shift between the waves arriving at the antenna elements due to their positions in space and the angle of arrival of the wave. Furthermore, the pattern of each element leads to a response that varies with the angle of arrival of the incoming plane wave. If it is the same for each element, the principle of pattern multiplication allows us to consider it as one multiplicative factor in the total pattern. The remaining angular dependence of the pattern is called the array factor, and it is determined only by the element positions and their amplitudes and phases represented by I_n. The array in Figure 2.1 is shown as a receiving

array; however, the receiving pattern is the same as the transmitting pattern by reciprocity [Ref. 4].

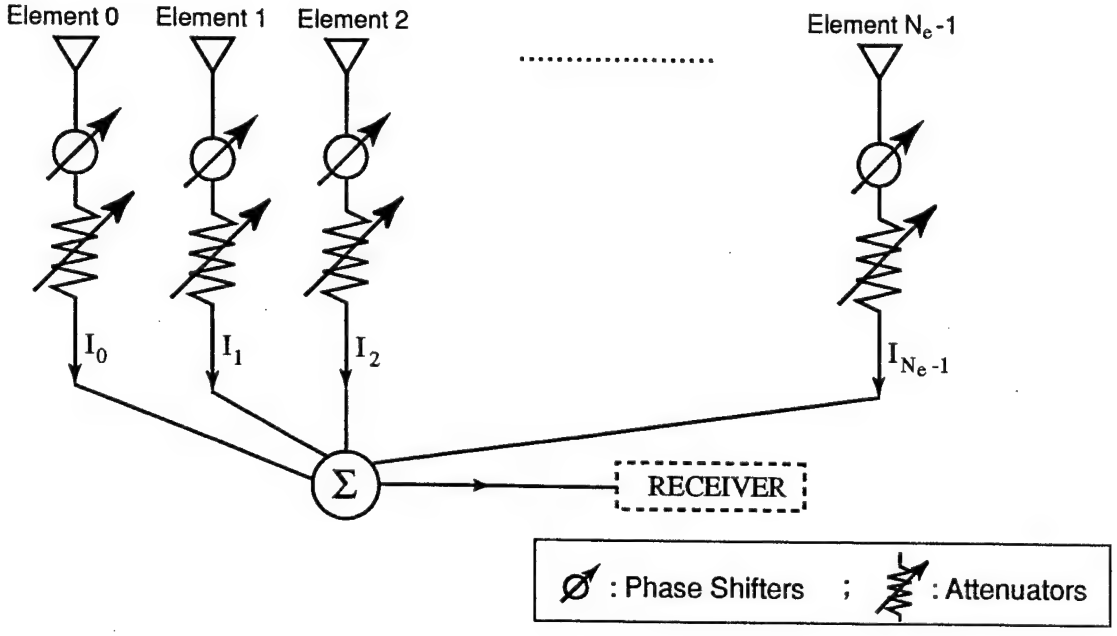

Figure 2.1: A Typical Linear Array. The Output Currents are Summed in a Summing Device Before Entering the Receiver.

Since the pattern of an array obtained by neglecting the patterns of the individual elements of the array is the array factor, then if we replace each element of the array with an isotropic point source, the resulting pattern is the array factor. The isotropic point source is an idealized antenna occupying a point in space and radiating uniformly in all directions. The radiation fields of a point source at the origin of a spherical coordinate system are proportional to $I_0e^{-jkr}/4\pi r$ where I_0 is the current of the point source, k is the wave-number equal to $2\pi/\lambda$, and r the radius of the sphere [Ref. 4]. The far-field pattern is obtained from

the angular dependence of the radiation fields. Thus the pattern of a point source is constant and given by

$$AF = I_0. \tag{2-2}$$

As elements are added to the array, each one with a different current, it is necessary to account for their relative field strengths as determined by their element currents.

The array factor for the array in Figure 2.1 is derived using the array in Figure 2.2 which has point sources for the array elements in place of the actual elements.

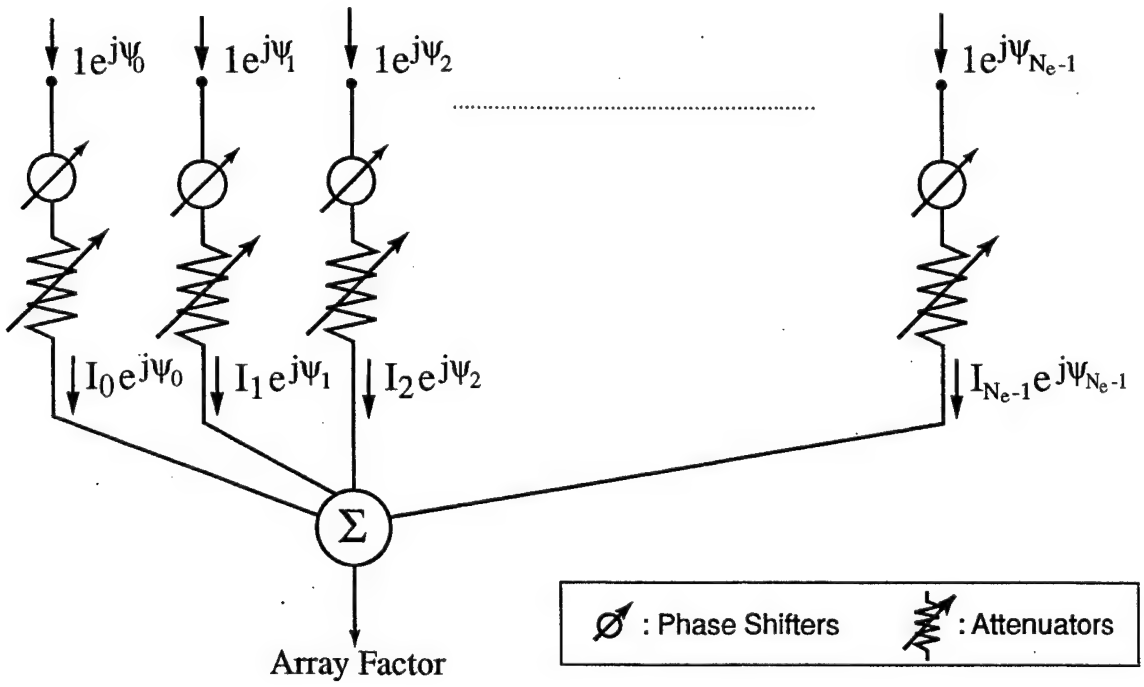

Figure 2.2: Equivalent Configuration of the Array in Figure 2.1 for Determining the Array Factor. The Elements of the Array are Replaced by Isotropic Point Sources.

The array factor for this receiving array is then the sum of the point source responses $\{e^{j\psi_0}, e^{j\psi_1}, \ldots, e^{j\psi_{N_e-1}}\}$ each weighted by the amplitude and phase shift $\{I_0, I_1, \ldots, I_{N_e-1}\}$ introduced in the transmission line connected to each element. Here $\psi_0, \psi_1, \ldots, \psi_{N_e-1}$ are the phases of an incoming plane wave at the elements locations designated $0, 1, \ldots, N_e - 1$. Usually these phases are relative to the coordinate origin; that is, the phase of the wave arriving at *n*th element leads the phase of the wave arriving at the origin by ψ_{N_e-1}. [Ref. 4]. Thus, the array factor of the array shown in Figure 2.2 is given by

$$AF = I_0 e^{j\psi_0} + I_1 e^{j\psi_1} + \cdots + I_{N_e-1} e^{j\psi_{N_e-1}}. \tag{2-3}$$

Now, consider a linear array of N_e elements as shown in Figure 2.3.

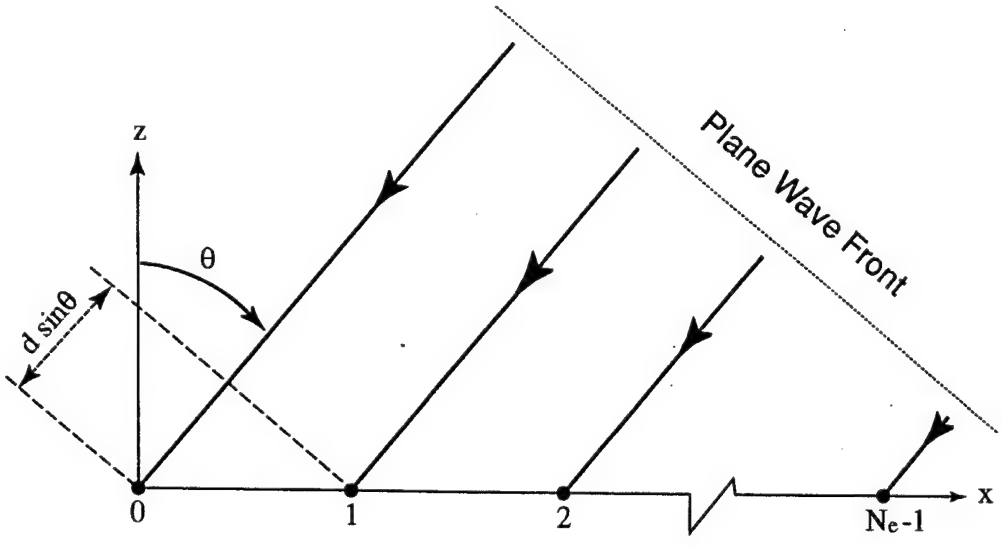

Figure 2.3: Equally Spaced Linear Array of Isotropic Point Sources.

The elements are equally spaced with a distance between elements equal to d. The angle θ is that of an incoming plane wave relative to the axis of the array. The isotropic sources

respond equally in all directions, but when their outputs are added together (each weighted according to I_n) a directional response is obtained. The phase of the wave arriving at the origin (n=0) is arbitrarily set to zero, $\psi_0=0$. The incoming wave at element 1 arrives before those at the origin since the distance is shorter by an amount $d\sin\theta$. The corresponding phase leads at element 1 relative to those at element 0 is $kd\sin\theta$. This process continues and Equation (2-3) becomes

$$AF = I_0 + I_1 e^{jkd\sin\theta} + I_2 e^{jk2d\sin\theta} + \cdots = \sum_{n=0}^{N_e-1} I_n e^{jkn d\sin\theta}. \tag{2-4}$$

Now consider the array to be transmitting. If the current has a linear phase progression (i.e., the relative phase between adjacent elements is the same), we separate out this phase explicitly as

$$I_n = A_n e^{jn\alpha} \tag{2-5}$$

where the *n+1* element leads the *n*th element in phase by α. Then Equation (2-4) becomes

$$AF = \sum_{n=0}^{N_e-1} A_n e^{jn(kd\sin\theta+\alpha)}. \tag{2-6}$$

Define ψ as

$$\psi = kd\sin\theta + \alpha \tag{2-7}$$

then

$$AF = \sum_{n=0}^{N_e-1} A_n e^{jn\psi}. \tag{2-8}$$

A very important special case of equally spaced linear arrays is that of the uniformly excited array. This is an array whose element current amplitudes are identical, so that

$$A_0 = A_1 = A_2 = \cdots = A_{N_e-1}. \tag{2-9}$$

The array factor from Equation (2-8) is then

$$AF = A_0 \sum_{n=0}^{N_e-1} e^{jn\psi} = A_0\left[1 + e^{j\psi} + e^{j2\psi} + \cdots + e^{j(N_e-1)\psi}\right]. \tag{2-10}$$

A few short steps are required to sum this geometric series. First multiply the last equation by $e^{j\psi}$ to obtain

$$AF\, e^{j\psi} = A_0\left[e^{j\psi} + e^{j2\psi} + \cdots + e^{jN_e\psi}\right]. \tag{2-11}$$

Subtracting Equation (2-11) from Equation (2-10) gives

$$AF(1 - e^{j\psi}) = A_0(1 - e^{jN_e\psi}) \tag{2-12}$$

or

$$AF = A_0 \frac{1 - e^{jN_e\psi}}{1 - e^{j\psi}}. \tag{2-13}$$

This may be rewritten in a more convenient form as follows

$$AF = A_0 \frac{e^{jN_e\psi} - 1}{e^{j\psi} - 1} = A_0 \frac{e^{jN_e\psi/2}}{e^{j\psi/2}}\left[\frac{e^{jN_e\psi/2} - e^{-jN_e\psi/2}}{e^{j\psi/2} - e^{-j\psi/2}}\right],$$

so that

$$AF = A_0 e^{j(N_e-1)\psi/2} \quad \frac{\sin(N_e\psi/2)}{\sin(\psi/2)}. \tag{2-14}$$

The phase factor of the array is given by $e^{j(N_e-1)\psi/2}$. If the array was centered about the origin, this phase factor would not be present since it represents the phase shift of the array phase center relative to the origin. Neglecting the phase factor, Equation (2-14) becomes

$$AF = A_0 \frac{\sin(N_e\psi/2)}{\sin(\psi/2)}. \tag{2-15}$$

The maximum value of the array factor is equal to A_0N_e and occurs when ψ=0. To normalize it so that the maximum value is equal to unity (if A_0=1) and is independent of the number of elements, Equation (2-15) is divided by N_e

$$AF_{norm} = \frac{1}{N_e} \frac{\sin(N_e\psi/2)}{\sin(\psi/2)}. \tag{2-16}$$

Now let θ_0 be the corresponding value of θ for which the array factor is maximum. Then from Equation (2-7) we have $\psi = kd\sin\theta_0 + \alpha = 0$, or

$$\alpha = -kd\sin\theta_0 = -\frac{2\pi d}{\lambda}\sin\theta_0. \tag{2-17}$$

Equation (2-17) represents the element-to-element phase shift in the excitation currents necessary to produce an array factor main beam maximum in a direction θ_0 relative to the line along which the array elements are aligned. This main beam scanning by phase control mode can be implemented by substituting Equation (2-17) into Equation (2-7) obtaining

$$\psi = kd(\sin\theta - \sin\theta_0) = \frac{2\pi d}{\lambda}(\sin\theta - \sin\theta_0). \quad (2\text{-}18)$$

Setting the phases of the array in this way is called "steering the beam" [Ref. 3].

C. TWO-ELEMENT INTERFEROMETER ANTENNA

For a two-element interferometer antenna (N_e=2), Equation (2-16) becomes

$$AF_{norm} = \frac{1}{2}\frac{\sin(\psi)}{\sin(\psi/2)}. \quad (2\text{-}19)$$

Assuming the two-element configuration is centered about the origin of the reference system, and using the trigonometric identity

$$\sin(2\psi) = 2\sin(\psi)\cos(\psi), \quad (2\text{-}20)$$

Equation (2-19) can be simplified further becoming

$$AF_{norm} = \frac{\sin(\psi/2)\cos(\psi/2)}{\sin(\psi/2)}$$

or

$$AF_{norm} = \cos(\psi/2). \quad (2\text{-}21)$$

A plot of the array factor using Equation (2-21) is shown in Figure 2.4 for d=6λ.

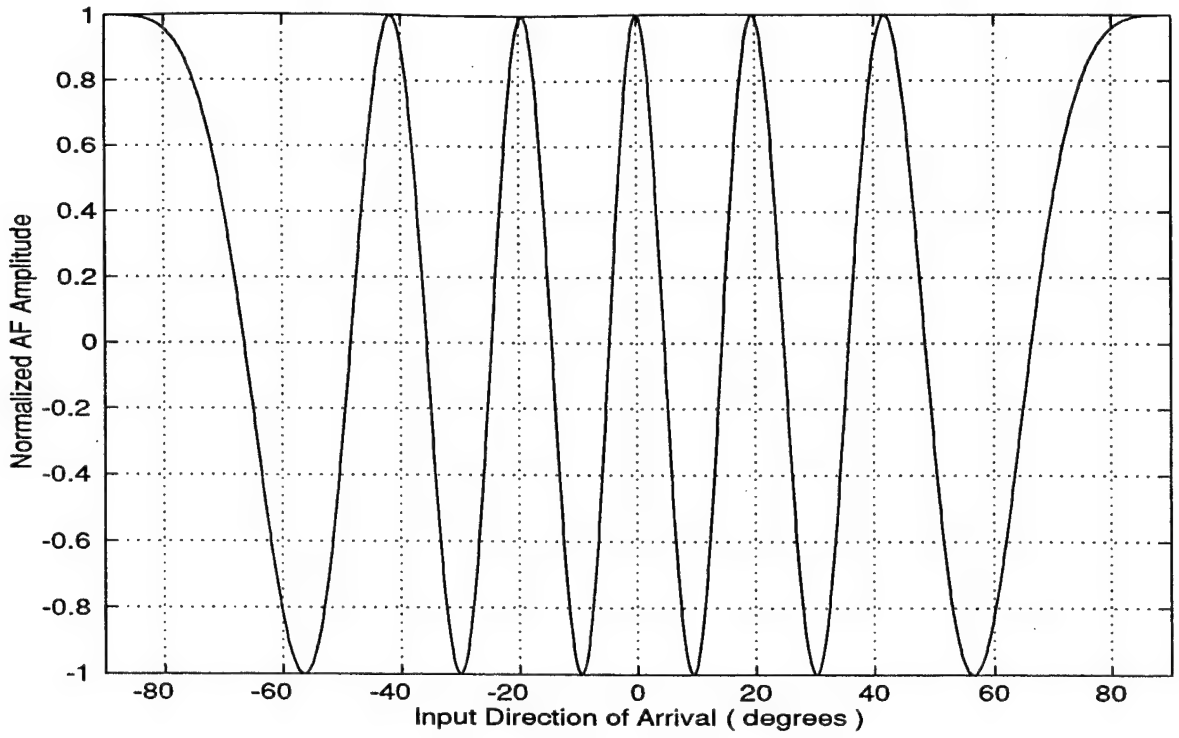

Figure 2.4: Array Factor Amplitude for a Two-Element Linear Array Separated by a Distance d=6λ.

The phase response of the two-element interferometer antenna with d=6λ is derived from Equation (2-18) with θ_0=0 and $-90° \leq \theta \leq 90°$ as illustrated in Figure 2.5a. The sawtooth waveform results by constraining ψ between -π and π.

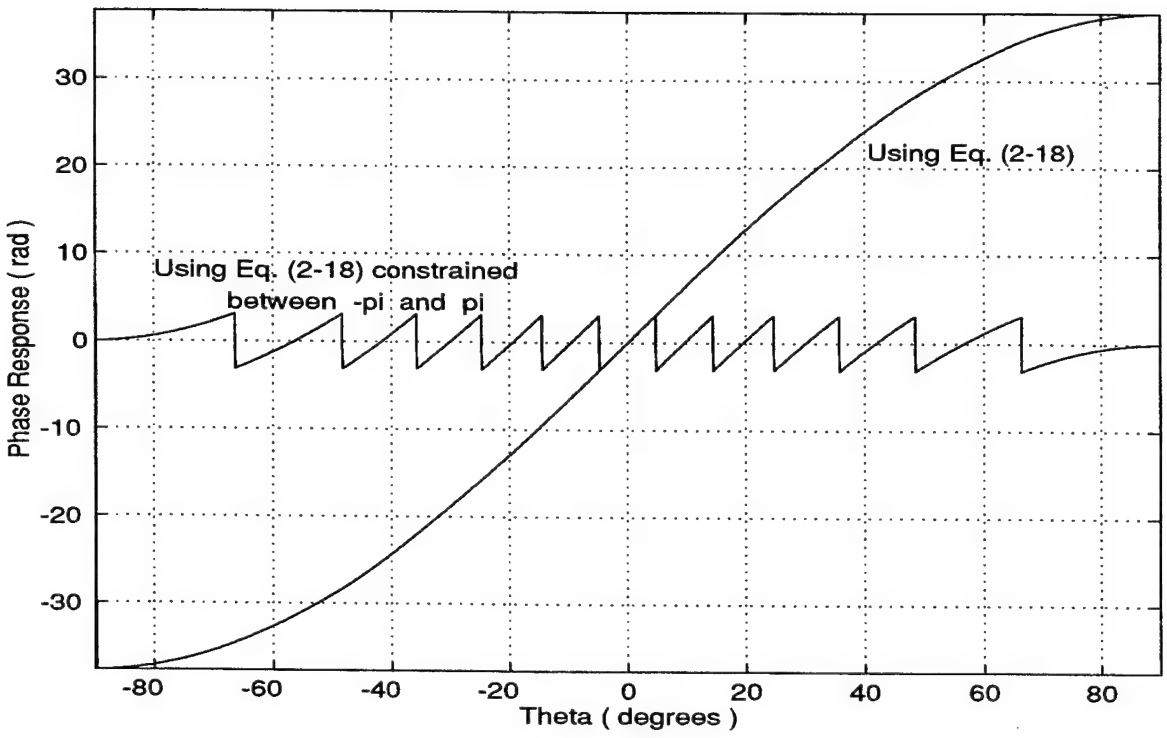

Figure 2.5a: Phase Response of a Two-Element Linear Array Separated by a Distance d=6 λ.

Figure 2.5b shows the resultant phase response folding waveform that will be encoded using the RNS.

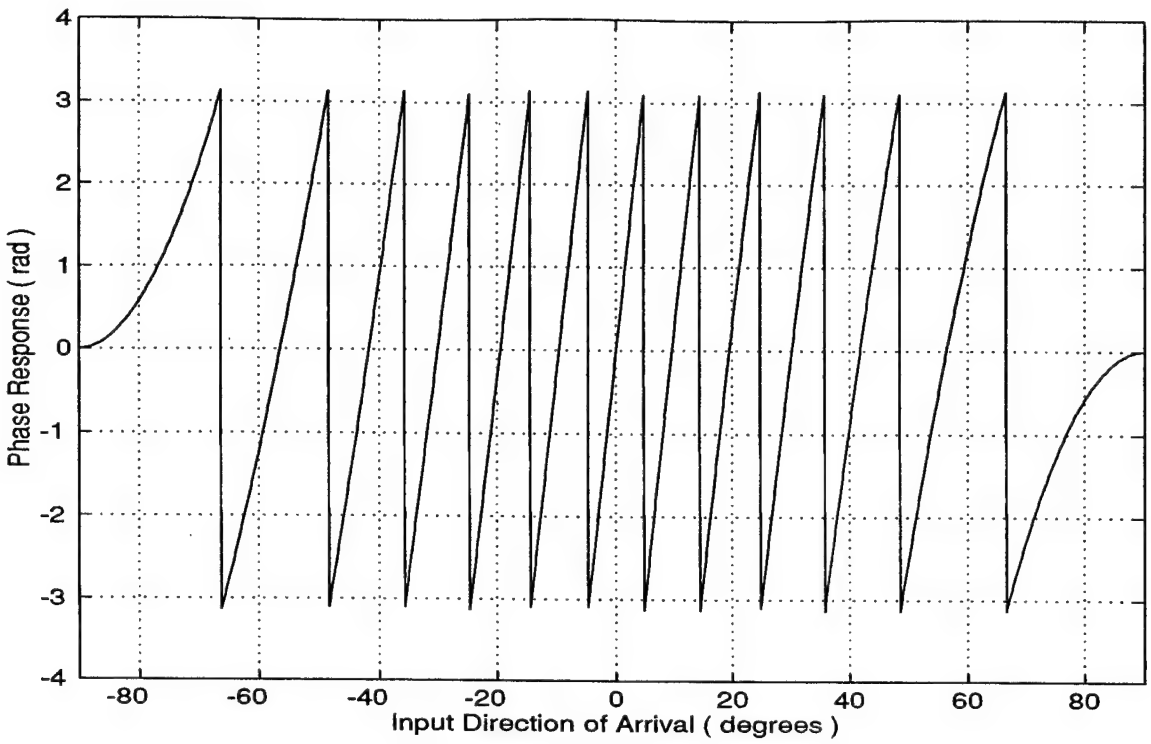

Figure 2.5b: Phase Response of a Two-Element Linear Array Separated by a Distance $d=6\lambda$ (ψ constrained to vary between $-\pi$ and π).

Note the sawtooth nature of this folding waveform. Also note the change in folding period as the input direction of arrival approaches $\pm 90°$.

III. SYMMETRICAL NUMBER SYSTEM ENCODING OF THE AMPLITUDE RESPONSE

A. THE SYMMETRICAL NUMBER SYSTEM (SNS)

The optimum SNS is composed of a number of Pairwise Relatively Prime (PRP) moduli m_i. The integers within each SNS modulus are derived by amplitude analyzing a symmetrically folded waveform with the period of the waveform equal to twice the PRP modulus, i.e., $2m_i$ [Ref. 5]. Given m, the integer values within twice the individual modulus are given by the row vector

$$\bar{x} = [0,1,\cdots,m-1,m-1,\cdots,1,0]. \tag{3-1}$$

From (3-1) the required number of threshold levels is m_i-1. By analyzing Equation (3-1) it is clear that the integers within each modulus do not form a complete system of length $2m_i$ by themselves due to the presence of ambiguities. However, the ambiguities that arise within the modulus can be resolved by using an N moduli set (m_1, m_2,...,m_N) and combining the values from all the channels together. By doing this, the SNS becomes a complete system having a one-to-one correspondence with the residue number system. For N equal to the number of PRP moduli, the dynamic range of this scheme is [Ref. 5, 6]

$$M = \prod_{i=1}^{N} m_i. \tag{3-2}$$

This dynamic range is also the position of the first repetitive moduli vector and the total number of quantization levels without ambiguities. As an example consider the moduli set m_1=3, m_2=4, and m_3=5. The first repetitive moduli vector occurs at an input *equal to 60*,

and the number of quantization levels without ambiguities is also 60 (0 to 59). Table 3.1 illustrates the SNS for the moduli set (3, 4, 5). Figure 3.1 shows the symmetrical folding waveforms and SNS states for m_1=3, m_2=4, and m_3=5. The individual states within the SNS represent the number of threshold levels crossed by the folding waveform. A total of m_i-1 threshold levels are required for each folding waveform.

Normalized	**Moduli**		
Input	m_1=3,	m_2=4,	m_3=5
0	0	0	0
1	1	1	1
2	2	2	2
3	2	3	3
4	1	3	4
5	0	2	4
6	0	1	3
7	1	0	2
8	2	0	1
9	2	1	0
10	1	2	0
11	0	3	1
12	0	3	2
.	.	.	.
.	.	.	.
.	.	.	.
52	1	3	2
53	0	2	3
54	0	1	4
55	1	0	4
56	2	0	3
57	2	1	2
58	1	2	1
59	0	3	0
60	0	3	0

Table 3.1: An Example to Illustrate the Optimum SNS Using Moduli Set m_1=3, m_2=4, m_3=5.

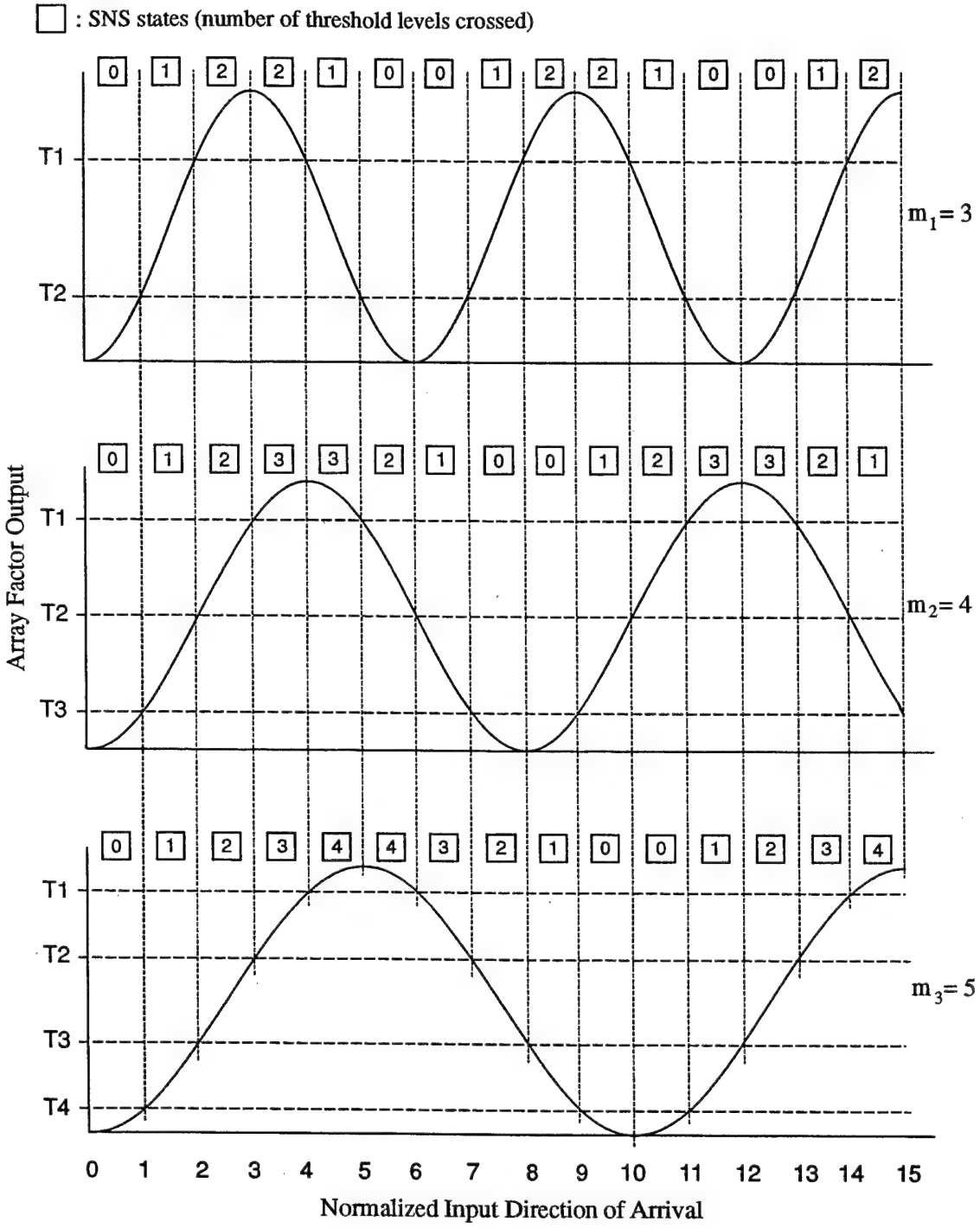

Figure 3.1: Optimum SNS Waveforms and Output Codes for m_1=3, m_2=4, and m_3=5.

B. SNS ANTENNA ARCHITECTURE

Figure 3.2 shows a schematic representation of the SNS antenna architecture for instantaneous direction finding. The array consists of four elements. Element 1 is combined with elements 2, 3, and 4. The three pairs of elements (1, 4), (1, 3), and (1, 2) form a three-baseline modular interferometer with m_1=3, m_2=4 and m_3=5 respectively.

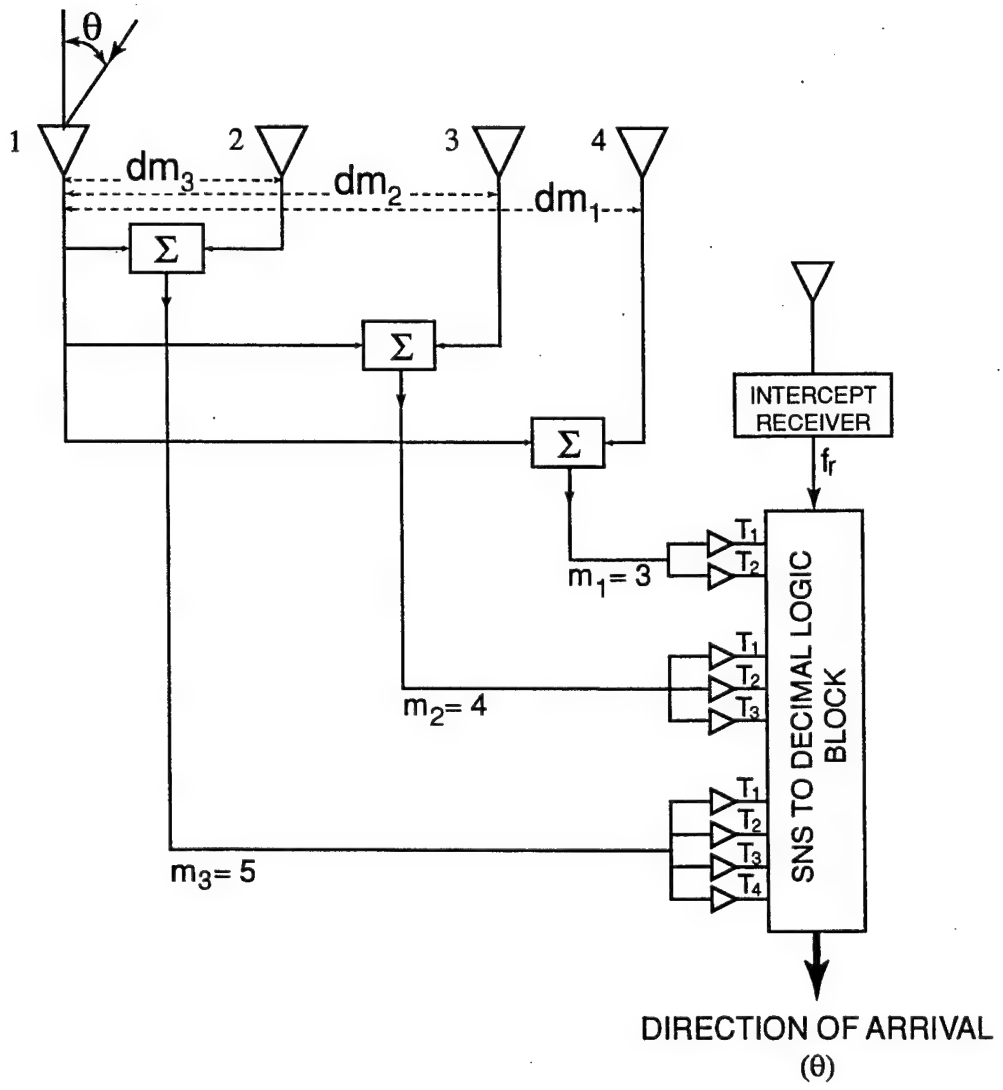

Figure 3.2: Schematic Representation of the Proposed SNS Antenna Architecture for Combat Direction Finding.

The array factor amplitude response from each pair of elements (corresponding to modulus m_i) is quantized using m_i-1 comparators. The comparator threshold levels are adjusted to midlevel quantize the folded amplitude response into the SNS format. The SNS-to-decimal logic block then recombines each channel and converts the SNS representation to a more familiar digital output.

The distance between each pair of elements must be determined in order to obtain the correct number of folds needed to cover the entire field of view (from 0 to ±90°) for the chosen moduli set. That is, the distance between each pair of elements must be derived as a function of the PRP modulus, m_i, so that the corresponding amplitude response has the correct number of folds. For a given modulus m_i, the number of folds needed to cover the dynamic range is given by

$$n_{i,SNS} = \frac{\text{dynamic range}}{2\,m_i} = \frac{M}{2m_i}, \tag{3-3}$$

where M is given by Equation (3-2). Next consider the array factor given by Equation (2-21). Define $\xi=\psi/2$ given by

$$\xi = \frac{\pi d}{\lambda}\sin\theta. \tag{3-4}$$

From Equation (3-4) we have that:

$$\begin{aligned} \theta = 0^\circ &\Rightarrow \xi = 0 \\ \theta = 90^\circ &\Rightarrow \xi = \frac{\pi d}{\lambda} \\ \theta = -90^\circ &\Rightarrow \xi = -\frac{\pi d}{\lambda}. \end{aligned} \tag{3-5}$$

Each fold of the array factor corresponds to a change in phase of 2π which implies

$$\xi(90^\circ) - \xi(-90^\circ) = 2\pi. \tag{3-6}$$

Substituting in Equation (3-6) the values of $\xi(\pm 90^\circ)$ found in Equation (3-5) we obtain

$$\frac{2\pi d}{\lambda} = 2\pi, \quad \therefore \quad d = \lambda. \tag{3-7}$$

Therefore, the distance between elements is given by

$$d_{i,SNS} = n_{i,SNS}\,\lambda = \left(\frac{M}{2m_i}\right)\lambda \tag{3-8}$$

where λ is the wavelength corresponding to the center frequency used to construct the antenna. For example, if an antenna is to be designed assuming a center frequency f_0=8.5 GHz using m_1=3, m_2=4 and m_3=5, the distance required between each pair of elements is:

$$\begin{aligned} d_1 &= 10\,\lambda \;\; = 35.29\ \text{cm} \quad (m_1 = 3) \\ d_2 &= 7.5\,\lambda = 26.47\ \text{cm} \quad (m_2 = 4) \\ d_3 &= \;6\,\lambda \;\; = 21.18\ \text{cm} \quad (m_3 = 5). \end{aligned}$$

With the correct distances between elements, the amplitude response from each pair of elements will be quantized using m_i-1 comparators. The function of the comparators is to generate the integers within each modulus by quantizing the amplitude response according to the modulus m_i with which it is associated. Finally the recombination of the SNS code from each pair of elements will be the instantaneous direction of arrival.

C. SIMULATION RESULTS

The array factor plot for the m_1=3 array as the input direction of arrival varies from -90° to 90° is shown in Figure 3.3. As shown the folding period changes as the angle θ goes from 0° to ± 90°.

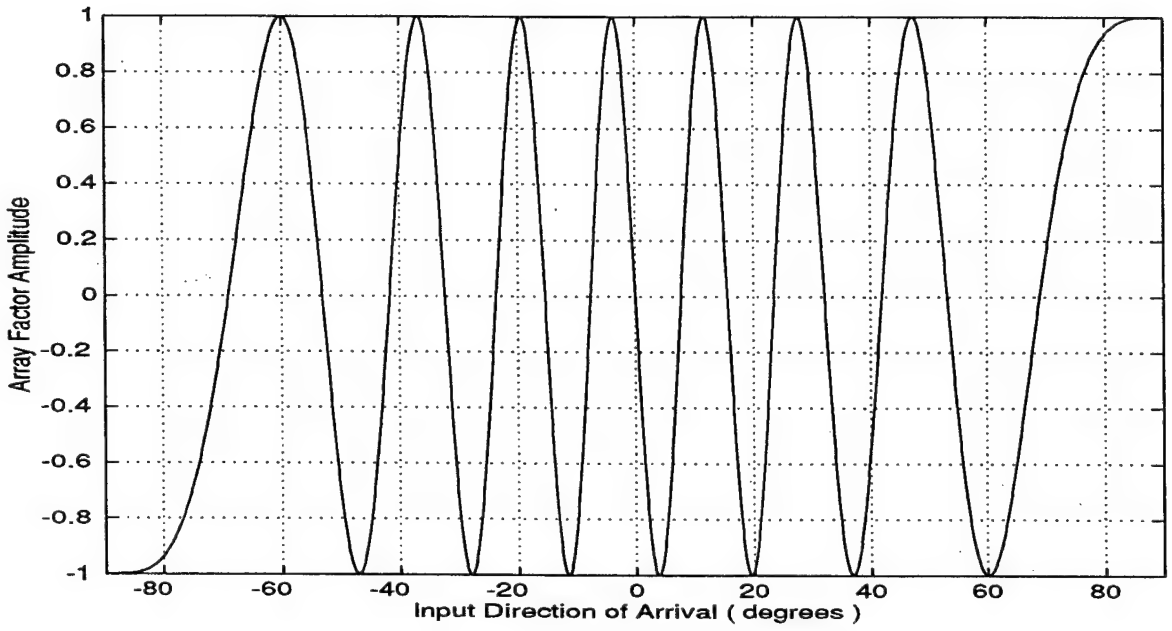

Figure 3.3: Array Factor as a Function of θ for a Two-Element Array Antenna With d=7.5 λ.

The SNS code cannot be applied to this waveform in a straight forward manner. However, if the array factor is examined as a function of sin(θ) as shown in Figure 3.4, the array factor corresponds to a symmetrically folded sinusoidal waveform ($-1 < \sin(\theta) < 1$) with a constant period, thereby satisfying the principal condition for applying the SNS code.

The chosen moduli have a dynamic range M=60, therefore the quantization width, considering the field of view (from 0° to ± 90°) that corresponds to the variation in sinθ

(from 0 to ± 1), will be equal to 2/60≈0.0333. For a true symmetrically folded sinusoidal waveform as a function of θ, with constant period, the quantization width would be constant, independent of the direction of arrival, and equal to 3° (180°/60). This, however, is not the case. Comparing Figures 3.3 and 3.4 it is possible never the less to establish a relationship between the constant quantization width (when the array factor is plotted as a function of sin(θ)) and the corresponding quantization width as a function of θ (when the array factor is plotted as a function of θ).

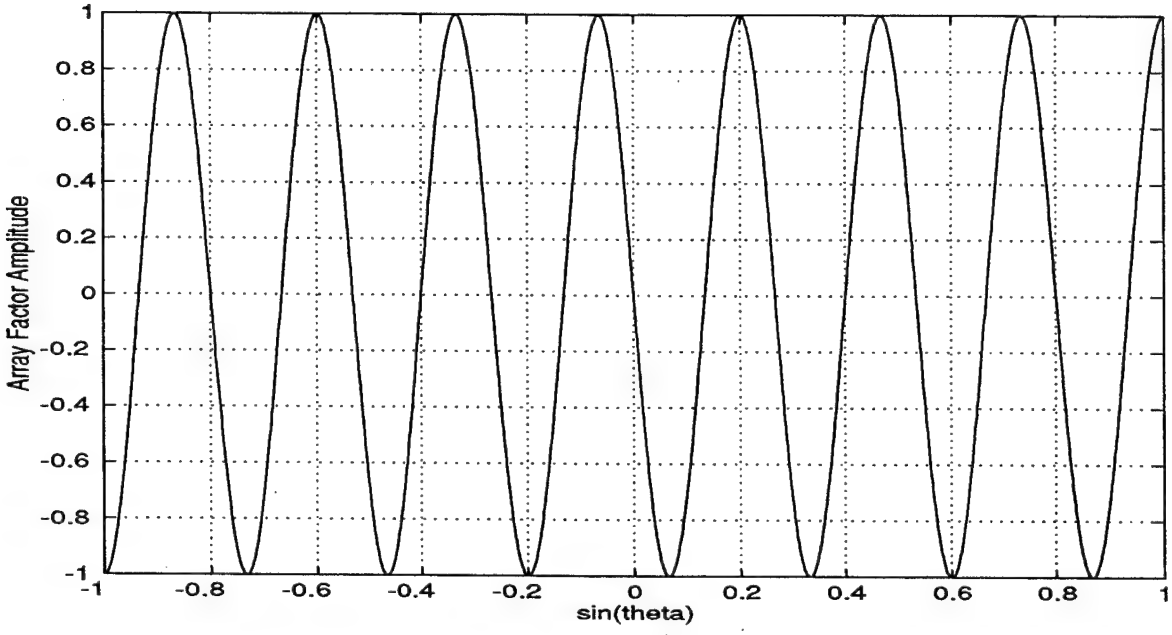

Figure 3.4: Array Factor as a Function of sin(θ) for a Two-Element Array Antenna With d=7.5 λ.

As a function of θ the quantization width depends on the direction of arrival of the incoming signal and is not uniform. The transition points from one quantization level to another quantization level occur at an angle θ_t given by

$$\theta_t = \sin^{-1}(x) \tag{3-9}$$

where x is given by

$$x = -1, -1+\frac{2}{M}, -1+\frac{4}{M}, \ldots, 1. \tag{3-10}$$

Table 3.2 shows the resulting transition points, θ_t, and the respective quantization widths.

The array factor for each pair of elements {(1, 4), (1, 3), and (1, 2)} corresponding to modulus m_1=3, m_2=4, and m_3=5 respectively are shown in Figures 3.5, 3.6, and 3.7. Also shown are the states within each modulus. The array factor is phased at -90° in all cases so that the SNS code '000' will correspond to our first quantization level at -90° (see Table 3.1). To obtain this proper phase relationship between pairs, a phase shift equal to π, $\pi/2$, and π was added to elements (1, 2), (1, 3), and (1, 4) respectively.

The next step is to separately quantize the array factor waveform corresponding to each pair of elements using the SNS encoding procedure explained in Section A of this chapter. The number of threshold levels (or comparators) depends on the modulus m_i that is being considered and is given by m_i-1 as previously noted. The matching threshold values for the comparators are found by simulation. The transition points from one quantization level to another occur at the values of θ_t shown in Table 3.2.

$\sin^{-1} x$	θ_t (degrees)	Quantization Width	$\sin^{-1} x$	θ_t (degrees)	Quantization Width
-1.0000	-90.0000		**0.0000**	0.0000	1.9102
-0.9666	-75.1649	14.8351	**0.0333**	1.9102	1.9123
-0.9333	-68.9605	6.2044	**0.0666**	3.8102	1.9166
-0.9000	-64.1581	4.8025	**0.1000**	5.7392	1.9231
-0.8666	-60.0736	4.0845	**0.1333**	7.6623	1.9318
-0.8333	-56.4427	3.6309	**0.1666**	9.5942	1.9429
-0.8000	-53.1301	3.3126	**0.2000**	11.5370	1.9564
-0.7666	-50.0555	3.0746	**0.2333**	13.4934	1.9726
-0.7333	-47.1666	2.8889	**0.2666**	15.4660	1.9916
-0.7000	-44.4270	2.7396	**0.3000**	17.4576	2.0136
-0.6666	-41.8103	2.6167	**0.3333**	19.4712	2.0390
-0.6333	-39.2965	2.5138	**0.3666**	21.5102	2.0680
-0.6000	-36.8699	2.4266	**0.4000**	23.5782	2.1011
-0.5666	-34.5181	2.3518	**0.4333**	25.6793	2.1389
-0.5333	-32.2310	2.2872	**0.4666**	27.8181	2.1819
-0.5000	-30.0000	2.2310	**0.5000**	30.0000	2.2310
-0.4666	-27.8181	2.1819	**0.5333**	32.2310	2.2872
-0.4333	-25.6793	2.1389	**0.5666**	34.5181	2.3518
-0.4000	-23.5782	2.1011	**0.6000**	36.8699	2,4266
-0.3666	-21.5102	2.0680	**0.6333**	39.2965	2.5138
-0.3333	-19.4712	2.0390	**0.6666**	41.8103	2.6167
-0.3000	-17.4576	2.0136	**0.7000**	44,4270	2.7396
-0.2666	-15.4660	1.9916	**0.7333**	47.1666	2.8889
-0.2333	-13.4934	1.9726	**0.7666**	50.0555	3.0746
-0.2000	-11.5370	1.9564	**0.8000**	53.1301	3.3126
-0.1666	-9.5942	1.9429	**0.8333**	56.4427	3.6309
-0.1333	-7.6623	1.9318	**0.8666**	60.0736	4.0845
-0.1000	-5.7392	1.9231	**0.9000**	64.1581	4.8025
-0.0666	-3.8102	1.9166	**0.9333**	68.9605	6.2044
-0.0333	-1.9102	1.9123	**0.9666**	75.1640	14.8351
0.0000	0.0000	1.9102	**1.0000**	90.0000	

Table 3.2: Equivalent Quantization Levels Transition Points and Quantization Level Width.

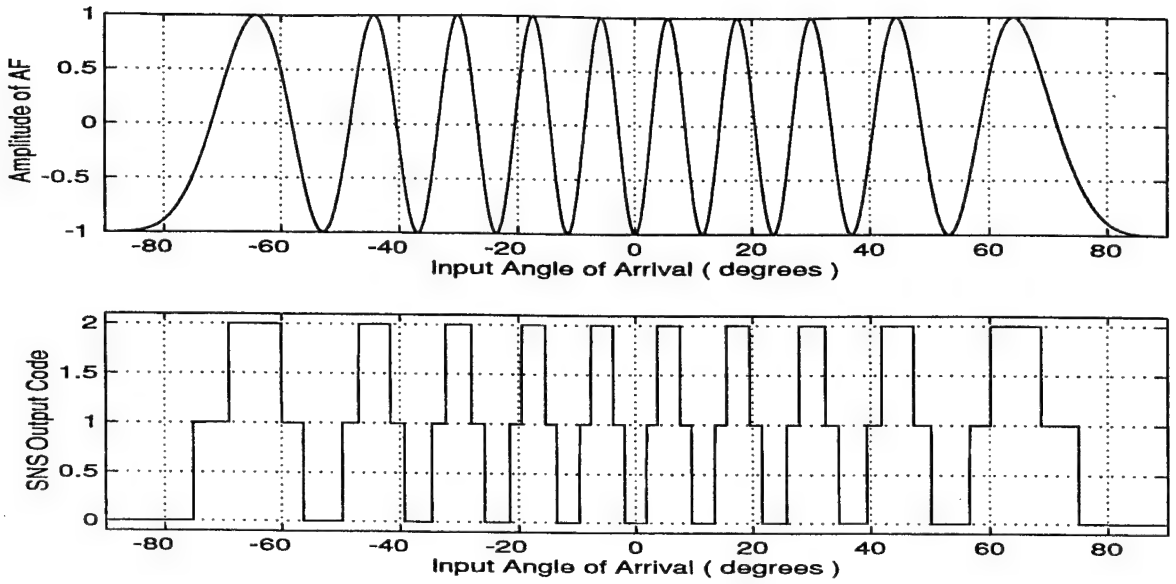

Figure 3.5: Array Factor Waveform and Respective SNS Quantization Code for the Pair of Elements (1, 4) Corresponding to Modulus m_1=3.

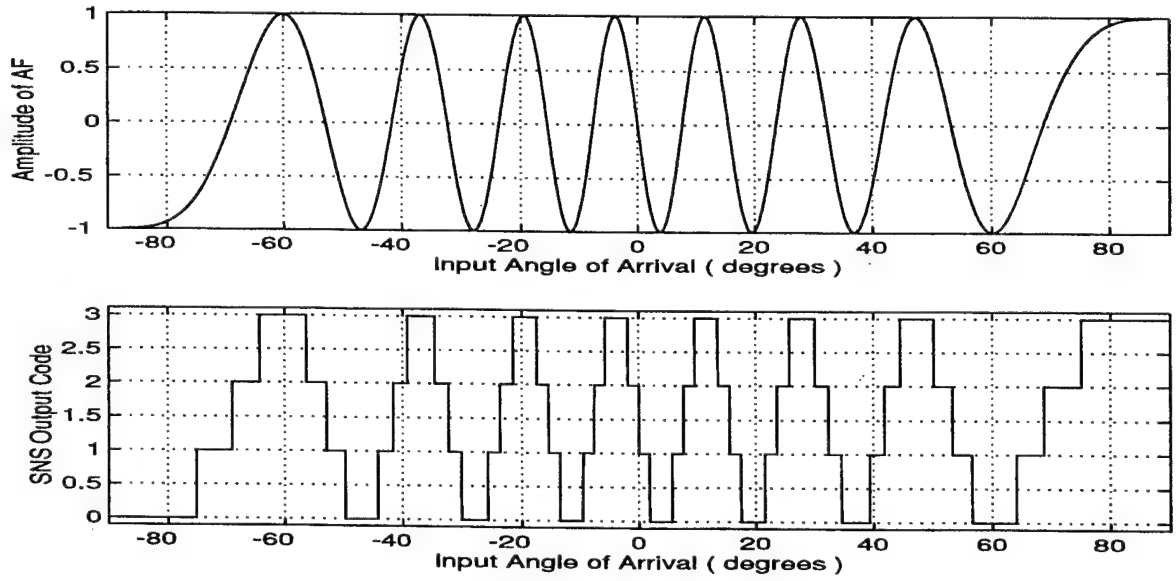

Figure 3.6: Array Factor Waveform and Respective SNS Quantization Code for the Pair of Elements (1, 3) Corresponding to Modulus m_2=4.

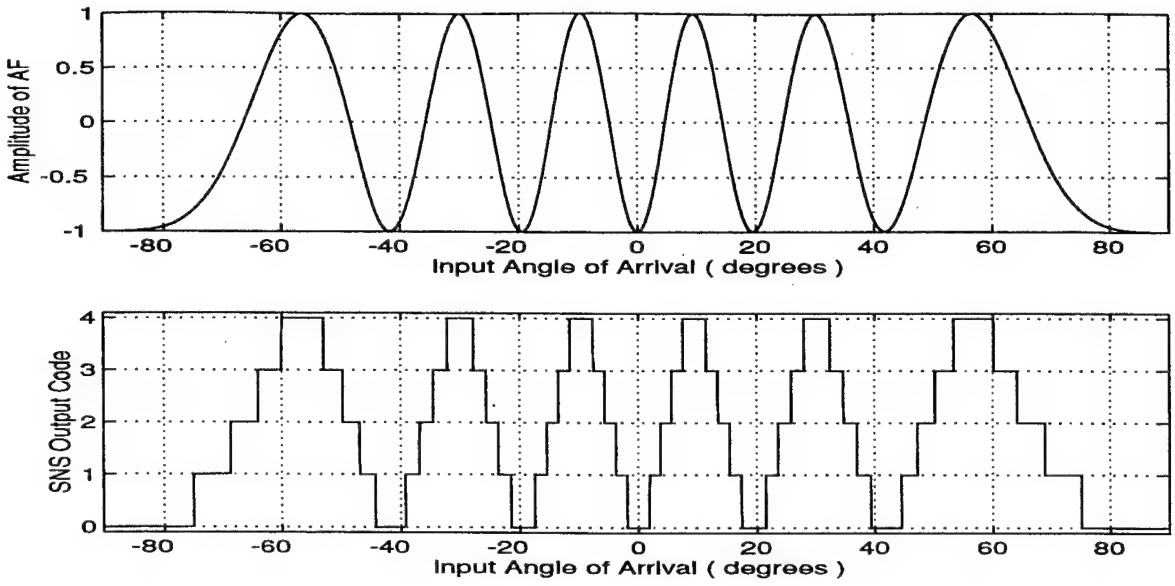

Figure 3.7: Array Factor Waveform and Respective SNS Quantization Code for the Pair of Elements (1, 2) Corresponding to Modulus m_3=5.

The normalized comparator matching threshold values for each pair of elements corresponding to modulus 3, 4, and 5 are shown in Table 3.3.

Elements	Modulus	T1	T2	T3	T4
(1, 2)	5	-0.8090	-0.3090	0.3090	0.8090
(1, 3)	4	-0.7071	0.0000	0.7071	------
(1, 4)	3	-0.5000	0.5000	------	------

Table 3.3: Normalized Comparator Matching Threshold Values for Each Pair of Elements.

The comparator states (or thermometer codes) from each channel are recombined in an SNS logic block to give the instantaneous resolved direction of arrival. Figure 3.8 shows the resolved direction of arrival or antenna transfer function corresponding to the 60 different possible combinations of the SNS for the moduli set (3, 4, 5). Note that the quantization width is not constant.

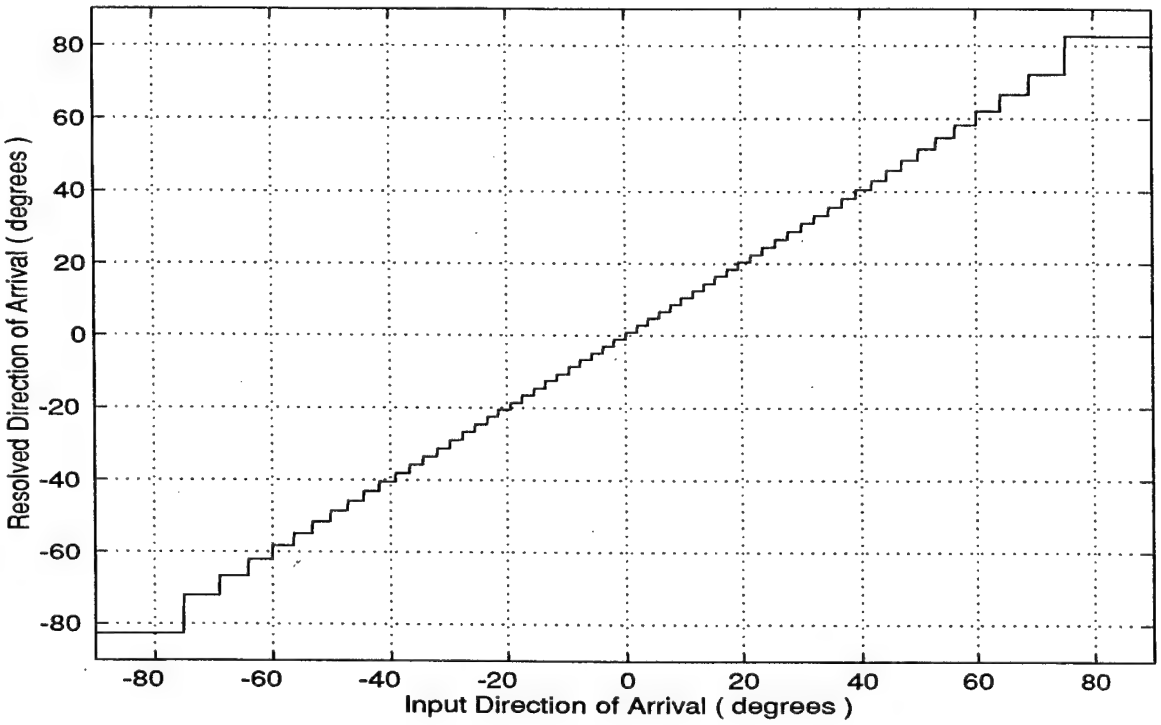

Figure 3.8: SNS Resolved Direction of Arrival for $-90° < \theta < 90°$(no element factor).

The actual amplitude response of a linear array antenna is given by Equation (2-1) which means that a multiplicative factor (the element factor) has to be taken into consideration in addition to the array factor. The effect of the element factor is to introduce

a drop-off in the antenna gain. The element factor will depend on the type of elements that are to be used in the array antenna (waveguides, dipoles, etc.). For example consider that this element factor is characterized by a *cosine* waveform. Taking this characterization into account, Equation (2-1) can be rewritten as follows

$$E(\theta, \phi = 0) = A_0 \cos\left(\frac{\Psi}{2}\right)\cos(\theta). \tag{3-11}$$

Figure 3.9 shows a plot of the electrical field response of the array assuming that the element factor is characterized by $\cos(\theta)$. The element factor modulates the array factor so that the resultant waveform no longer has a constant amplitude.

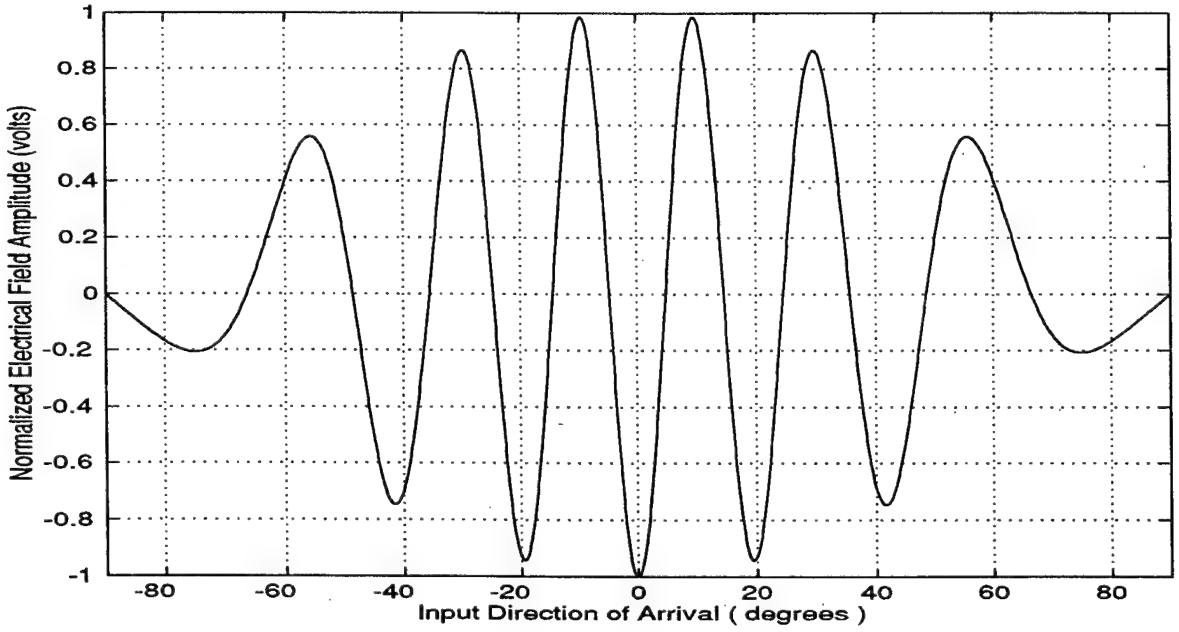

Figure 3.9: Amplitude of the Electrical Field Response of a Two Linear Array: Elements 1 and 2.

When the SNS quantization methodology is applied to the resultant waveform (same threshold levels) a number of errors result as shown in Figure 3.10. However, the results are still acceptable in a smaller interval ($-20° < \theta < 20°$). The antenna transfer function for this narrow region is shown in Figure 3.11. The encoding errors which exist at the code transition points are the result of some of the comparators not switching simultaneously as they should. These errors are easily isolated by using a few additional comparators in the minimum modulus channel [Ref. 5]. Investigation into the error isolation however, is beyond the scope of this thesis and is subject of future research.

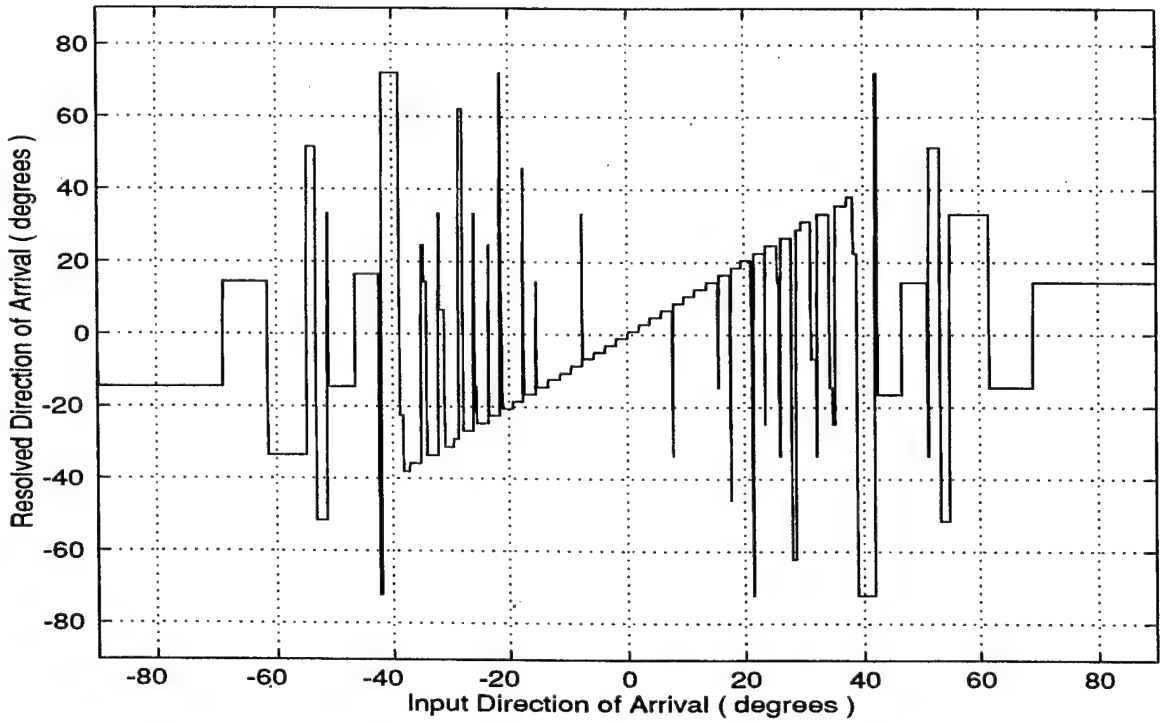

Figure 3.10: SNS Resolved Direction of Arrival for $-90° < \theta < 90°$ (element factor included).

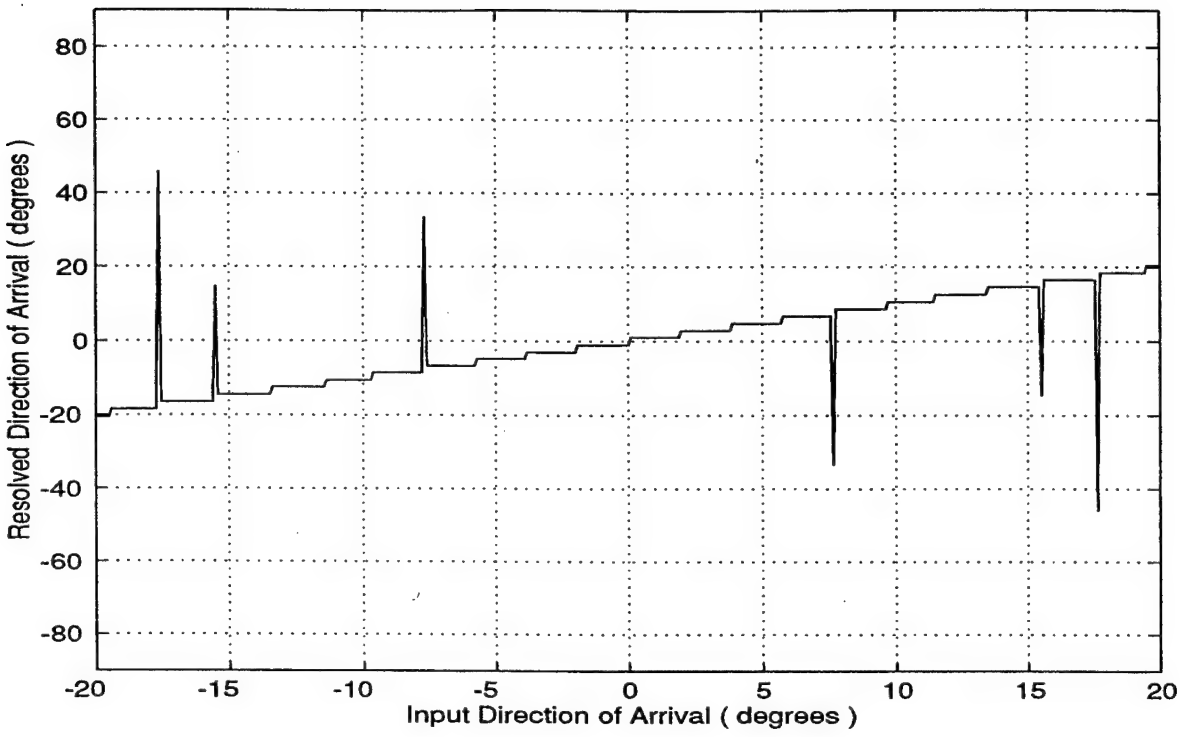

Figure 3.11: SNS Resolved Direction of Arrival for $-20° < \theta < 20°$(element factor included).

D. EXPERIMENTAL RESULTS

A linear antenna was built based on the theory developed previously using four rectangular waveguides mounted in a large ground plane. Figure 3.12 shows the configuration of the antenna (front plane, back plane, and mounted on the pedestal in the anechoic chamber). The connection between elements are as illustrated in Figure 3.2. Using the anechoic chamber facility at the Naval Postgraduate School, antenna pattern measurements (power response) for the H-field were taken for each pair of elements.

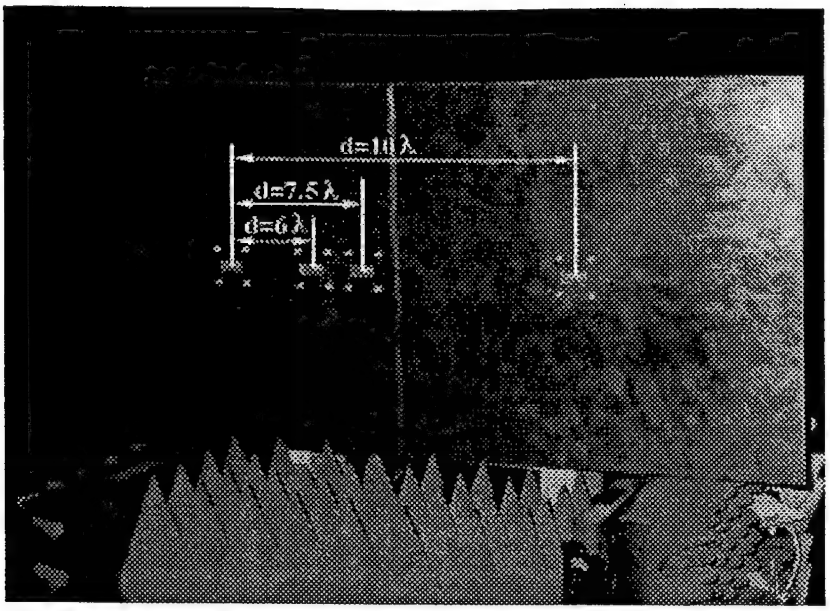

Figure 3.12.a: Photograph of the Built Antenna (Front Plane).

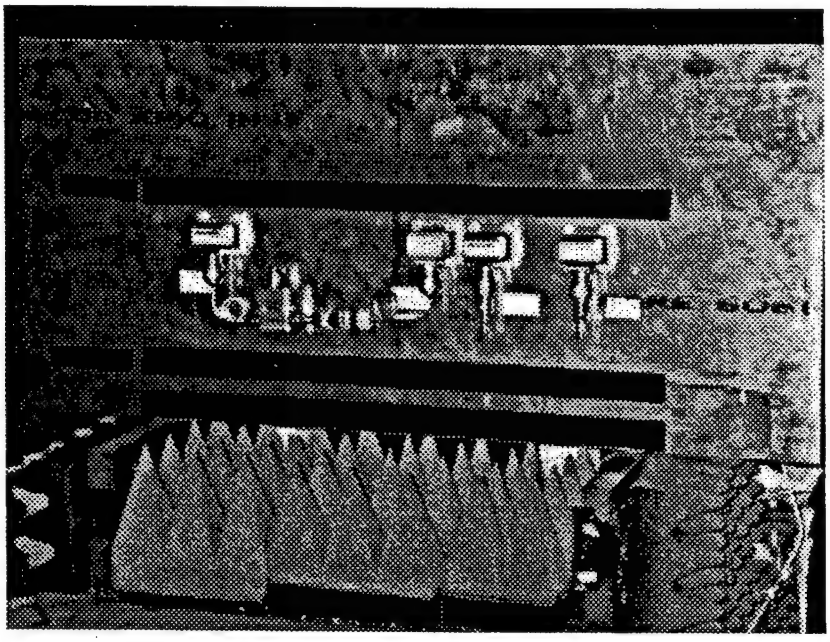

Figure 3.12.b: Photograph of the Built Antenna (Back Plane).

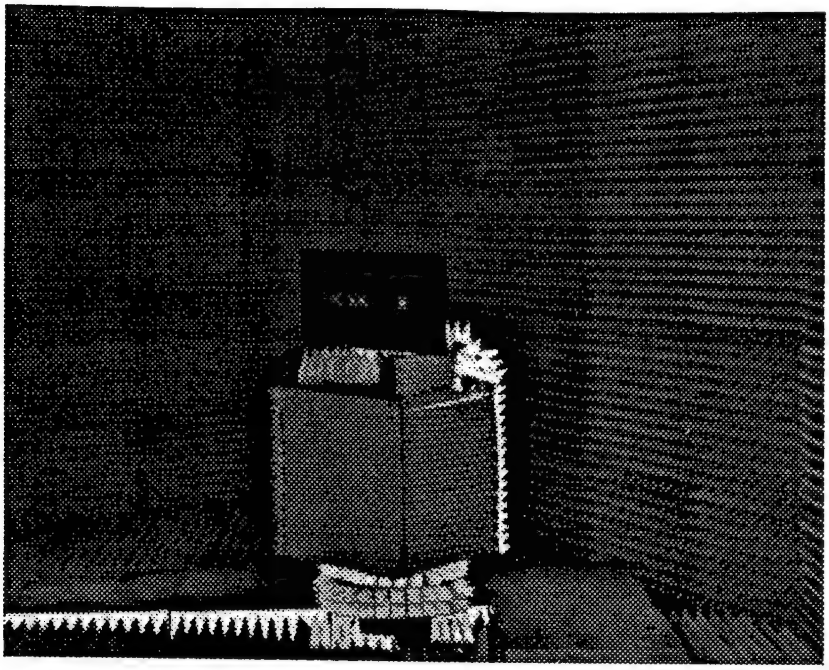

Figure 3.12.c: Photograph of the Built Antenna Mounted on the Pedestal in the Anechoic Chamber.

Before evaluating the experimental results, the simulated results for this particular antenna (rectangular waveguide elements) are examined. The theoretical element factor (EF) for a rectangular waveguide when analyzing the H-field is given by

$$EF = \frac{\cos(ka/2\sin\theta)}{\pi^2 - (ka/2\sin\theta)^2}\cos\theta \qquad (3\text{-}12)$$

where α is the width of the waveguide and k is the wave number [Ref. 3]. When Equation (3-12) is used as the element factor (instead of the $\cos(\theta)$ used previously in Section C), the resultant electrical field for each pair of elements is shown in Figure 3.13. Figure 3.14 shows the resolved direction of arrival obtained when this electrical field is processed using

the SNS architecture presented in Section A of this chapter. The results compare favorably to those shown in Figure 3-10.

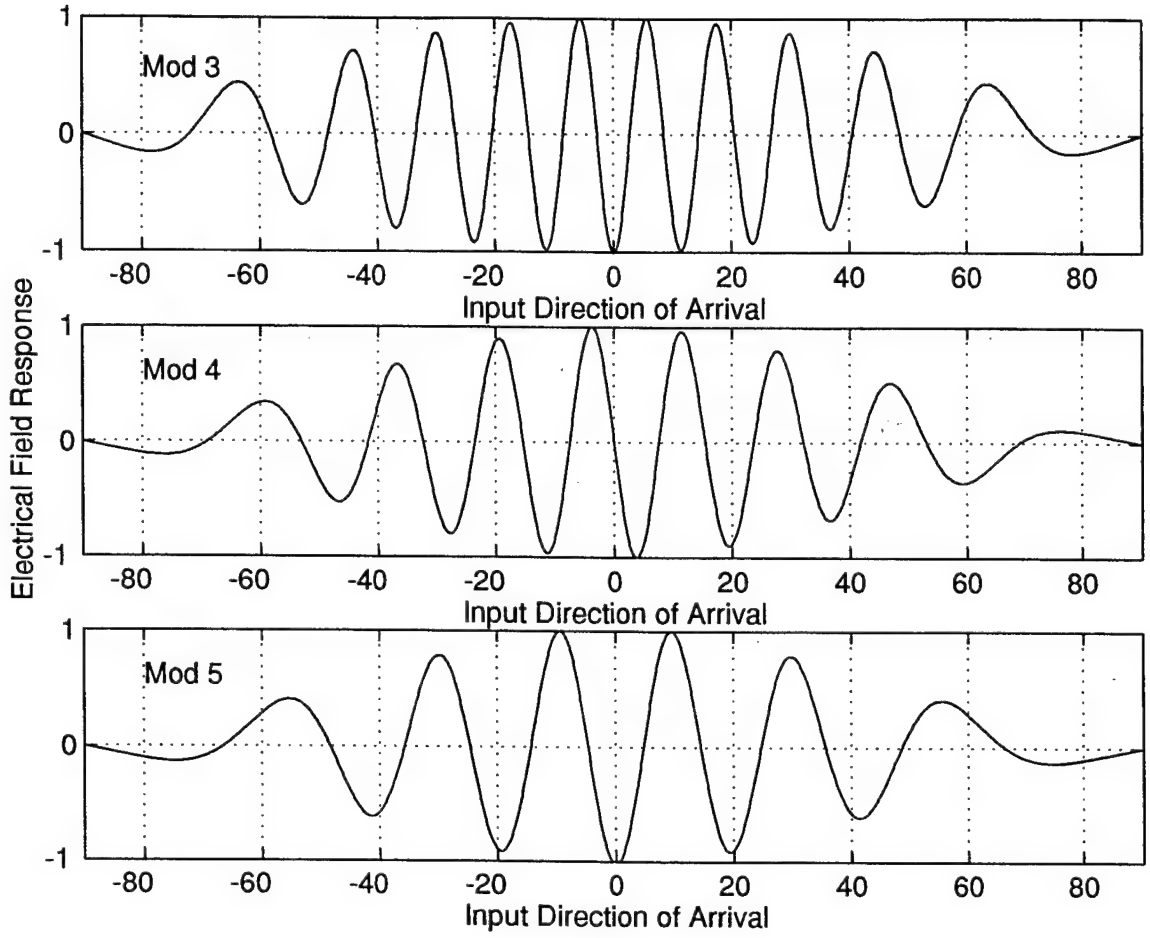

Figure 3.13: Electrical Field Response for Mod 3, Mod 4, and Mod 5 When Using Rectangular Waveguide Elements.

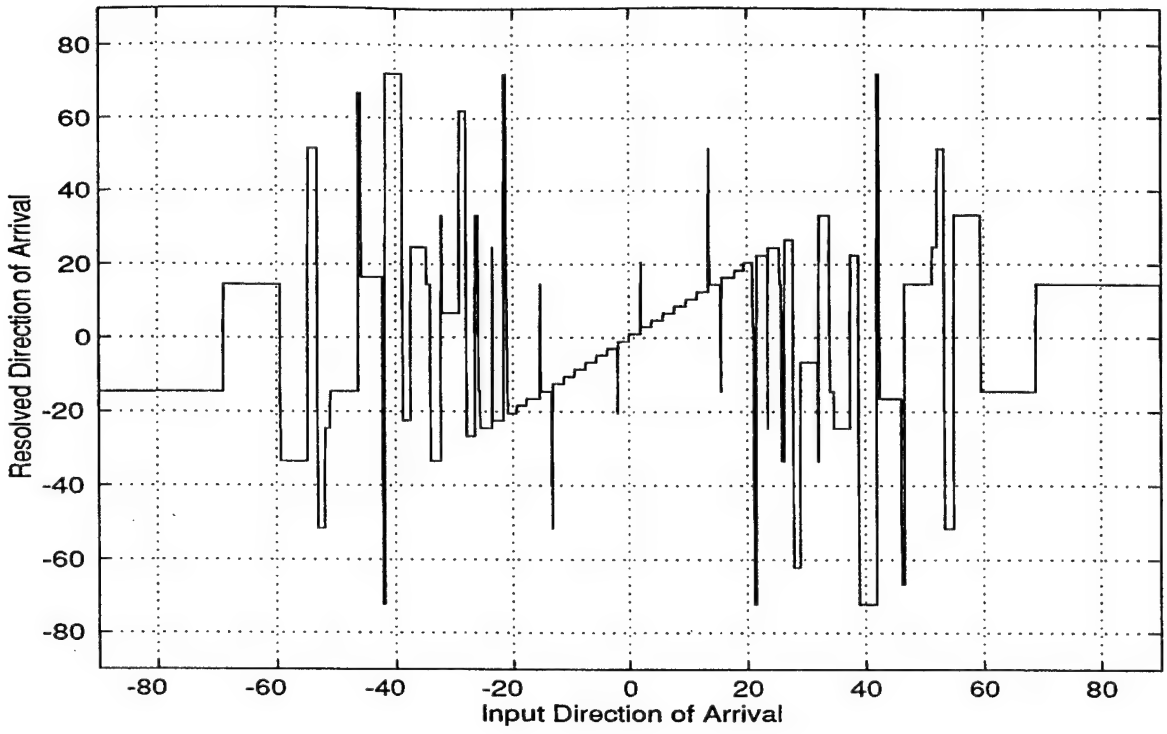

Figure 3.14: SNS Resolved Direction of Arrival as a Function of θ, When Using the EF for a Rectangular Waveguide.

The experimental measurements of the antenna pattern for each pair of elements is shown in Figure 3.15. Since the SNS architecture quantizes the amplitude of the received electrical field (not the power) it is necessary to convert to the collected measurements corresponding electrical field response. The relationship between the Power (P) and the Electrical Field (E) is given by

$$P = 20 \, \mathrm{Log}_{10} | E |. \qquad (3\text{-}13)$$

The absolute value of the electrical field is then

$$|E| = 10^{P/20}. \tag{3.14}$$

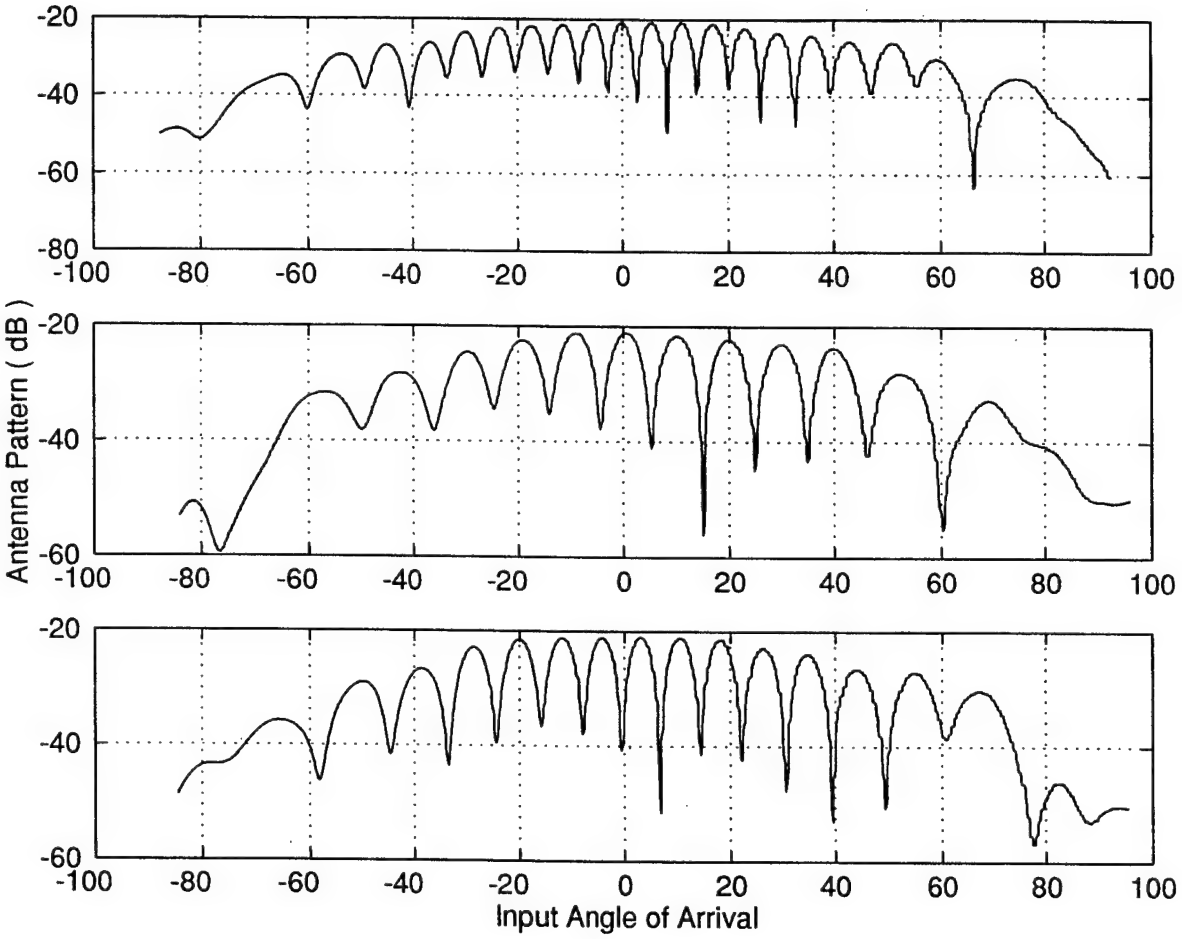

Figure 3.15: Antenna Pattern for Each Pair of Elements (Experimental Data).

Using Equation (3-14), the experimental measurements for each modulus (pair of elements) were used to calculate the absolute value of the electrical fields and are shown in Figure 3.16.

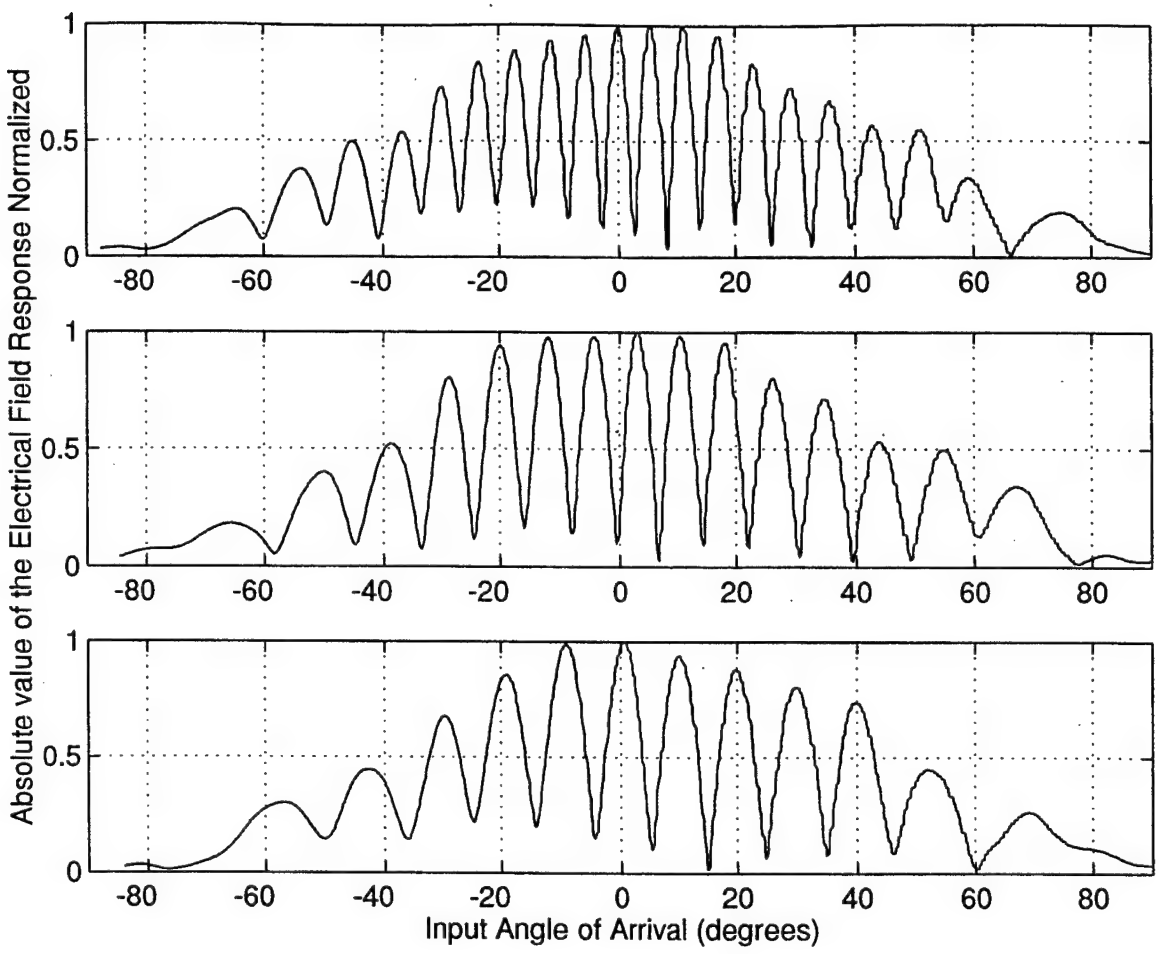

Figure 3.16: Absolute Value of the Electrical Field Response for Each Pair of Elements.

To obtain an approximation to the electrical field response for each pair of elements, the polarity for every odd lobe in Figure 3.16 is reversed. The result is shown in Figure 3.17.

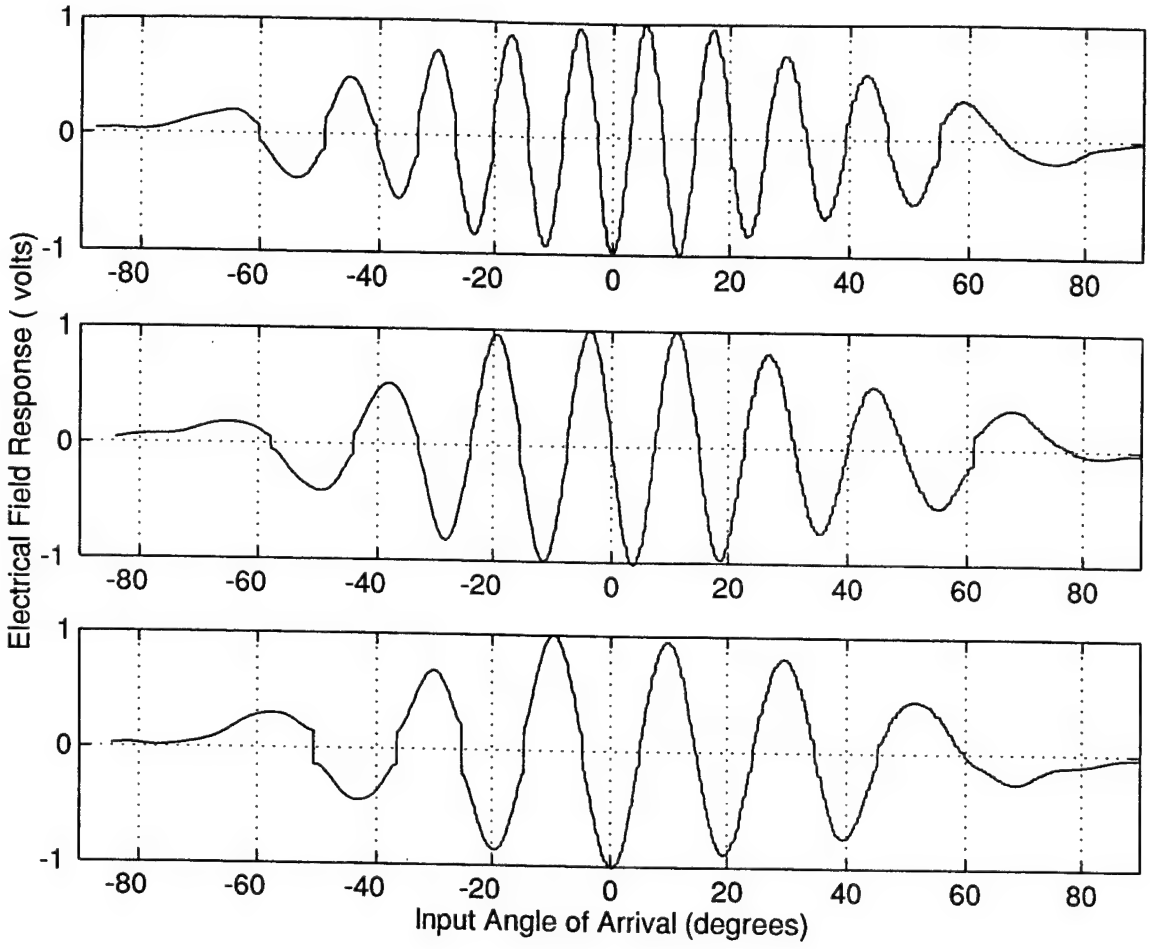

Figure 3.17: Electrical field Response for Each Pair of Elements Corresponding to Modulus 3, 4, and 5.

The electrical field measurements for each pair of elements, representing modulus 3, 4, and 5 is then quantized, and the output from each channel is recombined to obtain the resolved direction of arrival. The resolved direction of arrival is shown in Figure 3.18.

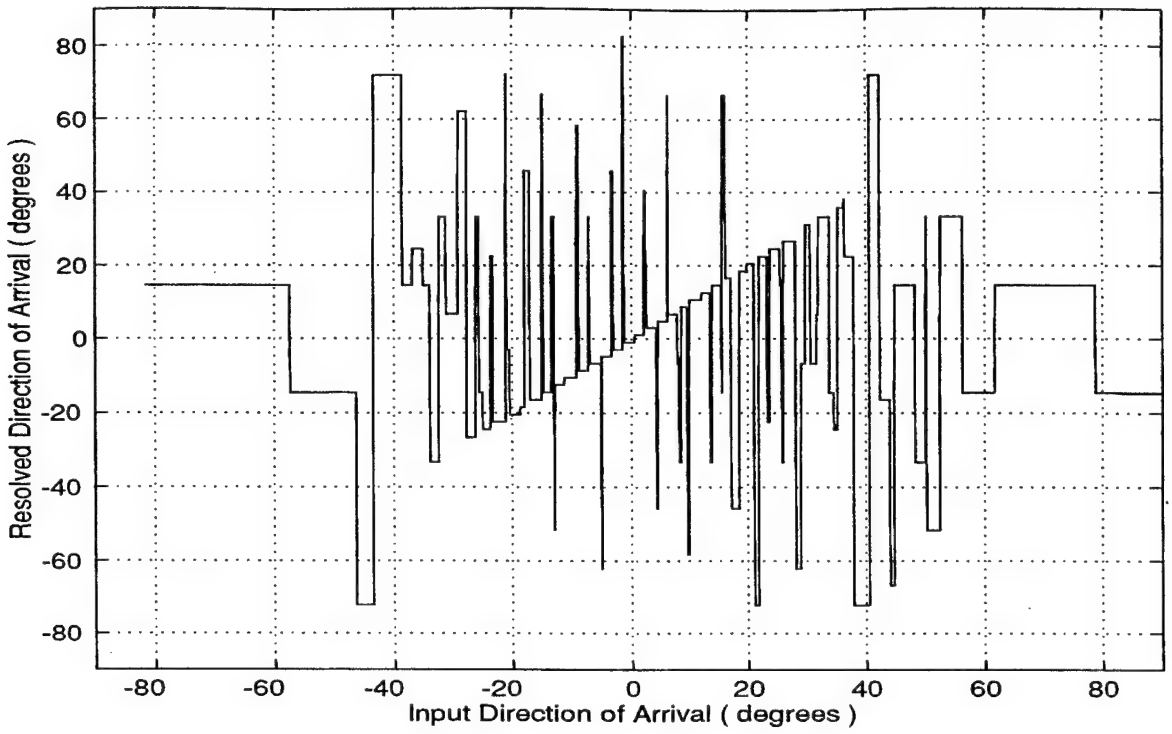

Figure 3.18: Resolved Direction of Arrival Using Experimental Data.

Comparing the experimental results (Figure 3.18) with the simulated results (Figure 3.14) shows a good deal of agreement. However, considering just the interval from 0° to ± 20°, we notice many more encoding errors in the experimental results. If the electrical field was available directly in the anechoic chamber, the approximation would not have been necessary and the number of encoding errors would have been more in line with those of Figure 3.14.

IV. RESIDUE NUMBER SYSTEM ENCODING OF THE PHASE RESPONSE

A. THE RESIDUE NUMBER SYSTEM (RNS)

The ancient study of the Residue Number System begins with a verse from a third-century book, Suan-ching, by Sun Tzu [Ref. 7]:

> We have things of which we do not know the number,
> If we count them by threes, the remainder is 2,
> If we count them by fives, the remainder is 3,
> If we count them by sevens, the remainder is 2,
> How many things are there?
> The answer, 23.

This 1700-year-old number system has been attracting a great deal of attention recently. Digital systems that use residue arithmetic units may play an important role in ultra-high speed, dedicated, real-time systems that support pure parallel processing of integer valued data. It is a "carry free" system that performs addition, subtraction, and multiplication as concurrent operations, side-stepping one of the principal arithmetic delays: managing carry information. Some applications such as fast Fourier transform, digital filtering, and image processing utilize the efficiencies of RNS arithmetic in addition and multiplication. The RNS has been employed efficiently in the implementation of digital processors.

Similar to the SNS, the RNS is also composed of a number of pairwise relatively prime moduli m_i [Ref. 6]. The integers within each RNS modulus are representative of a

saw-tooth waveform with the period of the waveform equal to the modulus. In this scheme, given m, the integer values within the individual modulus are given by the row vector

$$\vec{y} = [0, 1, \cdots, m-1]. \tag{4-1}$$

Again, the required number of comparators for each channel is m_i-1. Notice that all the integers within Equation (4-1) form a complete system of length m_i (no ambiguities). For N equal to the number of moduli, the dynamic range of this scheme, as well as the number of quantization levels, is given by

$$M = \prod_{i=1}^{N} m_i. \tag{4-2}$$

Table 4.1 illustrates the RNS for the moduli m_1=3, m_2=4, m_3=5. Figure 4.1 shows the RNS folding waveforms and the corresponding RNS states.

Normalized Input	Moduli $m_1=3$	$m_2=4$	$m_3=5$
0	0	0	0
1	1	1	1
2	2	2	2
3	0	3	3
4	1	0	4
5	2	1	0
6	0	2	1
7	1	3	2
8	2	0	3
9	0	1	4
10	1	2	0
11	2	3	1
12	0	0	2
.	.	.	.
.	.	.	.
.	.	.	.
52	1	0	2
53	2	1	3
54	0	2	4
55	1	3	0
56	2	0	1
57	0	1	2
58	1	2	3
59	2	3	4
60	0	0	0

Table 4.1: An Example to Illustrate the RNS Encoding Procedure for the Moduli $m_1=3$, $m_2=4$ and $m_3=5$.

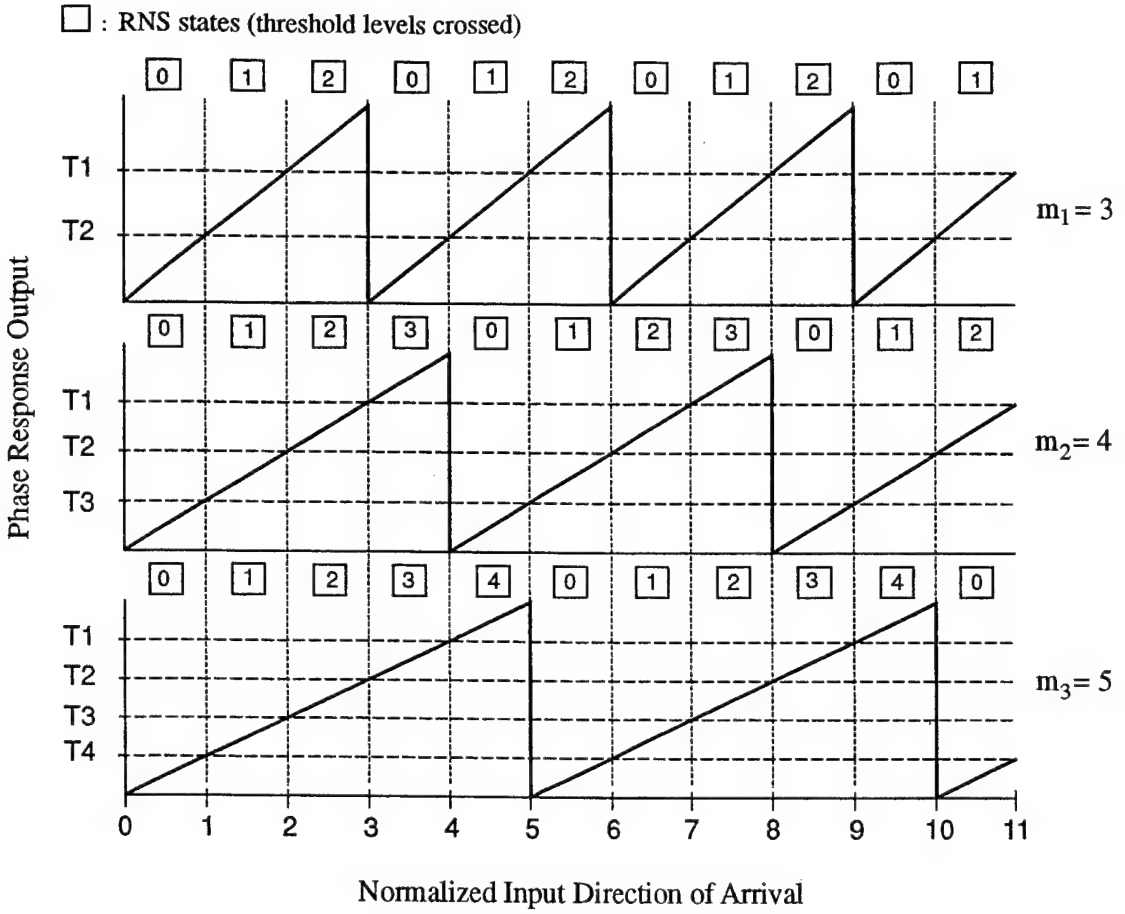

Figure 4.1: RNS Folding Waveforms and Output Codes for the Moduli m_1=3, m_2=4, and m_3=5.

B. RNS ANTENNA ARCHITECTURE

The phase response of a two-element interferometer corresponds to a saw-tooth folding waveform. The RNS antenna architecture being investigated is shown in Figure 4.2. Phase detectors are used to combine the individual pairs of elements. Also, the comparator threshold levels and logic block are particular to the RNS (see Table 4.1).

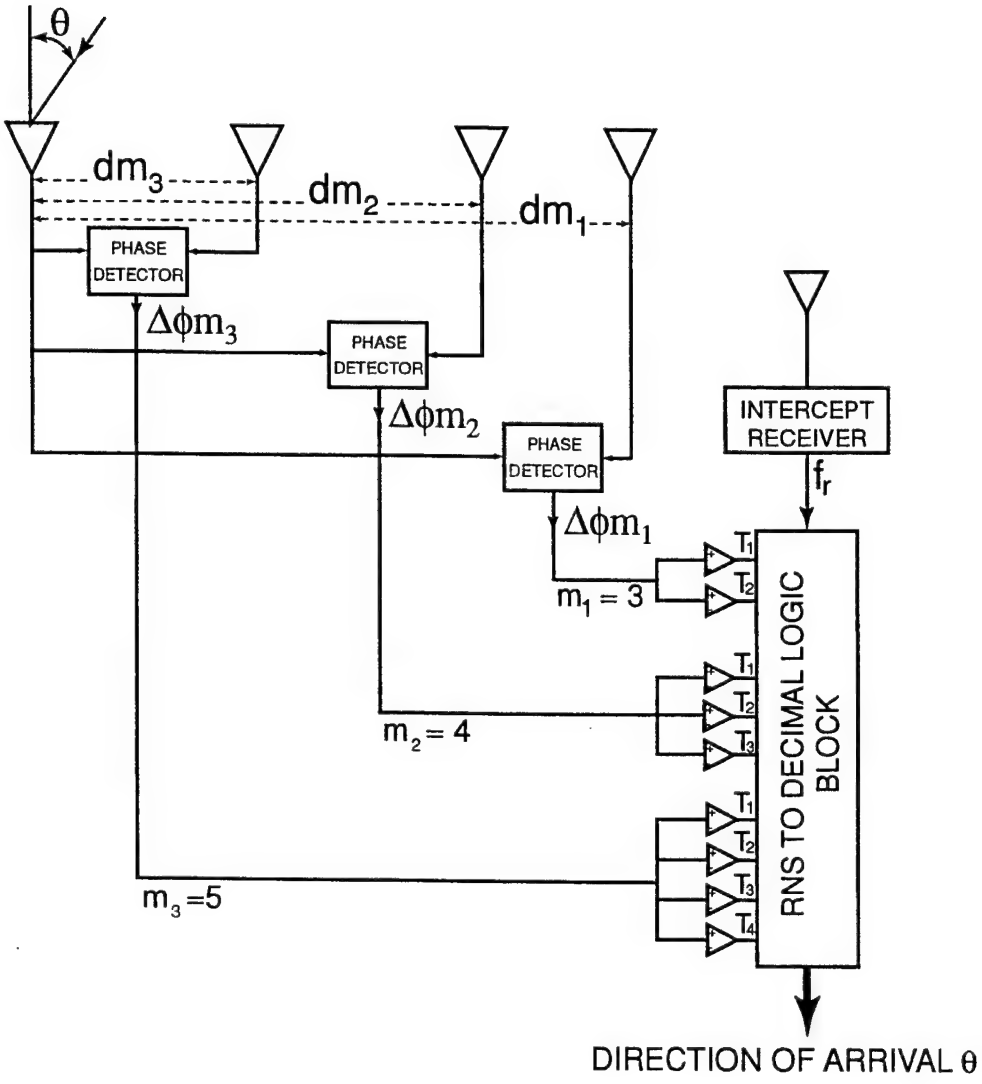

Figure 4.2: RNS Antenna Architecture.

The distance between each pair of elements must be derived as a function of the PRP modulus, m_i, so that the corresponding phase response has the correct number of folds. For a given modulus m_i, the number of folds needed to apply the RNS code within the dynamic range is given by

$$n_{i,RNS} = \frac{\text{dynamic range}}{m_i} = \frac{M}{m_i}. \tag{4-3}$$

Next consider the two element interferometer shown in Figure 1.1. The phase difference between the received signal due to the separation between elements is given by

$$\Delta\phi = \frac{2\pi d}{\lambda}\sin\theta. \tag{4-4}$$

From Equation (4-4) we have that:

$$\begin{aligned} \theta = 0^\circ &\Rightarrow \Delta\phi = 0 \\ \theta = 90^\circ &\Rightarrow \Delta\phi = \frac{2\pi d}{\lambda} \\ \theta = -90^\circ &\Rightarrow \Delta\phi = -\frac{2\pi d}{\lambda}. \end{aligned} \tag{4-5}$$

Since each fold of the phase response corresponds to a change in phase of 2π, we require that

$$\Delta\phi(90^\circ) - \Delta\phi(-90^\circ) = 2\pi \tag{4-6}$$

which implies (from Equation (4-5)

$$\frac{4\pi d}{\lambda} = 2\pi, \quad \therefore \quad d = \frac{\lambda}{2}. \tag{4-7}$$

Finally, the distance between elements is given by

$$d_{i,RNS} = n_{i,RNS}\left(\frac{\lambda}{2}\right) = \frac{M}{m_i}\left(\frac{\lambda}{2}\right). \tag{4-8}$$

Using the same moduli set with center frequency of f_0=8.5 GHz, the distances for each pair of elements are

$$d_1 = 10\,\lambda,$$
$$d_2 = 7.5\,\lambda,$$
$$d_3 = 6.0\,\lambda.$$

which are the same as those given for the SNS architecture. That is, the same hardware constructed for the SNS array can be used for the RNS array.

C. SIMULATION RESULTS

The correct distances between each pair of elements were found in Section B so that the output waveforms representative of modulus m_1=3, m_2=4, and m_3=5, have the correct number of folds required to quantize the entire phase response within the field of view (from 0° to ±90°). Figure 4.3 shows a plot of the phase response, as a function of the input direction of arrival for a two-element interferometer separated by a distance d=6λ. The saw-tooth waveform stretches out as θ, the input direction of arrival, goes from 0° to ±90°. However, if the phase response is plotted as a function of sin(θ), a perfect saw-tooth waveform is obtained as shown in Figure 4.4.

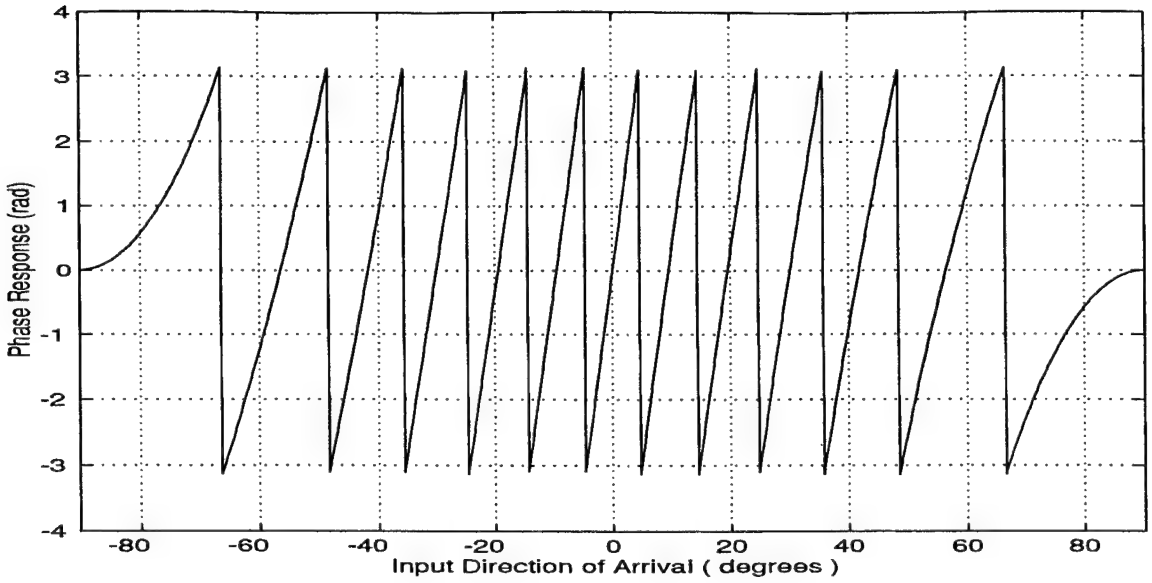

Figure 4.3: Phase Response as a Function of the Input Direction of Arrival for a Two-Element Interferometer with Separation $d_3=6\lambda$.

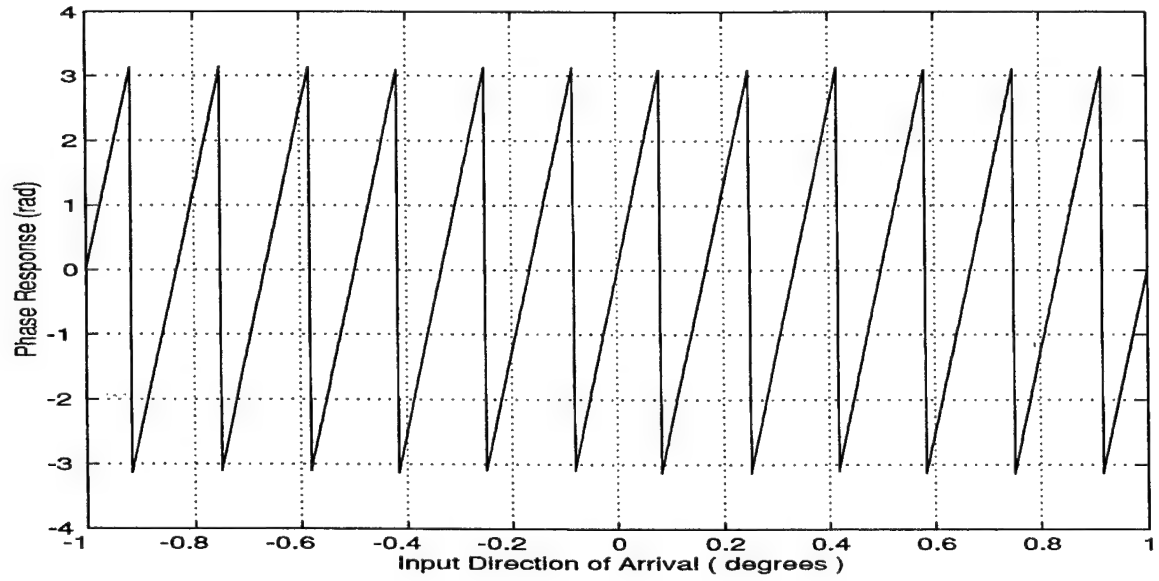

Figure 4.4: Phase Response as a Function of $\sin(\theta)$ for a Two-Element Interferometer with Separation $d_3=6\lambda$.

Based on these results, the same analysis that was performed when dealing with the array factor can be applied here. In Figures 4.5, 4.6, and 4.7, the phase response waveform and respective output quantization code for modulus m_1=3, modulus m_2=4, and modulus m_3=5 are plotted, as a function of the input direction of arrival.

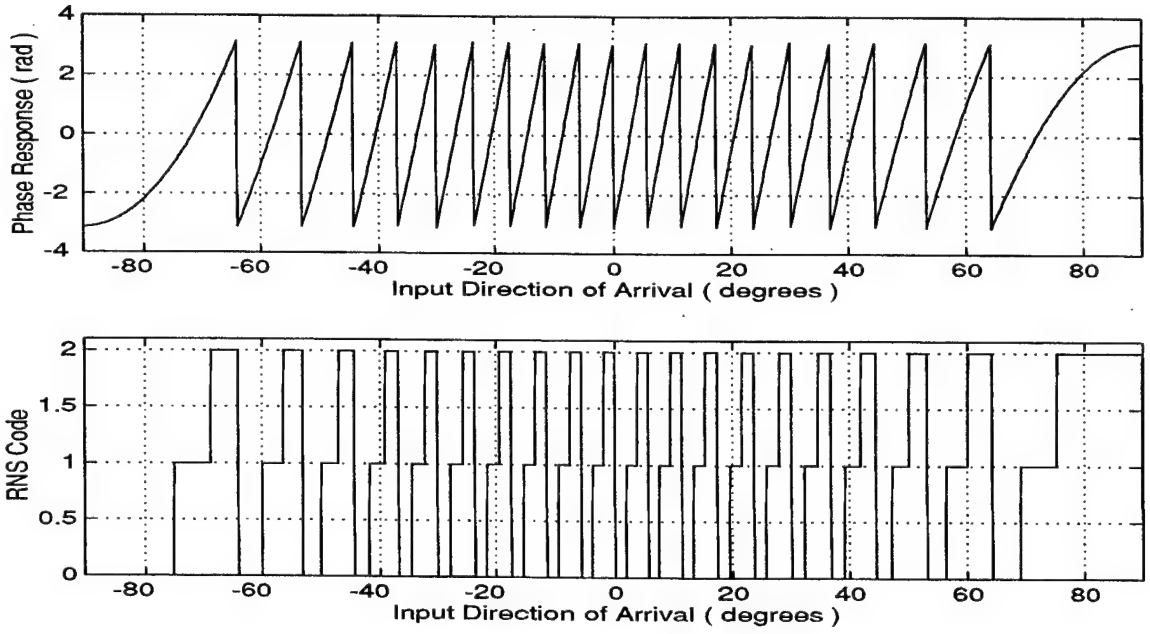

Figure 4.5: Phase Response Waveform and Respective RNS Quantization Code for the Pair of Elements (1, 4) Corresponding to Modulus m_1=3.

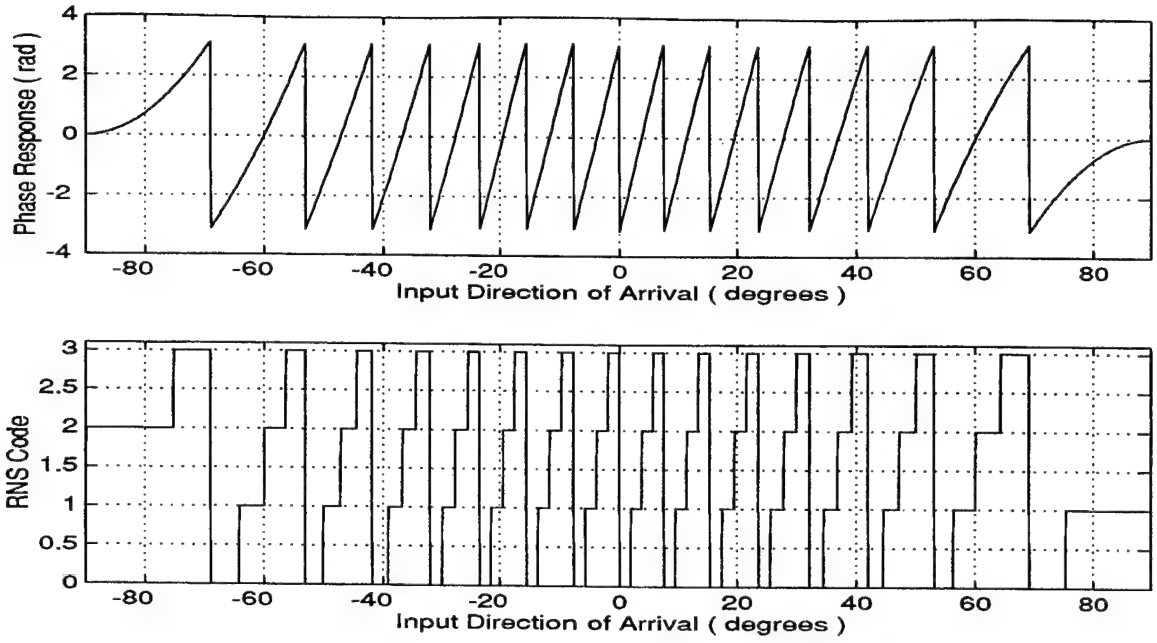

Figure 4.6: Phase Response Waveform and Respective RNS Quantization Code for the Pair of Elements (1, 3) Corresponding to Modulus m_2=4.

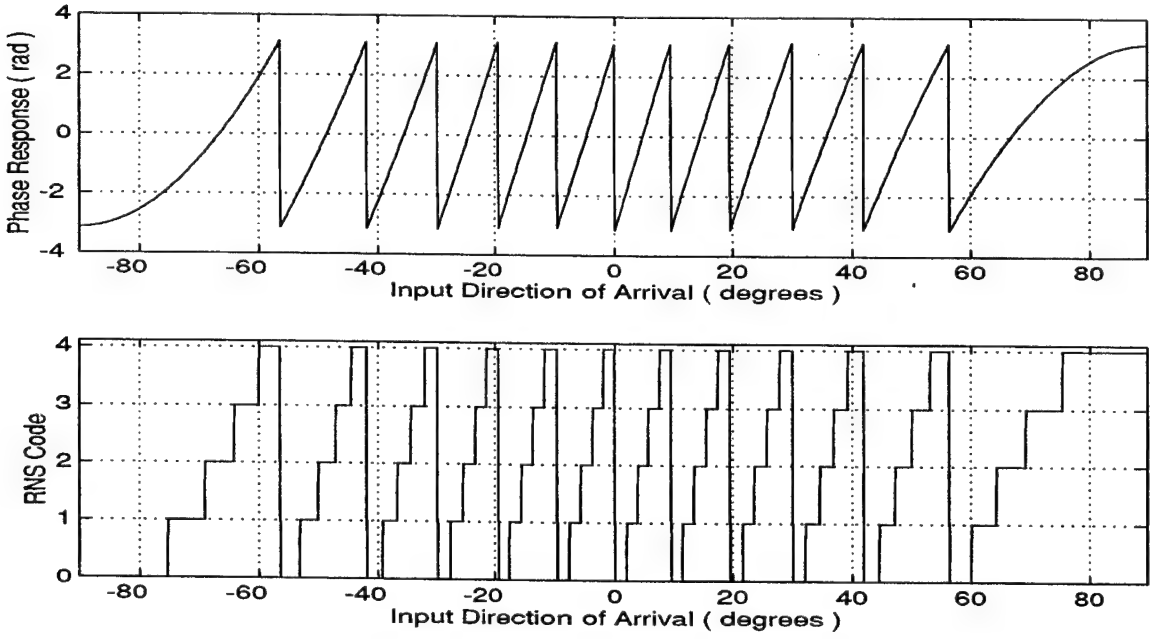

Figure 4.7: Phase Response Waveform and Respective RNS Quantization Code for the Pair of Elements (1, 2) Corresponding to Modulus m_3=5.

The quantization of the phase response from each pair of elements is made separately using a small bank of comparators. The number of threshold levels (and comparators) are the same as that for the array factor amplitude analysis. However, the matching threshold values are different as shown in Table 4.2.

Elements	Modulus	T1	T2	T3	T4
(1, 2)	5	-1.8850	-0.6283	0.6283	1.8850
(1, 3)	4	-1.5708	0.0000	1.5708	--------
(1, 4)	3	-1.0472	1.0472	--------	--------

Table 4.2: Comparator Threshold Levels for Each Pair of Elements When Considering the Phase Analysis.

For a specific input direction of arrival and pair of elements, there will be a corresponding integer (number of comparators in the on state) within the PRP modulus m_i. The value of those integers depends on the measured phase difference associated with each pair of elements for that specific input direction of arrival. The comparator state for each pair together can then be represented by 3 RNS codes. The 3 RNS codes are indexed to an RNS logic block to give the resolved direction of arrival. Table 4.3 shows the 3 RNS codes and the resolved direction of arrival.

3 RNS Codes	Resolved DOA (degrees)	3 RNS Code	Resolved DOA (degrees)
000	0.9551	**020**	-82.5824
111	2.8664	**131**	-72.0627
222	4.7809	**202**	-66.5593
033	6.7007	**013**	-62.1158
104	8.6382	**124**	-58.2581
210	10.5655	**230**	-54.7864
021	12.5152	**001**	-51.5928
132	14.4797	**112**	-48.6110
203	16.4618	**223**	-45.7968
014	18.4644	**034**	-43.1187
120	20.4907	**100**	-40.5534
231	22.5442	**211**	-38.0832
002	24.6287	**022**	-35.6940
113	26.7487	**133**	-33.3745
224	28.9091	**204**	-31.1155
030	31.1155	**010**	-28.9091
101	33.3745	**121**	-26.7487
212	35.6940	**232**	-24.6287
023	38.0832	**003**	-22.5442
134	40.5534	**114**	-20.4907
200	43.1187	**220**	-18.4644
011	45.7968	**031**	-16.4618
122	48.6110	**102**	-14.4797
233	51.5928	**213**	-12.5152
004	54.7864	**024**	-10.5655
110	58.2581	**130**	-8.6382
221	62.1158	**201**	-6.7007
032	66.5593	**012**	-4.7809
103	72.0627	**123**	-2.8664
214	82.5824	**234**	-0.9551

Table 4.3: RNS Code and Equivalent Resolved Direction of Arrival for Modulus 3, 4, and 5 Phased at 0° with Center Frequency f_0=8.5 GHz.

Figure 4.8, shows a plot of the resolved direction of arrival as a function of θ, the input direction of arrival. This new system gives the direction of arrival information over the complete field of view without ambiguity. However the accuracy varies depending on the actual direction of arrival of the incoming signal. Notice also that the quantization width increases as the direction of arrival approaches $\pm 90°$. The quantization error will be addressed in Chapter V.

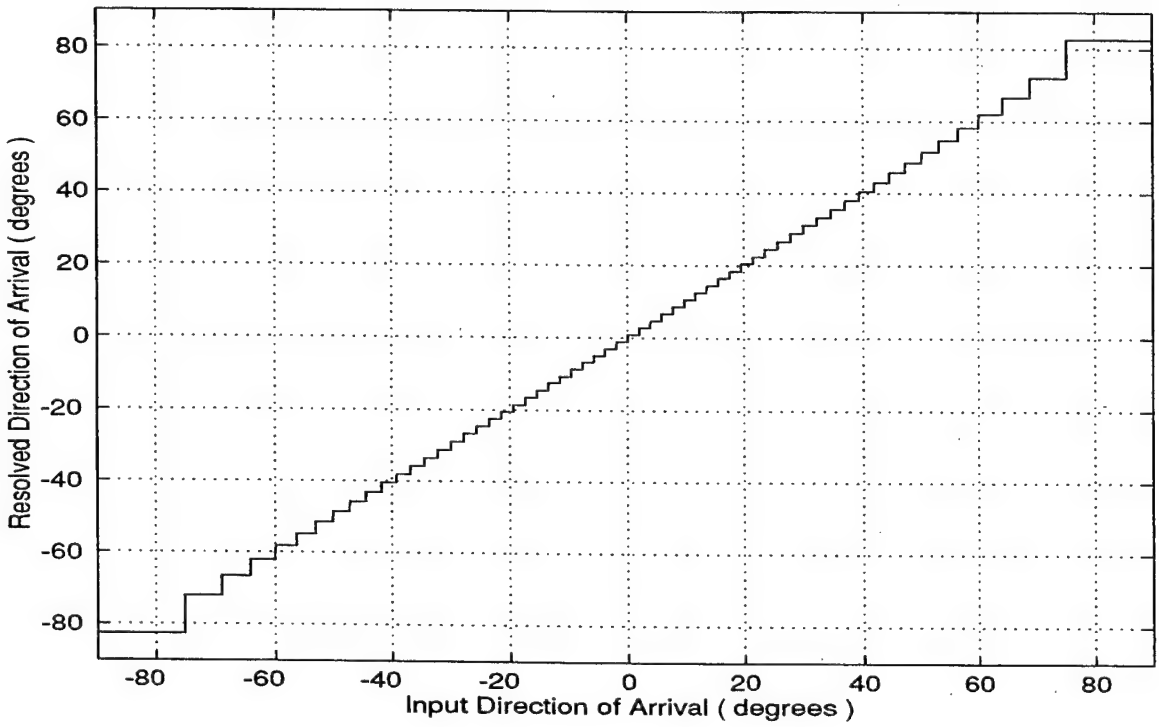

Figure 4.8: Resolved Direction of Arrival in Function of the Input Direction of Arrival.

D. EXPERIMENTAL RESULTS

Unfortunately it was not possible to obtain acceptable experimental results for the RNS antenna architecture. The main problem was the nonavailability of the phase detectors. Another problem was matching the elements with the correct length of cable in order to obtain the correct phase difference between each pair of elements. Future investigations are currently underway and will correct these problem.

V. FURTHER CONSIDERATIONS

A. OVERVIEW

Comparing the simulated results for the SNS antenna design with the results obtained for the RNS antenna design, it is clear that the second case permits acquiring the direction of arrival information over the complete field of view from 0° to ±90°. When using the SNS antenna it is impossible to obtain the direction of arrival information over the entire range from -90° to 90° due to the degradation in the amplitude response. Since the phase response has a "uniform" distribution (i.e., maximum and minimum with a constant value) over the complete field of view, it is possible to use the RNS code to quantize that signal correctly. Accordingly, only the phase analysis will be considered hereafter since the results shown are more encouraging. At this point we have not presented any results concerning the following aspects:

- quantization errors associated with this new antenna design,
- the antenna frequency response (incoming signal frequency different than the one used in the design),
- the required size of the antenna related to the moduli set and the frequency used to build the antenna, and
- the influence of the chosen moduli set on the accuracy and quantization error of the antenna.

These aspects are considered in this chapter for the RNS architecture (using the phase response). Some antennas design examples are given to show the degree of accuracy that can be reached with this direction finding architecture.

B. QUANTIZATION ERROR ASSOCIATED WITH THE RNS ARCHITECTURE

The conversion of an analog (continuous) signal into a digital (discrete) representation is called quantization. Graphically, the quantization process means that a straight line representing the relation between the input and output of a linear continuous system is replaced by a staircase characteristic [Ref. 8], as shown in Figure 4.8. The difference of two adjacent discrete values is called the quantum or step size. Signals applied to a quantizer, with the input-output characteristic of Figure 4.8, are sorted into amplitude slices, and all input signals within plus or minus half a quantum step of the midvalue of a slice are replaced in the output by the midvalue. The quantizer error consists of the difference between the input and output signals of the quantizer so that the maximum instantaneous value of this error is half of one quantum step, and the total range of variation is from minus half a step to plus half a step. By analyzing Figure 4.8 again, it is clear that the quantization error for the RNS antenna is not constant since the code widths are not constant. The Appendix contains the Matlab™ program code to calculate the quantization error for a predetermined moduli set as a function of the input direction of arrival. Figure 5.1 shows a plot of the characteristic quantization error curve associated with the resolved direction of arrival from Figure 4.8 for the moduli set (3, 4, 5) and for a frequency equal to 8.5 GHz. For this case, the results show that the quantization error varies from about ±1° over the input range ±20°, to a maximum of ±7.42° for direction of arrivals near ±90°. Figure 5.2 it is a plot of both the resolved direction of arrival and the associated quantization error as a function of the input direction of arrival.

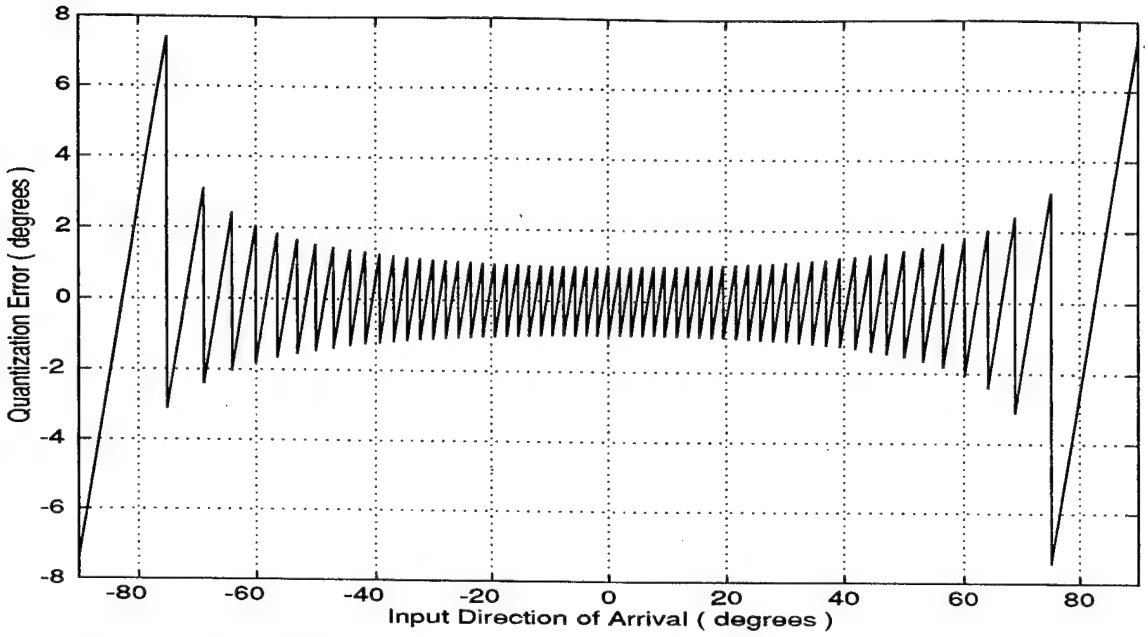

Figure 5.1: Characteristic Quantization Error Associated With the RNS Antenna When Considering the Moduli Set (3, 4, 5) and the $f_r=f_0=8.5$ GHz.

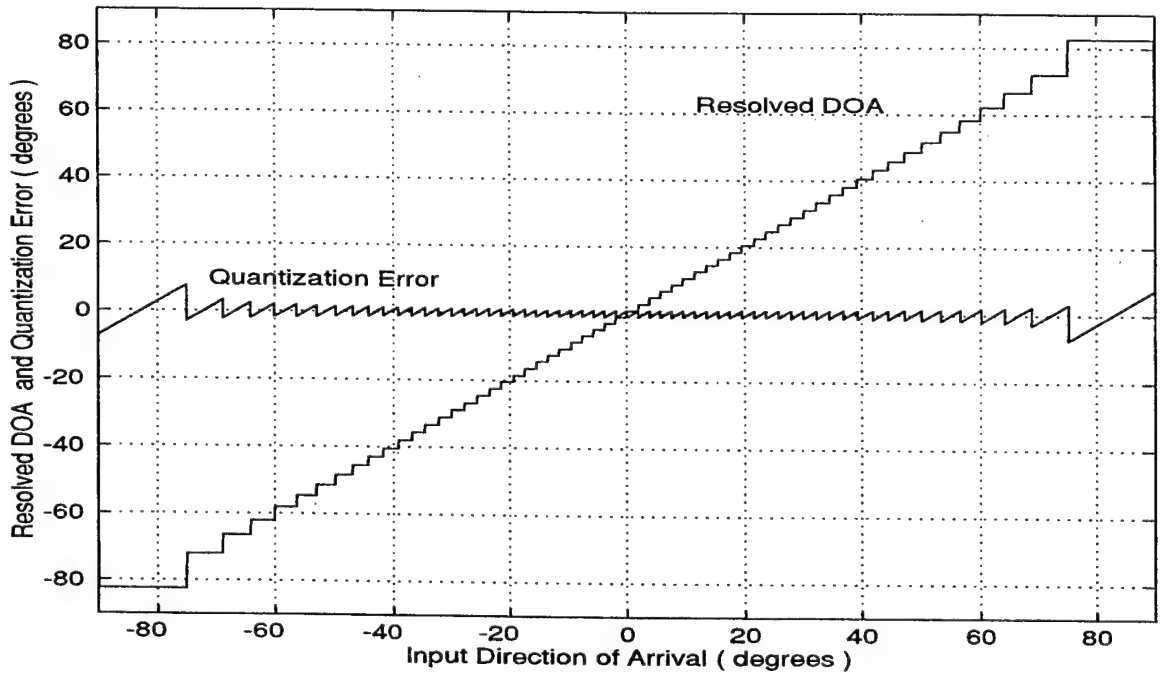

Figure 5.2: Resolved Direction of Arrival and Quantization Error.

C. RNS ANTENNA FREQUENCY RESPONSE

A frequency (f_0) was chosen to calculate the required distance between each pair of elements so that the correct number of folds (for each pair of elements) were available to apply the RNS code and process (quantize) correctly the phase response without ambiguities over the entire field of view. The simulated results shown previously are obtained assuming that the frequency of the incoming signal (f_r) was equal to f_0. In this case, the only error present is the quantization error. It is interesting to examine what happens when the frequency of the incoming signal has some other value different from f_0. Figure 5.3, shows the resolved direction of arrival for an incoming signal with a frequency f_r=4.25 GHz. Comparing these results with the results in Figure 4.8, we notice the following: the total number of quantization levels is reduced by half and the resolved direction of arrival has large errors as the input direction of arrival goes from 0° to ±90°.

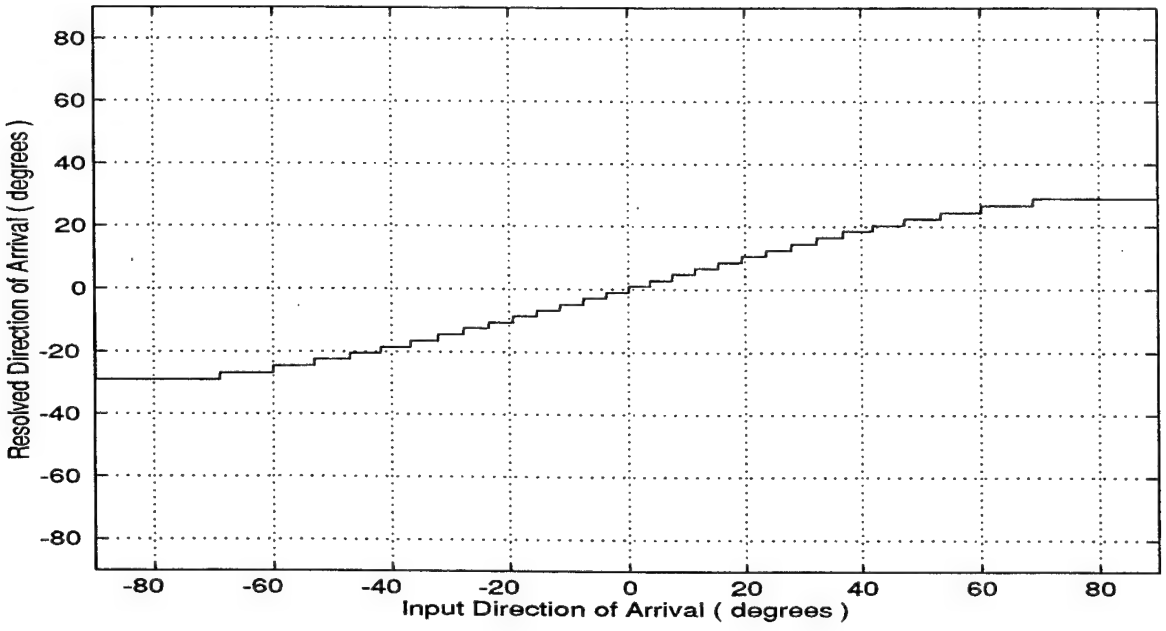

Figure 5.3: Resolved Direction of Arrival for an Incoming Signal With a Frequency f_r=4.25 GHz.

Alternatively, Figure 5.4 shows the resolved direction of arrival when the incoming signal frequency f_r=17 GHz. In this case, we notice that the total number of quantization levels doubles when compared with the simulated results shown in Figure 4.8 (f_r=f_0). As a result, the resolved directions of arrival are ambiguous because the same 3 RNS codes correspond to more that one direction of arrival. In addition the overall error is very high.

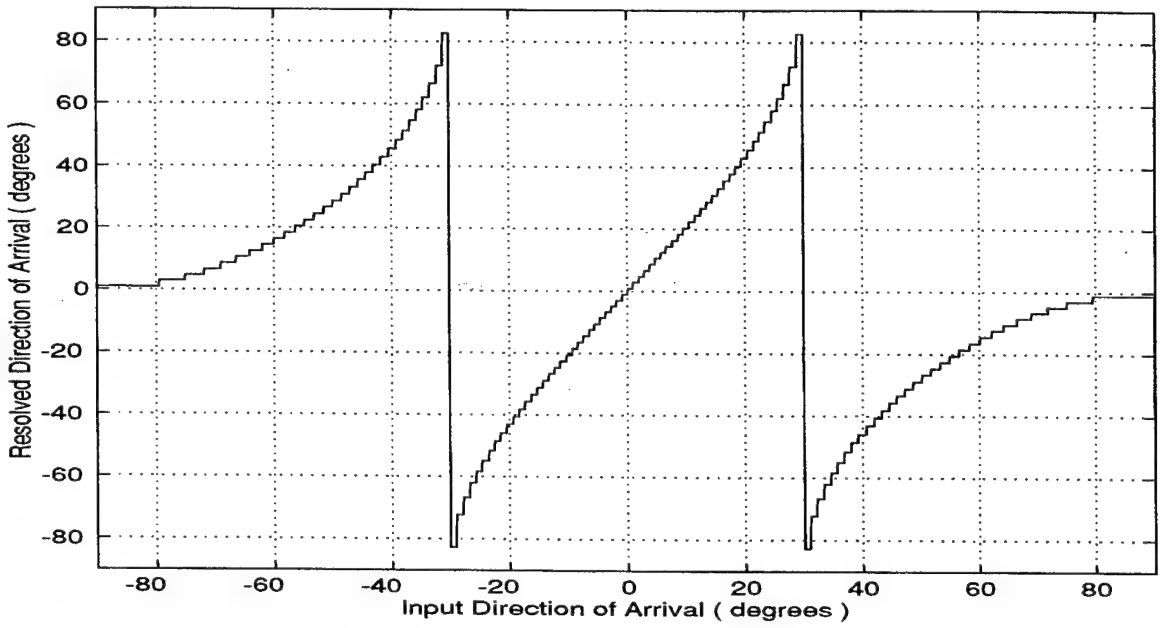

Figure 5.4: Resolved Direction of Arrival for an Incoming Signal With a Frequency f_r = 17 GHz.

The RNS antenna was designed assuming a moduli set (3, 4, 5) and a frequency (f_0) equal to 8.5 GHz. For a given PRP modulus m_i, Equation (4-3) gives the required number of folds to apply the RNS code within the dynamic range without ambiguities. It was found to be equal to 20 for modulus 3. In addition, the distance between each pair of elements is given by Equation (4-4). This distance is fixed when the antenna is built. On other hand, in

the presence of a signal with a frequency other than f_0, and from Equation (1-1), the phase difference between the received signal due to the separation between elements is given by

$$\Delta \phi = \frac{2 \pi d}{\lambda_r} \sin\theta. \tag{5-1}$$

Consider modulus 3, $d=10\lambda_0$. Substituting that value in Equation (5-1) gives

$$\Delta \phi = \frac{20 \pi \lambda_0}{\lambda_r} \sin\theta. \tag{5-2}$$

To analyze Equation (5-2), three distinct cases need to be considered according to the value of the ratio λ_0/λ_r.

- Case 1: $\lambda_0/\lambda_r = 1 \quad \Rightarrow \quad f_r = f_0$.

This can be considered the ideal case since the corresponding phase response (sawtooth waveform) will have the exact number of folds required to apply the RNS code within the dynamic range without ambiguities over the complete field of view (from 0° to ±90°).

- Case 2: $\lambda_0/\lambda_r < 1 \quad \Rightarrow \quad f_r < f_0$.

In this case the phase response waveform will have less folds than the required number to apply the RNS code within the dynamic range. No ambiguities will be present; however, the quantization error will increase since a smaller number of quantization levels will exist to cover the same field of view (from 0° to ±90°). This case is directly related to Figure 5.3 where the ratio $\lambda_0/\lambda_r=0.5$. The equivalent number of folds and quantization levels are one

half those found for the ideal case. Figure 5.5 shows the phase response for both situations: f_r=8.5 GHz and f_r=4.25 GHz for modulus m_3=5.

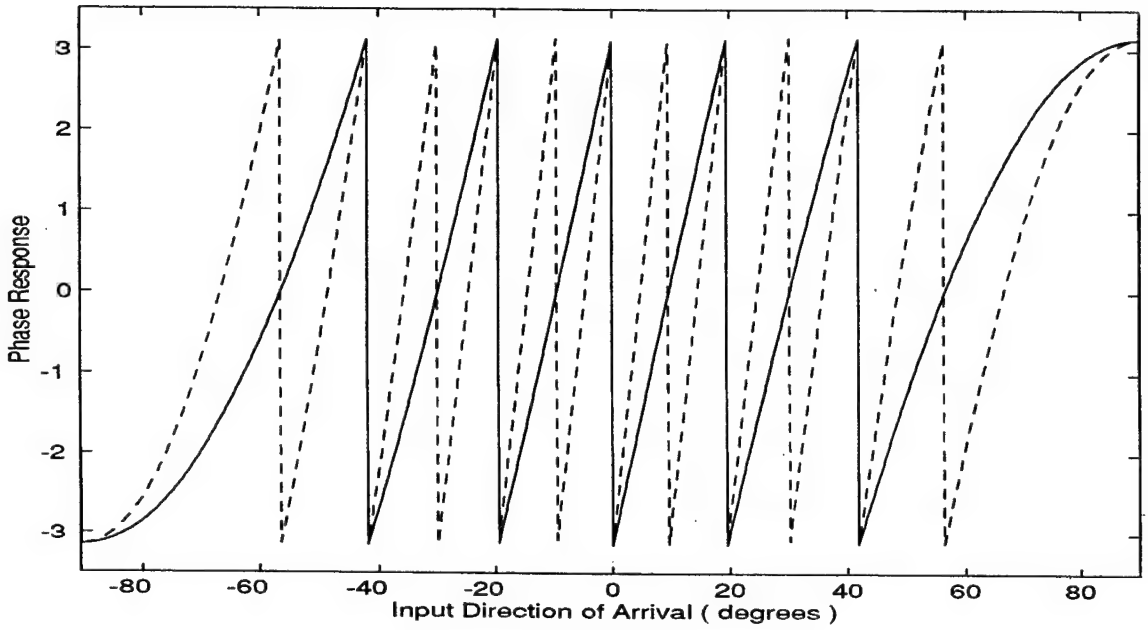

Figure 5.5: Phase Response Waveform (Mod 5) for f_r=8.5 GHz (Dashed) and f_r=4.25 GHz.

- Case 3: $\lambda_0/\lambda_r > 1 \quad \Rightarrow \quad f_r > f_0$.

For this case the resultant phase response will have more folds than the required number to apply the RNS code. As a result we start to have ambiguous resolved directions of arrival as observed in Figure 5.4. Here, the ratio λ_0/λ_r=2; therefore the number of folds and quantization levels are twice the values found for the ideal case, as illustrated in Figure 5.6 for modulus m_3=5.

In all cases, the number of folds present in the phase response waveform will be proportional to the ratio λ_0/λ_r.

In summary, for the results obtained in the third case, we won't be able to find the direction of arrival over the complete field of view without some ambiguous results. However, when the frequency of the incoming signal is smaller than f_0, we do not have any ambiguities, but the overall error of the resolved direction of arrival increases.

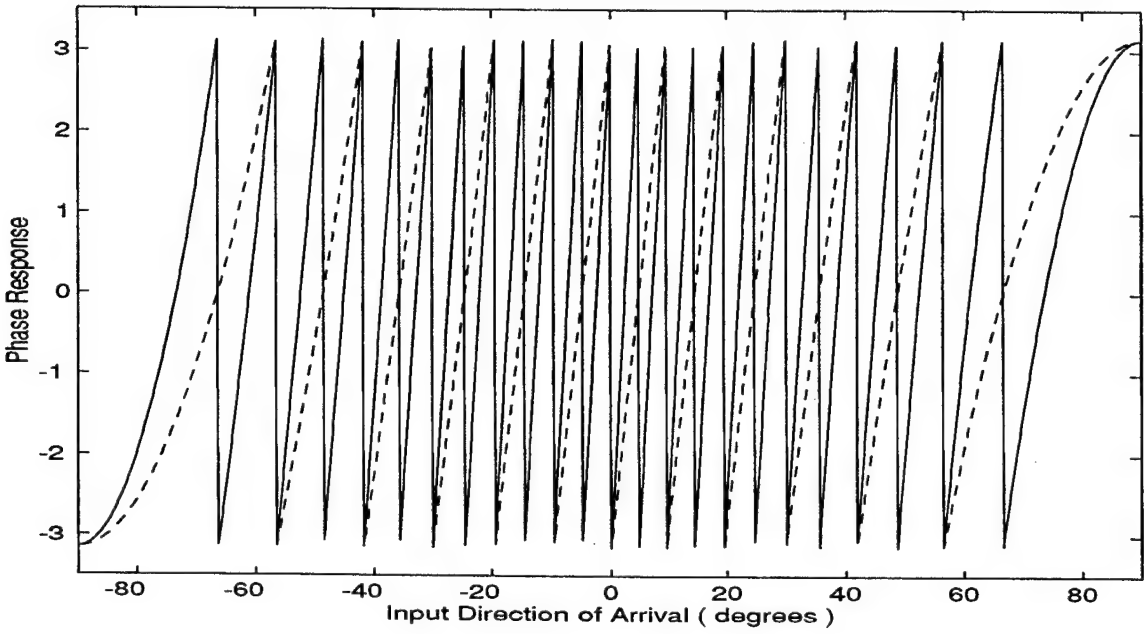

Figure 5.6: Phase Response Waveform (Mod 5) for f_r=8.5 GHz (Dashed) and f_r=17 GHz.

This suggests that, for example, if one of the requisites of our antenna is to be able to find the direction of arrival of any incoming signal with frequencies over some range, say 2 to 18 GHz, the higher frequency in that range should be chosen to build our antenna, i.e., 18 GHz for this case. By using this, the direction of arrival information will always be

obtained without ambiguities over the entire field of view. However, the overall quantization error will be different for each case depending on the number of quantization levels that will be used and, consequently, on the frequency value of the incoming signal.

At this point, we determine how *to correct* the additional error when the frequency of the incoming signal is different than f_0 (frequency used to build our antenna). To correct the error however, the frequency of the incoming signal must be known. With the measured frequency, the number of folds present in the phase response waveform is determined. The new number of folds present in the phase response over the entire field of view is given by

$$n_{i,fn} = \left(\frac{\lambda_0}{\lambda_r}\right) n_{i,RNS}. \tag{5-3}$$

Consider modulus 3 and f_r=4.25 GHz. For this particular case, the new number of folds ($n_{i,fn}$) *is equal* to 10. From Equation (4-3) and knowing that the number of quantization levels is equal to the dynamic range, the actual number of quantization levels (N_{QL}) for a specific frequency is given by

$$N_{QL} = n_{i,fn}\, m_i\,, \tag{5-4}$$

where $n_{i,fn}$ is the new number of folds and m_i represents the PRP modulus that is being considered. For our example, the number of quantization levels is equal to 30. With this number of quantization levels it is possible to find the transition points from one quantization level to another. The transition points will occur at some angle θ_t for which the $\sin(\theta_t)$ corresponds to some value in the range from 0 to ±1 given by

$$x(n) = \pm\frac{n}{N_{QL}} \tag{5-5}$$

for $n = 0, 1, 2,\ldots, N_{QL}$. Therefore, the transition angles are given by

$$\theta_t(n) = \sin^{-1}(x(n)). \tag{5-6}$$

Having the transition angles, the midvalue of each quantization level can easily be found, as well as the corresponding quantization error. The new midvalues for each quantization level are then indexed to the RNS logic block so that for each 3 RNS codes will correspond the correct resolved direction of arrival. Since the phase response waveform is always phased at 0° (see Figures 4.5, 4.6, and 4.7), it is possible to implement this new algorithm in our RNS logic block to obtain the correct resolved direction of arrival. Figure 5.7 shows the resolved direction of arrival and the quantization error for an incoming signal with a frequency f_r=4.25 GHz, using this new algorithm to introduce the corrections. With this new algorithm, the error in the resolved direction of arrival when the frequency of the incoming signal is smaller than f_0, becomes very small when compared with the results illustrated in Figure 5.3. Figure 5.8 shows the quantization error for this case using another scale.

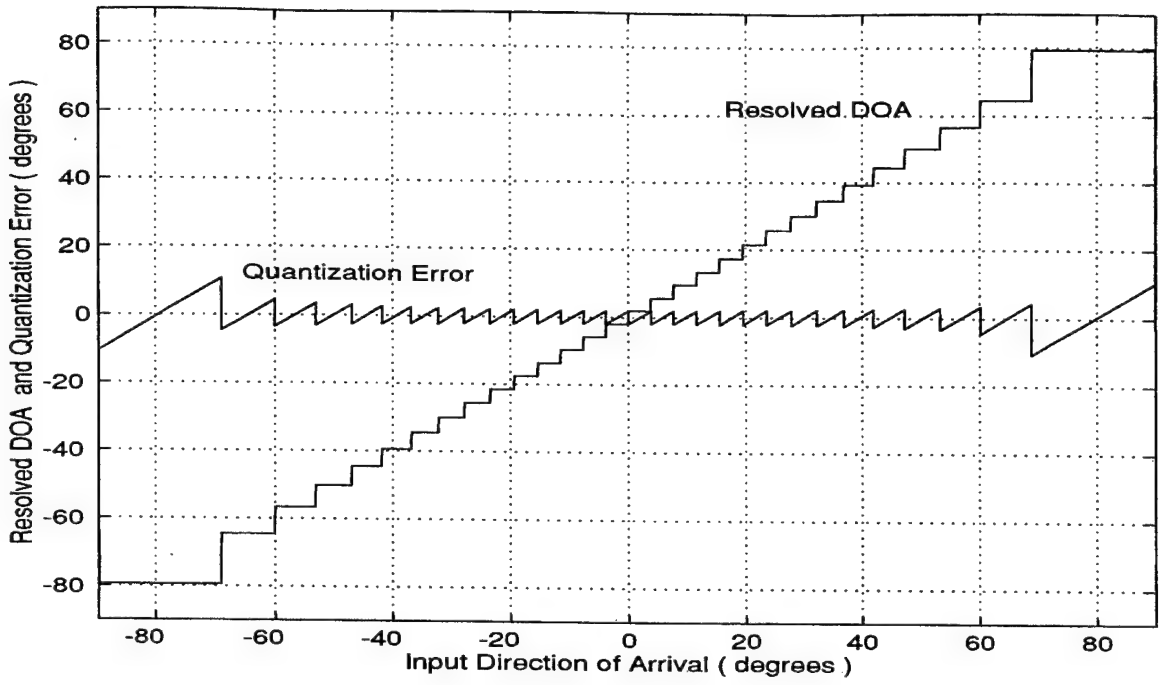

Figure 5.7: Resolved Direction of Arrival and Quantization Error for an Incoming Signal With a Frequency f_r=4.25 GHz.

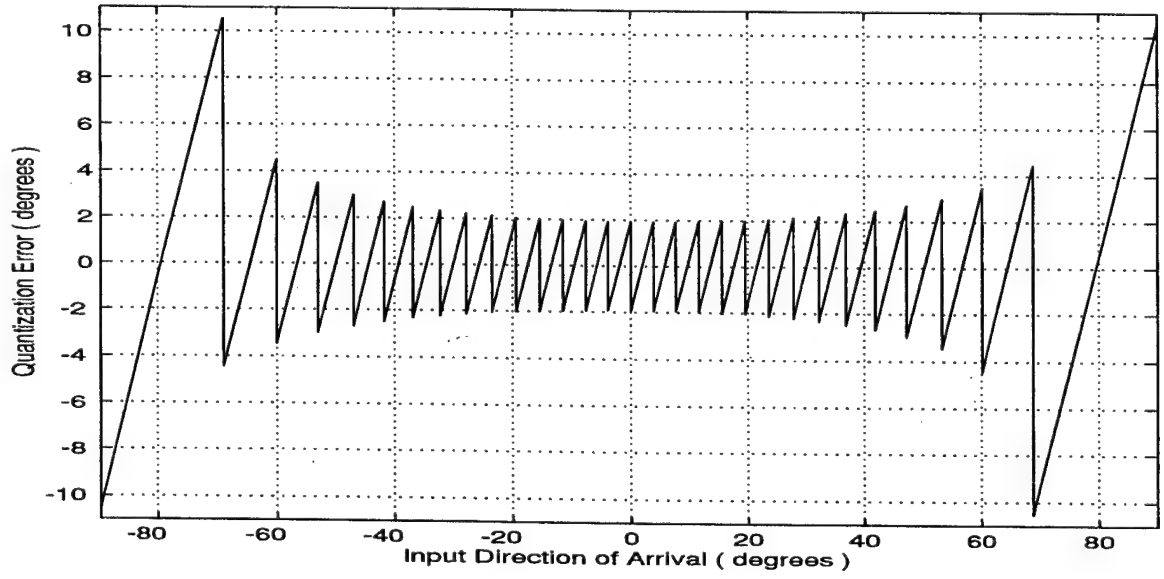

Figure 5.8: Characteristic Quantization Error Curve for an Incoming Signal With a Frequency f_r=4.25 GHz.

D. RELATIONSHIP BETWEEN ANTENNA SIZE, MODULI SET AND FREQUENCY CHOSEN TO BUILD THE ANTENNA

The size of the antenna is an important parameter when considering a new system to be implemented. The relationship between frequency and wavelength is given by $\lambda=c/f$ where c is the speed of light in free space. This relationship is important because the length of the DF antenna is given by the distance between the widest pair of elements which is proportional to the highest number of wavelengths (see Equation (4-8)) required to correctly apply the RNS code to a certain PRP moduli set. On other hand, when building the antenna, the highest frequency in the range of frequencies that are being observed must be chosen in order to be able to obtain the direction of arrival information over the entire field of view without ambiguities. Table 5.1 shows some different PRP moduli set combinations and the distance in wavelengths required for the widest pair of elements in the array.

PRP Moduli Set (m_1, m_2, m_3)	**Distance between the widest pair of elements**
(9, 13)	6.5 λ
(17, 20)	10 λ
(47, 50)	25 λ
(97, 101)	50.5 λ
(3, 4, 5)	10 λ
(5, 7, 9)	31.5 λ
(7, 9, 11)	49.5 λ
(11, 13, 15)	97.5 λ

Table 5.1: Distance Between the Widest Pair of Elements According to the Moduli Set.

For each case considered in Table 5.1, Figure 5.9 shows the required distance between the widest pair of elements as a function of the frequency used to build the antenna.

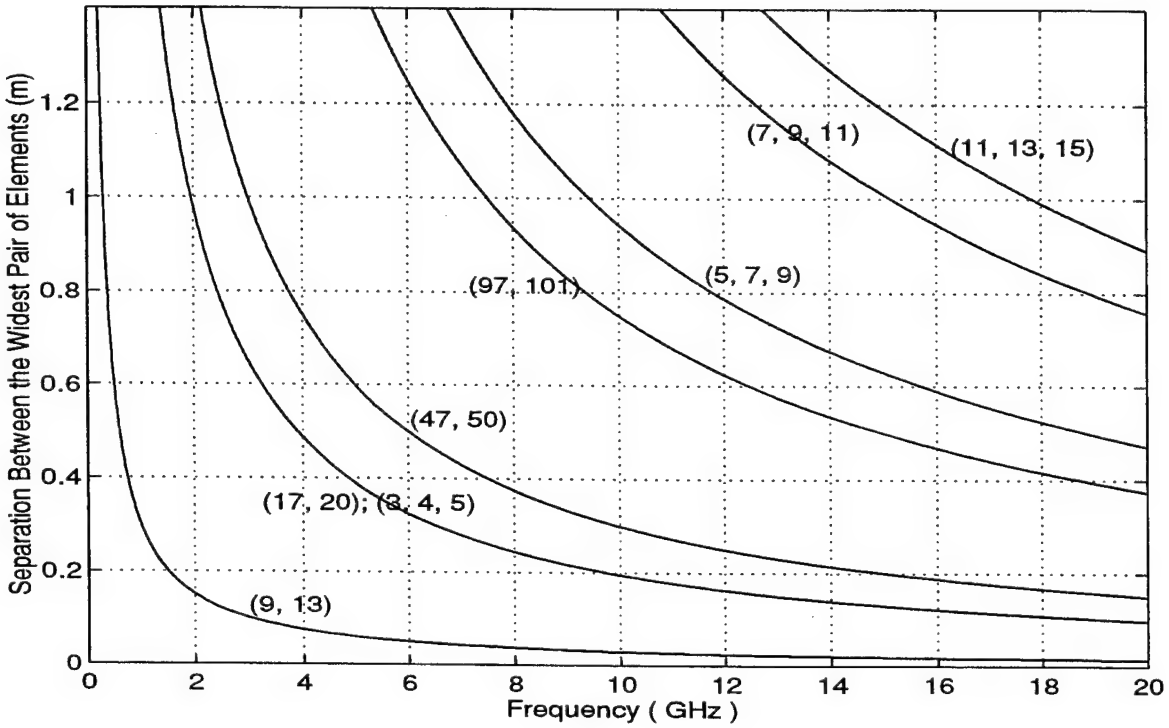

Figure 5.9: Required Distance Between the Widest Pair of Elements as a Function of the Frequency Used to Build the Antenna.

The results show that it is advantageous to chose a frequency as high as possible to build the antenna. First, with a higher frequency it is possible to obtain the direction of arrival information without ambiguities over a larger bandwidth. In addition, for the same moduli set, the size of the antenna becomes smaller when using higher frequencies to build it.

E. QUANTIZATION ERROR BEHAVIOR VS MODULI SET

Another interesting point is to investigate how the quantization error varies according to the chosen moduli set. The overall quantization error of the system is directly related to the chosen PRP moduli set, since it determines the dynamic range, and therefore the number of quantization levels available to quantize the phase response over the entire field of view. With a higher number of quantization levels, the quantization error is smaller. Therefore, a better performance of our antenna is to be expected. Figures 5.10 through 5.17 show the characteristic quantization error curve associated with each of the moduli set considered in Table 5.1, assuming that the antenna is build using a frequency (f_0) equal to 18 GHz.

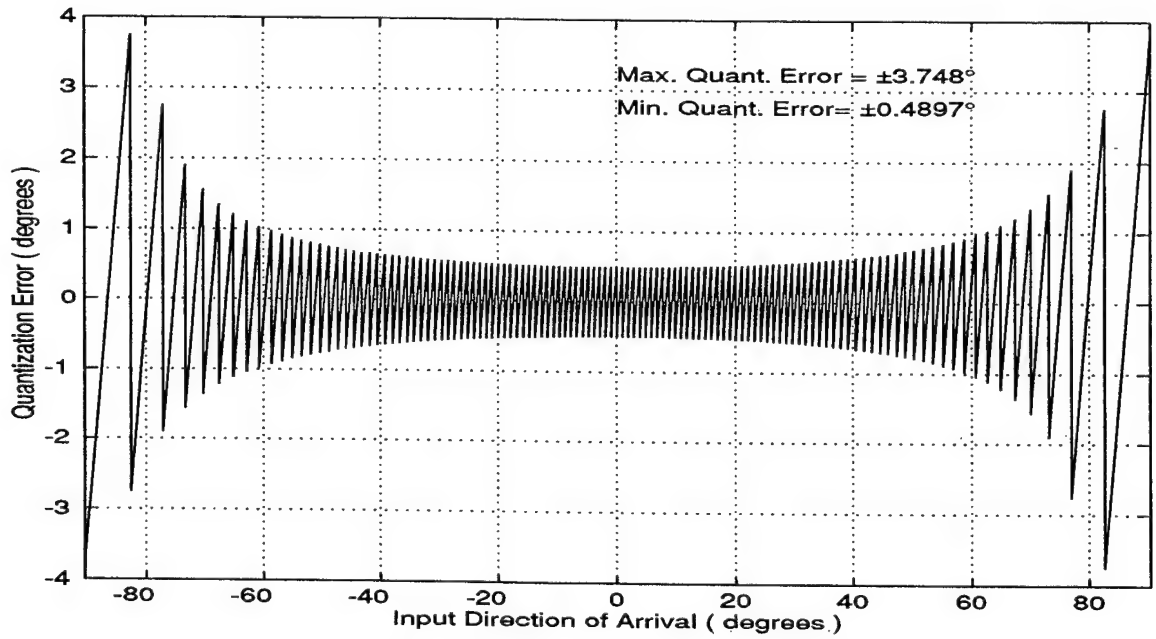

Figure 5.10: Characteristic Quantization Error Curve for the PRP Moduli Set (9, 13).

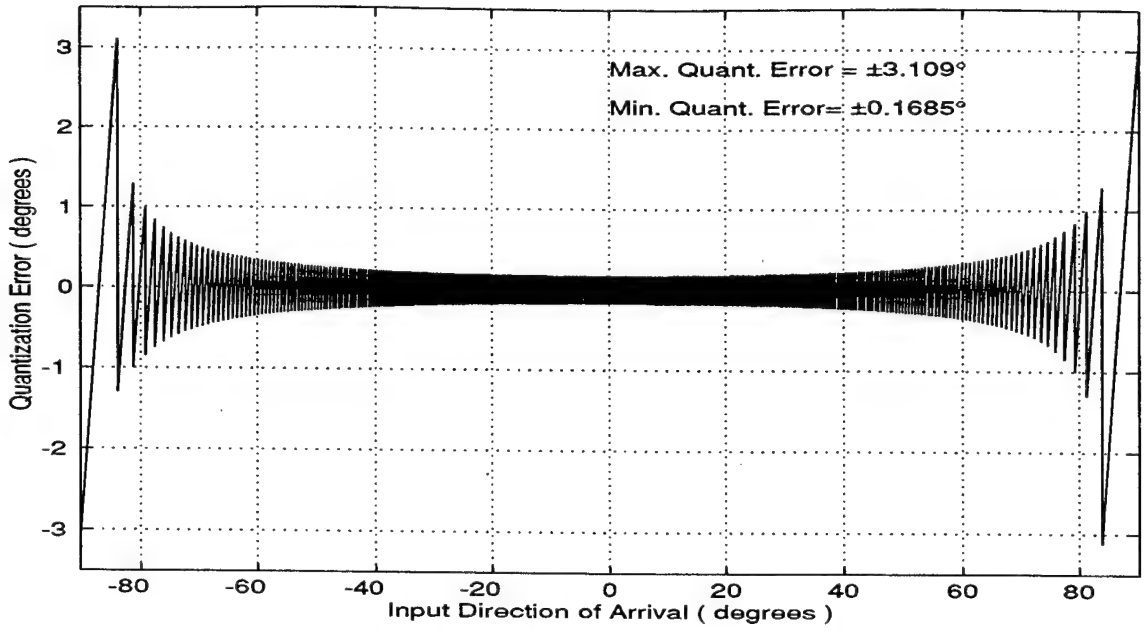

Figure 5.11: Characteristic Quantization Error Curve for the PRP Moduli Set (17, 20).

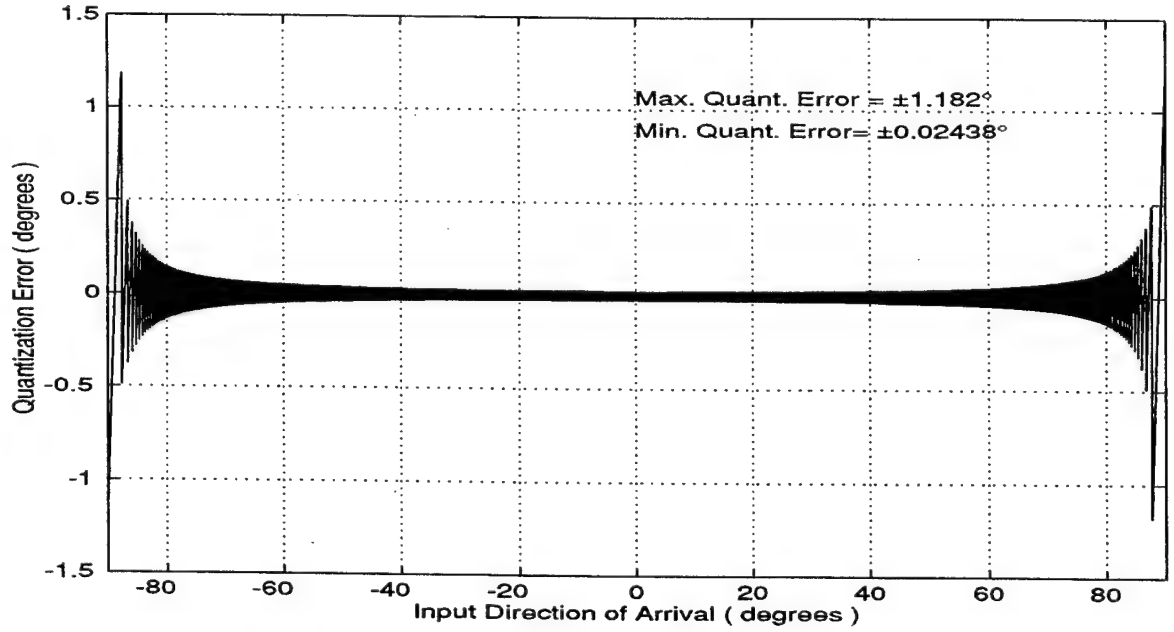

Figure 5.12: Characteristic Quantization Error Curve for the PRP Moduli Set (47, 50).

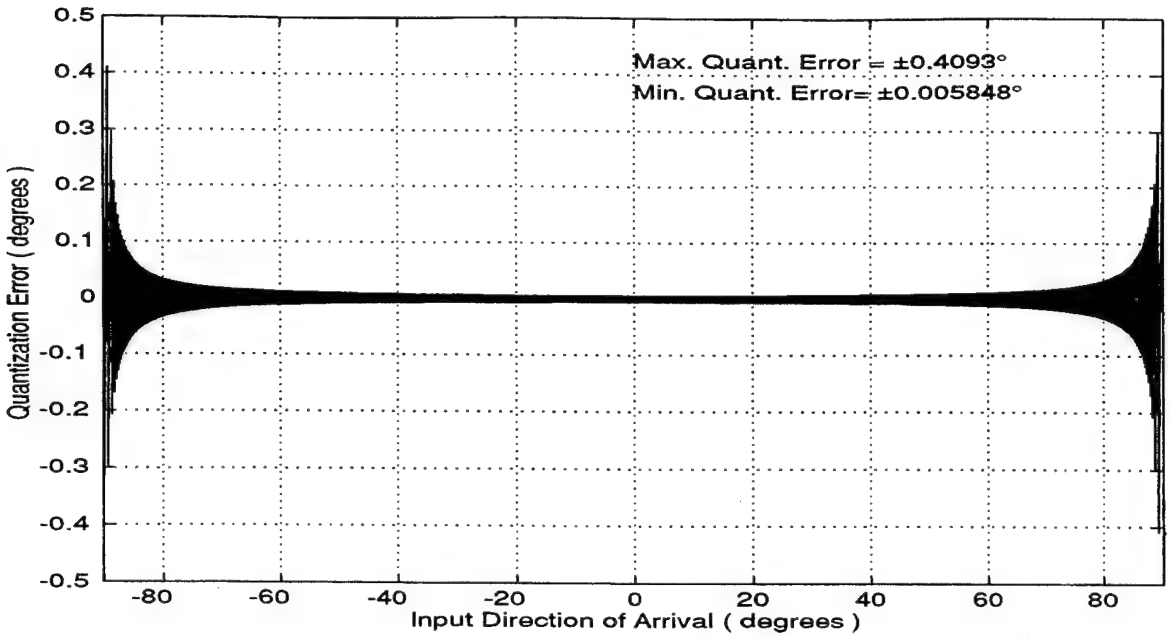

Figure 5.13: Characteristic Quantization Error Curve for the PRP Moduli Set (97, 101).

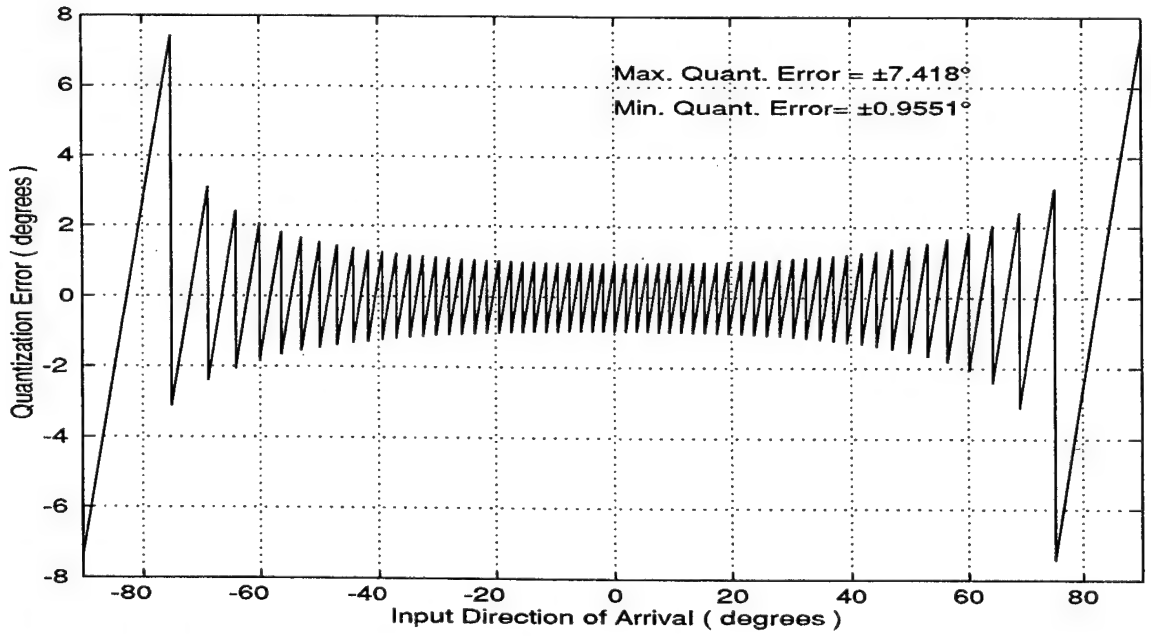

Figure 5.14: Characteristic Quantization Error Curve for the PRP Moduli Set (3, 4, 5).

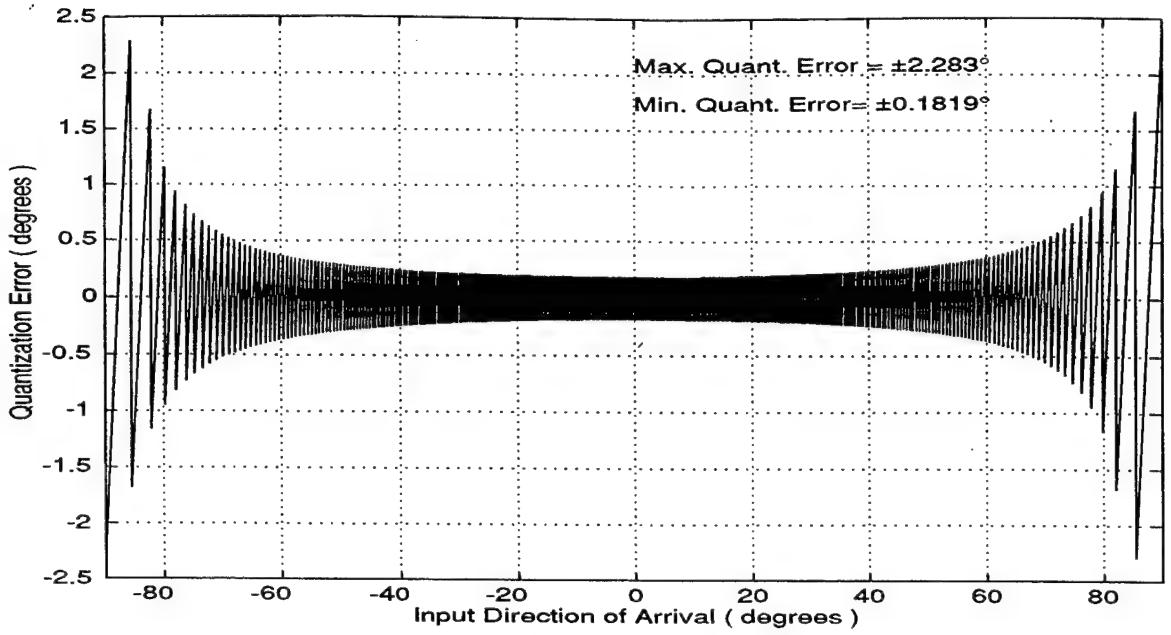

Figure 5.15: Characteristic Quantization Error Curve for the PRP Moduli Set (5, 7, 9).

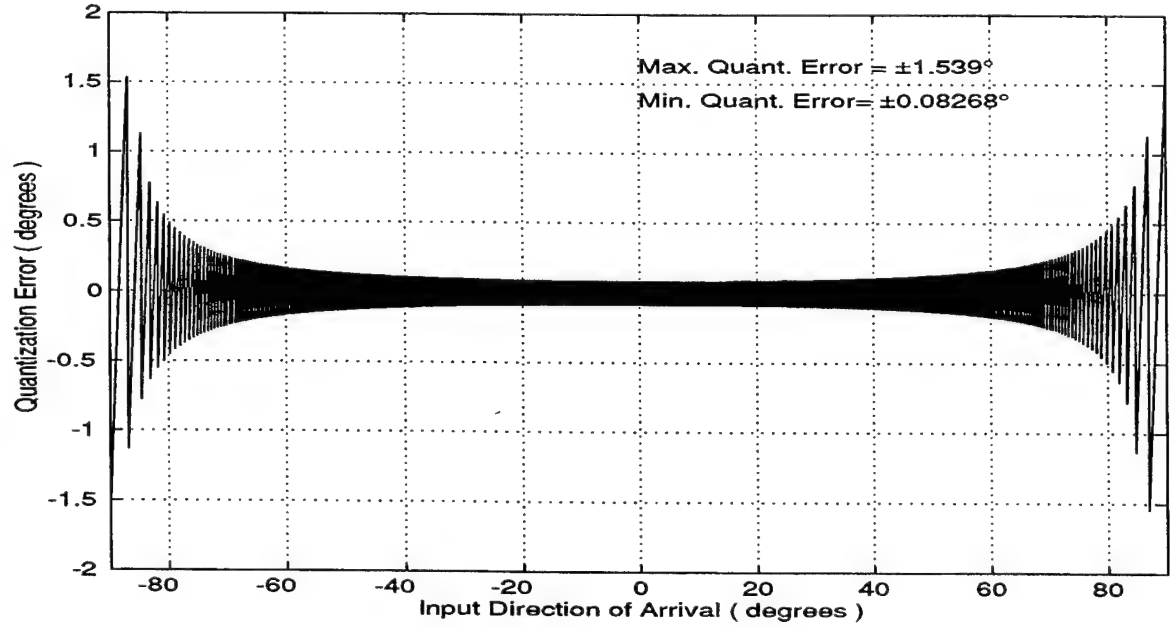

Figure 5.16: Characteristic Quantization Error Curve for the PRP Moduli Set (7, 9, 11).

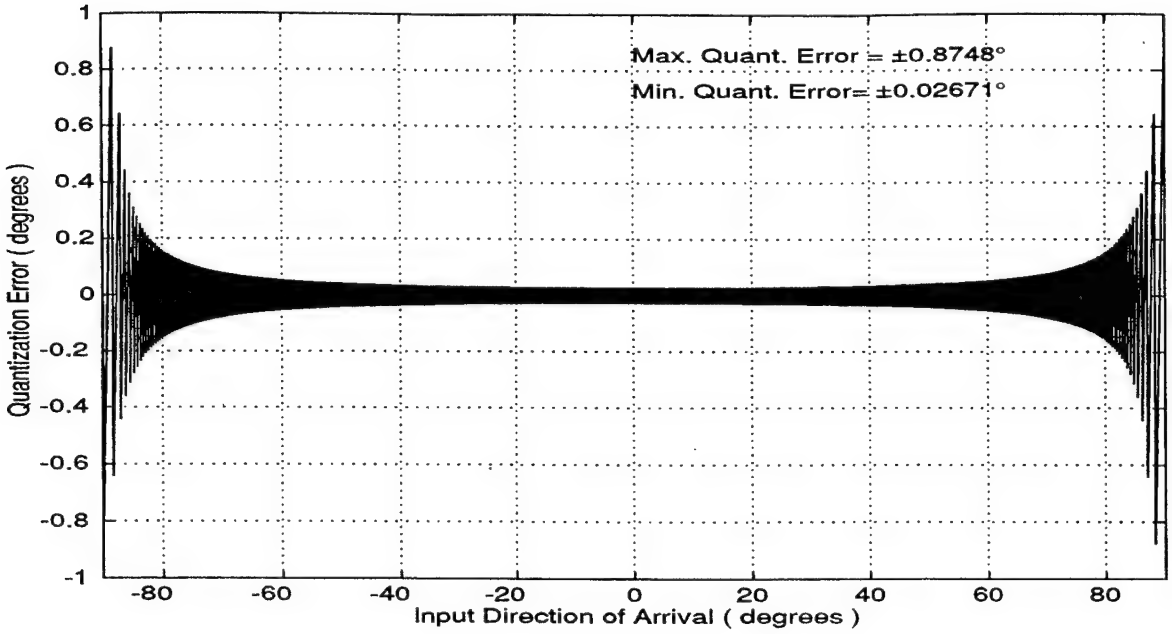

Figure 5.17: Characteristic Quantization Error Curve for the PRP Moduli Set (11, 13, 15).

Comparing the results obtained for each case it is clear that when using a N moduli set with N=2, the quantization error is smaller than when using a moduli set with N=3, assuming that the widest distance between elements is the same. Therefore, with a moduli set with N=2, it is possible to obtain a very high accuracy with relative small antenna sizes. However, the required number of comparators for this scheme (N=2) becomes very high when compared with the scheme using a moduli set with N=3. Table 5.2 contains a compilation of all information of each case considered in Table 5.1. In addition, the last column shows the equivalent *rms* accuracy of an interferometer (conventional methods) assuming that the direction of arrival is equal to 0° and the SNR is equal to 0 dB. The *rms* angular accuracy of an interferometer in radians [Ref. 1] is given by

$$\sigma_\theta = \frac{\Delta\alpha}{\pi\sqrt{SNR}}, \tag{5-7}$$

where $\Delta\alpha$ is the separation between adjacent nulls given by

$$\Delta\alpha = \frac{\lambda}{d\cos\theta}. \tag{5-8}$$

Moduli Set	Largest dist.	No. Comparators	Min. Quant. Error (deg.) $f_r = f_0 = 18$ GHz	Min. Quant. Error (deg.) $f_r = 2$ GHz	*RMS* Accuracy (deg.) Conv. Methods
(9, 13)	6.5 λ	20	± 0.4897	± 4.425	4.897
(17, 20)	10 λ	35	± 0.1685	± 1.517	1.827
(47, 50)	25 λ	95	± 0.0244	± 0.2194	0.729
(97, 101)	50.5 λ	196	± 0.0058	± 0.0526	0.365
(3, 4, 5)	10 λ	9	± 0.9551	± 8.729	1.827
(5, 7, 9)	31.5 λ	18	± 0.1819	± 1.638	0.579
(7, 9, 11)	49.5 λ	24	± 0.0827	± 0.744	0.368
(11,13, 15)	97.5 λ	36	± 0.0267	± 0.2404	0.187

Table 5.2: Comparison Between Different RNS Architecture Schemes and the Conventional Methods.

As shown in Table 5.2, with this new architecture it is possible to obtain the direction of arrival information with a substantial improvement in accuracy when compared with the conventional interferometer methods.

VI. SUMMARY AND CONCLUDING REMARKS

In this thesis two novel architectures for high-resolution wideband direction finding based in the SNS and RNS were developed and investigated. The first architecture incorporates a SNS encoding of the amplitude of the electrical field response (symmetrical folding waveform) of the phase response (sawtooth folding waveform) array. The second architecture incorporates a RNS encoding of the interferometer phase. In addition, an array antenna was constructed in a ground plane using rectangular waveguide elements with a center frequency f_0=8.5 GHz and the SNS architecture was tested.

The simulated results show that the SNS architecture is sensitive to the drop off in the antenna gain due to the element factor effect associated with the kind of individual elements used to build the antenna. In this case it is not possible to obtain the direction of arrival information over the entire field of view (from 0° to ±90°). However, we still have a small interval (from 0° to ±20°) where it is possible to have that information. The experimental results indicate a considerable agreement for this case.

For the RNS architecture the simulated results indicate that it provides a more robust solution to high-resolution DF having an excellent performance. In fact, since the phase response has an "uniform" distribution it is possible to obtain the direction of arrival information over the entire field of view. To avoid ambiguities in the resolved direction of arrival (over the entire field of view) the spacing between elements must be established for the highest frequency to be received. On other hand, the frequency of the incoming signal has to be known in order to make the necessary corrections in the RNS logic block using a fast correction algorithm to obtain the correct direction of arrival. The performance of the algorithm was quantified and shown to have excellent results over a large bandwidth.

The quantization error associated with both architectures depends on the moduli set that is chosen to build the antenna, which also determines the size of the antenna and the required number of comparators. Table 5.2, in Chapter V, illustrates some specifications for the RNS architecture using different moduli set combinations. It also shows the equivalent *rms* accuracy for the conventional methods according to the distance between the widest pair of elements. Comparing those values with the values found for the RNS architecture we notice a great improvement in accuracy with the new architecture.

The advantages of the RNS architecture over the conventional methods can be summarized as follows:

- Higher resolution, higher bandwidth capability,
- Small number of antenna elements,
- Small array size to achieve higher accuracy,
- Only few comparators are required, depending on the chosen moduli set,
- Full coverage from 0° to ±90° without ambiguities.

It was not possible to obtain acceptable experimental results for the RNS antenna architecture. The main problem was the nonavailability of the phase detectors. However, future investigations are currently underway and will correct this and another problems.

APPENDIX: MATLAB™ CODE

```
%Program 1
%This program 'Ampanal.m' calculates the resolved Direction of Arrival using the SNS
%code to process the amplitude response of the array for the moduli set (3, 4, 5).

clear all
whitebg
global m1
global m2
global m3
global fo
global fr
global ds
global rad
global M
global theta

obj=input('Do you want the Array Factor (1) or the Electrical field (2) analysis ?')
ds=input('What is the step size? ')
fo=input('What was the frequency used to built the antenna (GHz) ?')
fr=input('What is the frequency of the received signal (GHz) ?')

m1=3;
m2=4;
m3=5;
fo=fo*1e9;
fr=fr*1e9;

rad=pi/180;
theta=-90:ds:90;
c=3e8;
L=c/fo;
L1=c/fr;

%*****************************Dynamic Range*****************************
M=m1*m2*m3;

%*******************Distances Between Each Pair of Elements*****************
d1=0.5*M/m1*L;
d2=0.5*M/m2*L;
d3=0.5*M/m3*L;

%*****Generates the Array Factor or the Electrical field for Each Pair of Elements******
phi1=(2*pi*d1/L)*sin(theta*rad);
phi2=(2*pi*d2/L)*sin(theta*rad);
phi3=(2*pi*d3/L)*sin(theta*rad);

if obj==1
        mod1A=cos(0.5*(phi1)+pi);
```

```
        mod2A=cos(0.5*(phi2)+pi/2);
        mod3A=cos(0.5*(phi3)+pi);
else
        mod1A=cos(0.5*(phi1)+pi).*cos(theta*rad);
        mod2A=cos(0.5*(phi2)+pi/2).*cos(theta*rad);
        mod3A=cos(0.5*(phi3)+pi).*cos(theta*rad);
end

figure(1)
subplot(311)
plot(theta,mod1A)
axis([-90,90,-1,1]);
xlabel('Input Direction of Arrival ( degrees )')
grid

subplot(312)
plot(theta,mod2A)
axis([-90,90,-1,1]);
xlabel('Input Direction of Arrival ( degrees )')
ylabel('Array Factor Amplitude ')
grid

subplot(313)
plot(theta,mod3A)
axis([-90,90,-1,1]);
xlabel('Input Direction of Arrival ( degrees )')
grid

%**************Calculates the Threshold Values for Each Modulus***************
thresa

%*********Generates the Comparators RNS Output code for Modulus m1=3**********
for i=1:180/ds+1
 if mod1A(i)<=T1(1)
 mod1(i)=0;
 elseif mod1A(i)>T1(2)
 mod1(i)=2;
 else
 mod1(i)=1;
 end
end
end

%*********Generates the Comparators RNS Output code for Modulus m2=4**********
for i=1:180/ds+1
 if mod2A(i)<=T2(1)
 mod2(i)=0;
 elseif mod2A(i)<=T2(2)
 mod2(i)=1;
 elseif mod2A(i)<=T2(3)
 mod2(i)=2;
```

```
 else
 mod2(i)=3;
 end
end

%*********Generates the Comparators RNS Output code for Modulus m3=5**********
for i=1:180/ds+1
 if mod3A(i)<=T3(1)
 mod3(i)=0;
 elseif mod3A(i)<=T3(2)
 mod3(i)=1;
 elseif mod3A(i)<=T3(3)
 mod3(i)=2;
 elseif mod3A(i)<=T3(4)
 mod3(i)=3;
 else
 mod3(i)=4;
 end
end

%******Calculates the Resolved Direction of Arrival for the moduli Set (3, 4, 5)********
SNSLogicBlock

%*Plots the Resolved Direction of Arrival as a Function of the Input Direction of Arrival**
figure(2)
plot(theta,th,'g')
xlabel('Input Direction of Arrival ( degrees )')
ylabel('Resolved Direction of Arrival ( degrees )')
grid
axis([-90 90 -90 90])
```

```
% Program 2
% This program 'thresa.m' calculates the Threshold Values for the moduli set (3, 4, 5)
%when analyzing the Amplitude Response.

global m1
global m2
global m3
global fo
global ds
global M
global L

%*******Calculates the transition angles from one to another quantization level ********
x=-1:2/M:1;
y=asin(x);

%**************Calculates the Threshold Values for modulus m1=3***************
for l=1:m1-1
ang1(l)=y(l+1);
phi1(l)=(2*pi*d1/L)*sin(ang1(l));
T1(l)=cos(0.5*(phi1(l))+pi);
end

%**************Calculates the Threshold Values for Modulus m2=4***************
for r=1:m2-1
ang2(r)=y(r+1);
phi2(r)=(2*pi*d2/L)*sin(ang2(r));
T2(r)=cos(0.5*(phi2(r))+pi/2);
end

%**************Calculates the Threshold Values for Modulus m3=5***************
for h=1:m3-1
ang3(h)=y(h+1);
phi3(h)=(2*pi*d3/L)*sin(ang3(h));
T3(h)=cos(0.5*(phi3(h))+pi);
end
```

```
%Program 3
%This program 'SNSLogicBlock.m' calculates the resolved direction of arrival according
to the 3-SNS code.

global ds
global m1
global m2
global m3
global fo
global fr
global M
global theta

%****Combines the SNS Code coming from each channel m1=3, m2=4, and m3=5*****
res=[mod1' mod2' mod3'];

%***Calculates the Resolved Direction of Arrival according to the 3-SNS Code value****
for u=1:180/ds+1
if res(u,:)==([0,0,0])
  th(u)=-82.5824;
  elseif res(u,:)==([1,1,1])
  th(u)=-72.0627;
  elseif res(u,:)==([2,2,2])
  th(u)=-66.5593;
  elseif res(u,:)==([2,3,3])
  th(u)=-62.1158;
  elseif res(u,:)==([1,3,4])
  th(u)=-58.2581;
  elseif res(u,:)==([0,2,4])
  th(u)=-54.7864;
  elseif res(u,:)==([0,1,3])
  th(u)=-51.5928;
  elseif res(u,:)==([1,0,2])
  th(u)=-48.6110;
  elseif res(u,:)==([2,0,1])
  th(u)=-45.7968;
  elseif res(u,:)==([2,1,0])
  th(u)=-43.1187;
  elseif res(u,:)==([1,2,0])
  th(u)=-40.5534;
  elseif res(u,:)==([0,3,1])
  th(u)=-38.0832;
  elseif res(u,:)==([0,3,2])
  th(u)=-35.6940;
  elseif res(u,:)==([1,2,3])
  th(u)=-33.3745;
  elseif res(u,:)==([2,1,4])
  th(u)=-31.1155;
  elseif res(u,:)==([2,0,4])
  th(u)=-28.9091;
  elseif res(u,:)==([1,0,3])
```

```
th(u)=-26.7487;
elseif res(u,:)==([0,1,2])
th(u)=-24.6287;
elseif res(u,:)==([0,2,1])
th(u)=-22.5442;
elseif res(u,:)==([1,3,0])
th(u)=-20.4907;
elseif res(u,:)==([2,3,0])
th(u)=-18.4644;
elseif res(u,:)==([2,2,1])
th(u)=-16.4618;
elseif res(u,:)==([1,1,2])
th(u)=-14.4797;
elseif res(u,:)==([0,0,3])
th(u)=-12.5152;
elseif res(u,:)==([0,0,4])
th(u)=-10.5655;
elseif res(u,:)==([1,1,4])
th(u)=-8.6382;
elseif res(u,:)==([2,2,3])
th(u)=-6.7007;
elseif res(u,:)==([2,3,2])
th(u)=-4.7809;
elseif res(u,:)==([1,3,1])
th(u)=-2.8664;
elseif res(u,:)==([0,2,0])
th(u)=-0.9551;
elseif res(u,:)==([0,1,0])
th(u)=0.9551;
elseif res(u,:)==([1,0,1])
th(u)=2.8664;
elseif res(u,:)==([2,0,2])
th(u)=4.7809;
elseif res(u,:)==([2,1,3])
th(u)=6.7007;
elseif res(u,:)==([1,2,4])
th(u)=8.6382;
elseif res(u,:)==([0,3,4])
th(u)=10.5655;
elseif res(u,:)==([0,3,3])
th(u)=12.5152;
elseif res(u,:)==([1,2,2])
th(u)=14.4797;
elseif res(u,:)==([2,1,1])
th(u)=16.4618;
elseif res(u,:)==([2,0,0])
th(u)=18.4644;
elseif res(u,:)==([1,0,0])
th(u)=20.4907;
elseif res(u,:)==([0,1,1])
th(u)=22.5442;
```

```
elseif res(u,:)==([0,2,2])
th(u)=24.6287;
elseif res(u,:)==([1,3,3])
th(u)=26.7487;
elseif res(u,:)==([2,3,4])
th(u)=28.9091;
elseif res(u,:)==([2,2,4])
th(u)=31.1155;
elseif res(u,:)==([1,1,3])
th(u)=33.3745;
elseif res(u,:)==([0,0,2])
th(u)=35.6940;
elseif res(u,:)==([0,0,1])
th(u)=38.0832;
elseif res(u,:)==([1,1,0])
th(u)=40.5534;
elseif res(u,:)==([2,2,0])
th(u)=43.1187;
elseif res(u,:)==([2,3,1])
th(u)=45.7968;
elseif res(u,:)==([1,3,2])
th(u)=48.6110;
elseif res(u,:)==([0,2,3])
th(u)=51.5928;
elseif res(u,:)==([0,1,4])
th(u)=54.8;%54;
elseif res(u,:)==([1,0,4])
th(u)=58.2581;
elseif res(u,:)==([2,0,3])
th(u)=62.1158;
elseif res(u,:)==([2,1,2])
th(u)=66.5593;
elseif res(u,:)==([1,2,1])
th(u)=72.0627;
elseif res(u,:)==([0,3,0])
th(u)=82.5824;
end
end
```

```
%Program 4
%This program 'Phanalnew' calculates the Resolved Direction of Arrival using the RNS
%code to process the phase response of the array for the moduli set (3, 4, 5).

clear all
whitebg
global m1
global m2
global m3
global fo
global fr
global ds
global rad
global M
global theta

ds=input('What is the step size? ')
fo=input('What was the frequency used to built the antenna (GHz) ?')
fr=input('What is the frequency of the received signal (GHz) ?')

m1=3;
m2=4;
m3=5;
fo=fo*1e9;
fr=fr*1e9;

rad=pi/180;
theta=-90:ds:90;
c=3e8;
L=c/fo;
L1=c/fr;

%*****************************Dynamic Range*****************************
M=m1*m2*m3;

%*******************Distances Between Each Pair of Elements*****************
d1=0.5*M/m1*L;
d2=0.5*M/m2*L;
d3=0.5*M/m3*L;

%**************Generates the Array Factor for Each Pair of Elements**************
phi1=(2*pi*d1/L1)*sin(theta*rad);
mod1p=angle(exp(j*((phi1+pi))));

phi1=(2*pi*d2/L1)*sin(theta*rad);
mod2p=angle(exp(j*((phi1)+pi)));

phi1=(2*pi*d3/L1)*sin(theta*rad);
mod3p=angle(exp(j*((phi1)+pi)));
```

```
figure(1)
subplot(311)
plot(theta,mod1p)
axis([-90,90,-4,4]);
xlabel('Input Direction of Arrival ( degrees )')
grid

subplot(312)
plot(theta,mod2p)
axis([-90,90,-4,4]);
xlabel('Input Direction of Arrival ( degrees )')
ylabel('Phase Response ( pi ) ')
grid

subplot(313)
plot(theta,mod3p)
axis([-90,90,-4,4]);
xlabel('Input Direction of Arrival ( degrees )')
grid

%**************Calculates the Threshold Values for Each Modulus***************
thres

%*********Generates the Comparators RNS Output code for Modulus m1=3**********
for i=1:180/ds+1
 if mod1p(i)<=T1(1)
 mod1(i)=0;
 elseif mod1p(i)>T1(2)
 mod1(i)=2;
 else
 mod1(i)=1;
 end
end
end

%*********Generates the Comparators RNS Output code for Modulus m2=4**********
for i=1:180/ds+1
 if mod2p(i)<=T2(1)
 mod2(i)=0;
 elseif mod2p(i)<=T2(2)
 mod2(i)=1;
 elseif mod2p(i)<=T2(3)
 mod2(i)=2;
 else
 mod2(i)=3;
 end
end

%*********Generates the Comparators RNS Output code for Modulus m3=5**********
for i=1:180/ds+1
```

```
if mod3p(i)<=T3(1)
mod3(i)=0;
elseif mod3p(i)<=T3(2)
mod3(i)=1;
elseif mod3p(i)<=T3(3)
mod3(i)=2;
elseif mod3p(i)<=T3(4)
mod3(i)=3;
else
mod3(i)=4;
end
end

%******Calculate the Resolved Direction of Arrival and the Quantization Error*********
%************************for the moduli Set (3, 4, 5)************************
RNSlogicBlock

%*********Plots the Resolved Direction of Arrival and the Quantization Error*********
%******************as a function of the Input Direction of Arrival******************
figure(2)
plot(theta,th,'g')
hold
xlabel('Input Direction of Arrival ( degrees )')
ylabel('Resolved DOA  and Quantization Error ( degrees )')
axis([-90 90 -90 90])
plot(y([2:size(y,2)]),k,'r')
grid
```

```
%Program 5
%This program 'thres.m' calculates the Threshold values for the moduli set (3, 4, 5)
%when analyzing the phase response.

global m1
global m2
global m3
global fo
global fr
global ds
global M
global L

%*******Calculate the transition angles from one to another quantization level*********
x=-1:2/M:1;
y=asin(x);

%**************Calculate the Threshold Values for modulus m1=3****************
for l=1:m1-1
ang1(l)=y(l+1);
phi1(l)=(2*pi*d1/L)*sin(ang1(l));
T1(l)=angle(exp(j*((phi1(l))+pi)));
end

%**************Calculate the Threshold Values for modulus m2=4****************
for r=1:m2-1
ang2(r)=y(r+1);
phi2(r)=(2*pi*d2/L)*sin(ang2(r));
T2(r)=angle(exp(j*((phi2(r))+pi)));
end

%**************Calculate the Threshold Values for modulus m3=5****************
for h=1:m3-1
ang3(h)=y(h+1);
phi3(h)=(2*pi*d3/L)*sin(ang3(h));
T3(h)=angle(exp(j*((phi3(h))+pi)));
end
```

```
% Program 6
%This program 'RNSlogicBlock.m' calculates the Resolved Direction of Arrival and
%Quantization Error according to the 3-RNS code. It also uses an algorithm to calculate the
%correct quantization level midvalue when the frequency of the received signal (fr) is
%different form the center frequency (fo) used in the antenna design.

global rad
global m1
global m2
global m3
global fo
global fr
global M
global theta

%*****Calculate the total number of quantization levels over the entire field of view*****
%**********and the transition angles from one to another quantization level**********
nf=fr/fo*M/m1;
nql=nf*m1;
p=0:2/nql:1;
if max(p)~=1
p=[p 1];
end
p=[ -rot90(p(2:size(p,2)))' p];
trang=1/rad*asin(p);

%**Calculate the quantization level width and the midvalues for each quantization level***
for n=1:size(p,2)-1
midval(n)=trang(n)+(trang(n+1)-trang(n))/2;
qlw(n)=midval(n)-trang(n);
end

if rem(size(midval,2),2)==0
a=midval;
b=size(a,2)/2;
end
if rem(size(midval,2),2)==1
a=midval;
b=(size(a,2)+1)/2;
end

if size(a,2)~=60
a=[zeros(1,b) a zeros(1,b)];
end
b=size(a,2)/2;
for n=2:2*size(trang,2)-1
if rem(n,2)==0
y(n)=trang((n)/2);
else
y(n)=trang((n+1)/2);
end
```

```
end

%**********************Calculate the Quantization Error**********************
for n=1:size(trang,2)-1
c(n)=(trang(n+1)-trang(n))/2;
end
for r=1:2*size(trang,2)-2
if rem(r,2)==0
k(r)=c(r/2);
else
k(r)=-c((r+1)/2);
end
end

%****Combines the RNS Code coming from each channel m1=3, m2=4, and m3=5*****
res=[mod3' mod4' mod5'];

for u=1:180/ds+1
 if res(u,:)==([0,0,0])
 th(u)=a(b+1);
 elseif res(u,:)==([1,1,1])
 th(u)=a(b+2);
 elseif res(u,:)==([2,2,2])
 th(u)=a(b+3);
 elseif res(u,:)==([0,3,3])
 th(u)=a(b+4);
 elseif res(u,:)==([1,0,4])
 th(u)=a(b+5);
 elseif res(u,:)==([2,1,0])
 th(u)=a(b+6);
 elseif res(u,:)==([0,2,1])
 th(u)=a(b+7);
 elseif res(u,:)==([1,3,2])
 th(u)=a(b+8);
 elseif res(u,:)==([2,0,3])
 th(u)=a(b+9);
 elseif res(u,:)==([0,1,4])
 th(u)=a(b+10);
 elseif res(u,:)==([1,2,0])
 th(u)=a(b+11);
 elseif res(u,:)==([2,3,1])
 th(u)=a(b+12);
 elseif res(u,:)==([0,0,2])
 th(u)=a(b+13);
 elseif res(u,:)==([1,1,3])
 th(u)=a(b+14);
 elseif res(u,:)==([2,2,4])
 th(u)=a(b+15);
 elseif res(u,:)==([0,3,0])
 th(u)=a(b+16);
 elseif res(u,:)==([1,0,1])
```

```
th(u)=a(b+17);
elseif res(u,:)==([2,1,2])
th(u)=a(b+18);
elseif res(u,:)==([0,2,3])
th(u)=a(b+19);
elseif res(u,:)==([1,3,4])
th(u)=a(b+20);
elseif res(u,:)==([2,0,0])
th(u)=a(b+21);
elseif res(u,:)==([0,1,1])
th(u)=a(b+22);
elseif res(u,:)==([1,2,2])
th(u)=a(b+23);
elseif res(u,:)==([2,3,3])
th(u)=a(b+24);
elseif res(u,:)==([0,0,4])
th(u)=a(b+25);
elseif res(u,:)==([1,1,0])
th(u)=a(b+26);
elseif res(u,:)==([2,2,1])
th(u)=a(b+27);
elseif res(u,:)==([0,3,2])
th(u)=a(b+28);
elseif res(u,:)==([1,0,3])
th(u)=a(b+29);
elseif res(u,:)==([2,1,4])
th(u)=a(b+30);
elseif res(u,:)==([0,2,0])
th(u)=a(b-29);
elseif res(u,:)==([1,3,1])
th(u)=a(b-28);
elseif res(u,:)==([2,0,2])
th(u)=a(b-27);
elseif res(u,:)==([0,1,3])
th(u)=a(b-26);
elseif res(u,:)==([1,2,4])
th(u)=a(b-25);
elseif res(u,:)==([2,3,0])
th(u)=a(b-24);
elseif res(u,:)==([0,0,1])
th(u)=a(b-23);
elseif res(u,:)==([1,1,2])
th(u)=a(b-22);
elseif res(u,:)==([2,2,3])
th(u)=a(b-21);
elseif res(u,:)==([0,3,4])
th(u)=a(b-20);
elseif res(u,:)==([1,0,0])
th(u)=a(b-19);
elseif res(u,:)==([2,1,1])
th(u)=a(b-18);
```

```
 elseif res(u,:)==([0,2,2])
 th(u)=a(b-17);
 elseif res(u,:)==([1,3,3])
 th(u)=a(b-16);
 elseif res(u,:)==([2,0,4])
 th(u)=a(b-15);
 elseif res(u,:)==([0,1,0])
 th(u)=a(b-14);
 elseif res(u,:)==([1,2,1])
 th(u)=a(b-13);
 elseif res(u,:)==([2,3,2])
 th(u)=a(b-12);
 elseif res(u,:)==([0,0,3])
 th(u)=a(b-11);
 elseif res(u,:)==([1,1,4])
 th(u)=a(b-10);
 elseif res(u,:)==([2,2,0])
 th(u)=a(b-9);
 elseif res(u,:)==([0,3,1])
 th(u)=a(b-8);
 elseif res(u,:)==([1,0,2])
 th(u)=a(b-7);
 elseif res(u,:)==([2,1,3])
 th(u)=a(b-6);
 elseif res(u,:)==([0,2,4])
 th(u)=a(b-5);
 elseif res(u,:)==([1,3,0])
 th(u)=a(b-4);
 elseif res(u,:)==([2,0,1])
 th(u)=a(b-3);
 elseif res(u,:)==([0,1,2])
 th(u)=a(b-2);
 elseif res(u,:)==([1,2,3])
 th(u)=a(b-1);
 elseif res(u,:)==([2,3,4])
 th(u)=a(b);
 end
 end
end
end
```

```
%Program 7
%This program 'Quanterror' calculates the Quantization Error for any PRP N moduli set,
%where N is equal to 2 or 3, and any frequency.

clear all
whitebg
ds=input('What is the step size? ')
N=input('What is the moduli set size (2 or 3) ?')
if N==2
m1=input('What is the value of modulus m1 ?')
m2=input('What is the value of modulus m2 ?')
end

if N==3
m1=input('What is the value of modulus m1 ?')
m2=input('What is the value of modulus m2 ?')
m3=input('What is the value of modulus m3 ?')
end

fo=input('What was the frequency used to built the antenna (GHz) ?')
fr=input('What is the frequency of the received signal (GHz) ?')

%**********Number of Folds Over the Entire field of View for Modulus m1**********
nf=fr/fo*M/m1;

%********Total Number of Quantization Levels Over the Entire Field of View*********
nql=nf*m1;

%*************Generates the Quantization Level Transistion Angles****************
p=0:2/nql:1;
if max(p)~=1
p=[p 1];
end
p=[ -rot90(p(2:size(p,2)))' p];
trang=1/rad*asin(p);

%**************Calculates the Midvalue of Each Quantization Level***************
for n=1:size(p,2)-1
midval(n)=trang(n)+(trang(n+1)-trang(n))/2;
qlw(n)=midval(n)-trang(n);
end

%********************Calculates the Quantization Error************************
for n=2:2*size(trang,2)-1
if rem(n,2)==0
y(n)=trang((n)/2);
else
y(n)=trang((n+1)/2);
end
end
```

```
for n=1:size(trang,2)-1
c(n)=(trang(n+1)-trang(n))/2;
end

for r=1:2*size(trang,2)-2
if rem(r,2)==0
k(r)=c(r/2);
else
k(r)=-c((r+1)/2);
end
end

%**********Plots the Resolved Direction of arrival and Quantization Error**********
%****************as a Function of the Input Direction of Arrival******************
figure(1)
plot(y([2:size(y,2)]),k,'r')
xlabel('Input Direction of Arrival ( degrees )')
ylabel(' Quantization Error ( degrees )')
axis([-90 90 -round(max(k)+0.5) round(max(k)+0.5)])
grid
```

LIST OF REFERENCES

1. Curtis Schleher, Ph. D., *Introduction to Electronic Warfare*, Artech House Inc., Dedham, MA, 1987.

2. R. Baron, K. P. Davis, C. P. Hofman, "Passive Direction Finding and Signal Location," Microwave Journal, September 1982.

3. Constantine A. Balanis, *Antenna Theory, Analysis and Design*, Harper & Row, Publishers, Inc., York, NY, 1982.

4. Stuzman Thiele, *Antenna Theory and Design*, Wiley & Sons, Inc., 1981.

5. P. E. Pace, J. L. Schafer, and D. Styer, "Optimum Analog Preprocessing for Folding ADC's," IEEE Transactions on Circuits and Systems-II: Analog and Digital Signal Processing, Vol. 42, N0. 12, December 1995.

6. P. E. Pace, P. A. Ramamoorthy, David Styer, "A Preprocessing Architecture for Resolution Enhancement in High-Speed Analog-to-Digital Converters," IEEE Transactions on Circuits and Systems, Vol. 41, No. 6, June 1994.

7. Fred J. Taylor, "Residue Arithmetic: A tutorial with Examples," IEEE Computer Magazine, May 1984.

8. Simon Haykin, *An Introduction to Analog and Digital Communications*, by John Wiley & Sons, Inc., 1989.

INITIAL DISTRIBUTION LIST

	No.Copies
1. Defense Technical Information Center 8725 John J. Kingman Rd.,STE 0944 Ft. Belvoir, VA 22060-6218	2
2. Dudlley Knox Library Naval Postgraduate School 411 Dyer Rd. Monterey, CA 93943-5101	2
3. Chairman, Code PH Department of Physics Naval Postgraduate School Monterey, CA 93943-5121	1
4. Chairman, Code EC Department of Electrical and Computer Engineering Naval Postgraduate School Monterey, CA 93943-5121	1
5. Professor Phillip E. Pace, Code EC/PC Department of Electrical and Computer Engineering Naval Postgraduate School Monterey, CA 93943-5121	3
6. Professor Robert M. Keolian, Code PH/KN Department of Physics Naval Postgraduate School Monterey, CA 93943-5121	1
7. Professor David C. Jenn, Code EC/JN Department of Electrical and Computer Engineering Naval Postgraduate School Monterey, CA 93943-5121	1
8. LT. Luis E. Moita Rodrigues Rua S. Francisco Xavier, No. 112 Bairro do Restelo 1400 Lisboa Portugal	2
9. Space and Naval Warfare System Command Department of the Navy PMW-178 Attn: CAPT. Connell Washington, DC 20363-5100	1